2017

Use of ultraviolet laser ablation electrospray ionization mass spectrometry for plant metabolite imaging

Katherine-Jo Galayda
Iowa State University

Follow this and additional works at: https://lib.dr.iastate.edu/etd

Part of the Analytical Chemistry Commons

Use of ultraviolet laser ablation electrospray ionization mass spectrometry for plant
metabolite imaging

by

Katherine-Jo Galayda

A dissertation submitted to the graduate faculty

in partial fulfillment of the requirements for the degree of

DOCTOR OF PHILOSOPHY

Major: Analytical Chemistry

Program of Study Committee:
Robert S. Houk, Major Professor
Young-Jin Lee
Joseph Burnett
Robbyn Anand
Basil Nikolau

Iowa State University

Ames, Iowa

2017

DEDICATION

I would like to dedicate my dissertation to the woman who pushes me to be a better woman than I was the day before, my mother, Mary Galayda. I love you more than you will ever know.

TABLE OF CONTENTS

**CHAPTER 3   ANTHOCYANIN IMAGING IN *SOLENOSTEMON
SCUTELLARIODES (COLEUS) LEAVES USING ULTRAVIOLET
LASER ABLATION ELECTROSPRAY IONIZATION
MASS SPECTROMETRY**... 49

**CHAPTER 4   DETERMINING LIPID CHANGES DURING AUTOPHAGY
IN *ARABIDOPSIS THALIANA* PLANTS USING MASS SPECTROMETRY
IMAGING**…………………………………………………………………… 81

ACKNOWLEDGMENTS

Firstly, I would like to thank Dr. R. Sam Houk for being my research advisor. The freedom you allowed me to have while being a graduate student allowed me to become the researcher that I am today. I am also forever grateful that you allowed me to enter your research group at a time where my future as a graduate student at ISU was uncertain, it meant the world to me and always will. Secondly, I would like to thank my research committee for their continued support and advice these last six years. I know you have your own students and projects, but taking time out of your busy schedules to help me was so selfless, and I truly appreciate it. Thirdly, I would like to thank Stan Bajic for his willingness to assist me when instruments broke and put up with me when I got a little carried away. Your coffee with cream, no sugar will be arriving shortly! And lastly, I would like to thank the Houk group members (past and present) for their support and friendship over the past 6 years, especially the awesome Patrick McVey. I am honored to have worked with such great scientists.

A special shout out to my family and friends as well. Mom, dad, MB thanks for believing in me when everyone else had their doubts (eh, it's alright!). And to my friends, both in Iowa and back east, thanks for putting up with my crazy loud self. You guys keep me sane and I want you all to know how proud I am to call you my friend and I cannot wait to see what the future holds for all of us! I am your number one fan!

ABSTRACT

This dissertation describes a variety of plant studies by laser ablation electrospray ionization mass spectrometry imaging. (LAESI MSI). During the LAESI process, a plant sample is ablated when a laser is fired at it. The resultant neutral plume is ionized and enters the mass spectrometer by an electrospray stream. In all experiments an ultraviolet (UV; 355 Nd:YAG) laser was used. Once ions enter the mass spectrometer and are detected, a spectrum is produced for a particular area on the plant. The rest of the plant is ablated and spectra are combined for image creation.

Unlike other forms of mass spectrometry, MSI allows for chemical and spatial information which can help understand the diversity of plants, where one cell may contain different chemicals compared to its neighboring cell. Plants studied in this dissertation included peonies, coleus, and *Arabidopsis thaliana*. A variety of metabolites were imaged, including flavonoids, anthocyanins and lipids. Analyte images allowed further insight into biological processes, such as the malonylshisonin pathway in coleus leaves, and effects of lipids during autophagy in *Arabidopsis thaliana*. LAESI MSI was also shown in this dissertation to be a potentially faster more sensitive technique than other forms of mass spectrometry.

CHAPTER 1. GENERAL INTRODUCTION

Basic Principles of Mass Spectrometry

Mass spectrometry (MS) is an analytical technique that is widely used in many areas ranging from forensics, biology and the medical sciences due to its versatility, selectivity, and sensitivity.[1-3] While several forms of mass spectrometry exist, the basic principle remains the same. Figure 1 shows a schematic of a typical MS run. Briefly, in order for a sample to be detected, it must become ionized, often by gaining or losing a proton. Common forms of ionization include electrospray ionization (ESI) and chemical ionization.[4-6] Once ionization occurs, ions travel through a mass analyzer, such as a time of flight (TOF), and are further separated by their mass to charge ratio (m/z). These ions can now be detected and a mass spectrum is produced for analysis.

Most MS analyses performed today are coupled with separation techniques, such as gas chromatography (GC) or liquid chromatography (LC).[7] LC and GC are useful for biologically interesting chemicals since they can distinguish isomers that cannot normally be differentiated by MS alone.[8] While GC-MS and LC-MS are particularly useful for obtaining quantitative data, sample preparation involving extractions of plant and animal tissue renders these techniques useless in obtaining spatial information. Mass spectrometry imaging, a relatively new technique in the history of MS, offers a solution to this limitation.

Mass Spectrometry Imaging

The basic principle of mass spectrometry imaging (MSI) is demonstrated in Figure 2. A sample is ablated using either a laser, ion beam or some other ablation source, and ionized by a

number of techniques described further below. Ions enter the mass spectrometer and a mass spectrum is produced from each individual sample location. The resultant mass spectrum contains all the ions from that area on the sample, making it unique to that specific area. When the entire sample area is fully ablated, spectra are binned, and images for ions of interest can be created.

MSI results in chemical and spatial information and is thus gaining popularity in biomedical sciences, forensics, and metabolomics.[9-11] In the early stages of MSI, most work was performed on mammalian tissues, such as rat brains and human tumors. Popular studies on these tissues include imaging of peptides[12], lipids[13], and drugs[14-16]. In recent years MSI has also included imaging of plant samples. Plants have highly diverse metabolic profiles that are unique both between different plants species and neighboring cells on the same plant, MSI serves as a useful tool for obtaining spatial information.[7,17,18] Common plant samples include fungus, Arabidopsis, and marigold.

The process of generating spatially resolved information (i.e. data processing) is the same for all various mass spectrometry imaging techniques. The difference lies in ionization methods, which can be broken down into two categories: ionization either at reduced pressure or ambient pressure. The most common reduced pressure methods for plant samples include matrix assisted laser desorption ionization (MALDI) and secondary ion mass spectrometry (SIMS). While there are several ambient pressure techniques, this chapter will focus specifically on desorption electrospray ionization (DESI) and laser ablation electrospray ionization (LAESI). MALDI, SIMS, DESI, and LAESI are discussed below. Table 1 compares the four techniques.

Reduced Pressure MSI

In vacuum MSI, volatile compounds usually cannot be detected because the compounds are lost when the sample is evacuated. When compared to ambient methods, sample preparation is much more involved since water must be removed from the sample before ionization.[7] However, with good sensitivity and ability to achieve spot sizes down to 20 nm, vacuum MSI is the preferred platform for a variety of samples, including plant materials.

MALDI

Matrix assisted laser desorption ionization (MALDI) is the most common form of MSI and involves co-crystallization of the sample with a matrix. While the exact ionization processes are still debated[19,20] it is believed that ionization involves the matrix absorbing the laser energy causing desorption of both the matrix and sample. Overall, MALDI is a good ionization technique for imaging large molecules with little fragmentation occurring due to the laser energy being absorbed by the matrix,[17] although matrix effects, such as delocalization of analyte ions and un-uniform matrix coating can occur.

SIMS

Secondary ion mass spectrometry (SIMS) uses a high energy ion beam instead of a laser. Ionization occurs when the primary ion beam (usually Ar^+) strikes the sample surface inducing a series of collisions. Secondary ions are released when their kinetic energy is increased above the binding energy of the substrate.[21-23] The main advantage of SIMS MSI is its very high spatial resolution in the nm range.[24] It is often used to image organic and inorganic compounds but only of molecular weights less than ~1000 Da.

Ambient Pressure MSI

To circumvent problems in reduced pressure MSI, including the inability to ionize volatile compounds, ambient MSI techniques can be used. In ambient MSI, there is little to no sample preparation (most techniques do not require a matrix) and since ionization occurs externally to the mass spectrometer, it is amenable to a variety of MS instruments.[25] Imaging of living plants is possible since there is no applied matrix. However, ambient methods have lower sensitivity and larger laser spot sizes compared to reduced pressure.[7] Since spatial dislocation and chemical modifications can arise with reduced pressure matrix applications, ambient pressure ionization can be used as a complement to these reduced pressure methods.[25]

DESI

Desorption electrospray ionization (DESI) is a popular ambient pressure MSI technique where an ESI stream is directed toward the sample surface with the help of a nebulizer gas and a high applied voltage. The sample is then desorbed and ionized. Newly formed ions then enter the mass spectrometer and are detected. Since the electrospray stream cannot be focused as well as a laser, the ionization spot size is typically 200 µm with a spatial resolution of about 100 µm, though 30 µm spot sizes has been reported.[26] Since DESI is similar to regular electrospray, polar compounds are appropriate for this technique.

LAESI

Laser ablation electrospray ionization (LAESI) is another ambient pressure technique and will be discussed in depth throughout this dissertation. Figure 3 shows the ionization schematic. A laser is fired onto a solid sample causing a neutral plume to form. This ablated plume is then ionized by an external electrospray and ions of both the electrospray and sample enter the mass spectrometer. LAESI can be used for a number of analytes with typical laser spot sizes around

200-300 µm.[27] One feature of LAESI is its high depth penetration.[28] This is particularly advantageous for plant samples whose tough outer cuticle can be hard to puncture using other forms of ionization.

Spengler, Muddiman and Shiea have utilized similar ionization techniques including atmospheric pressure infrared laser desorption/ionization, matrix assisted laser desorption electrospray ionization (MALDESI) and electrospray-assisted laser desorption ionization (ELDI).[29-34] Spengler's technique involves an IR Nd:YAG laser at wavelength 2.94 µm and is similar to LAESI as no matrix is used, whereas MALDESI utilizes a matrix such as 2,5-dihydroxybenzoic acid (DHB) or ice.[29,30,33,34]. Spengler has worked on determining phospholipids in biological samples such as mouse brains, while early studies by Muddiman included the use of a N_2 UV laser (wavelength 355 nm) to image peptides and amino acids. Recent work by Muddiman has moved away from UV lasers towards IR (2.94 µm) lasers.[33-37] Shiea's technique, ELDI, the earliest form of this method, has imaged inks, fungus, and human tissues employs a UV laser for ablation.[31,32,38]

The term LAESI was coined in 2007 by Vertes who soon introduced its capabilities with MSI in 2008.[39,40] Early studies involved MSI of variegated *A. squarrosa* leaves, but have since investigated a variety of materials such as rat brains,[41] fish tissues,[42] sage leaves,[43] and *Escherichia coli* colonies.[44] A mid-infrared (2.94 µm) laser was used in all these experiments. Additional LAESI experiments by van Beek include MSI of pesticides in rose leaves, corn kernels, and lemon skins using a mid-IR laser.[45] These experiments demonstrated the many uses of LAESI including depth profiling[43] and imaging the localization of cancers in rat brain tissue and pesticides on rose leaves.[41,45]

Most of these methods use IR lasers, while a few utilize UV lasers. There seems to be several potential advantages to using a UV laser over an IR laser when it comes to MSI. Since a UV laser can be focused to a smaller diffraction limited spot size than an IR laser, spatial resolution is potentially improved, leading to smaller laser spot sizes.[46,47] When using IR lasers, ablation occurs due to heating of the water in the sample which in turn ablates the analyte.[7,17,48,49] If the sample is "dry," a matrix must be used leading to longer sample preparation times and potential matrix effects. A UV laser, however, is amenable to dry samples and thus allows for a wider range of samples to be studied.

With the idea that a UV laser can be used on dry samples and can achieve better spatial resolution than IR, LAESI MSI has been combined with a UV laser in this dissertation. With the smaller spot size, UV-LAESI can spatially resolve plant metabolites. This is particularly advantageous in the field of plant metabolomics where genotyping, comparisons of mutant plants with their wild type, and identifying biomarkers are studied.[50] In this study, a Nd:YAG 355 nm UV laser was coupled to a Waters Synapt G2-S high resolution mass spectrometer (Figure 4). While UV lasers have been used for ambient MSI in the past, most studies were done on animal or human tissues, with the exception of a single study on fungus by Shiea.[33]

Overall, this dissertation shows that UV-LAESI MSI is a novel technique that has the capabilities of studying plant materials, such as coleus and *Arabidopsis thaliana* leaves. Little sample preparation is required and rapid analysis is feasible.

Dissertation Organization

This dissertation is organized into five chapters. The first chapter (above) serves as a background on different laser ablation mass spectrometry imaging techniques, an introduction to

laser ablation electrospray ionization (LAESI) for mass spectrometry imaging, and the use of

LAESI in metabolomics profiling. Chapters 2, 3, and 4 are manuscripts prepared for submission

to a peer reviewed journal. Chapter 2 further describes the LAESI-MSI setup and the validation

of the resultant images by comparing them to results previously published using different

ionization techniques. Chapter 3 demonstrates the use of LAESI by spatially determining

anthocyanins on various species of coleus leaves. LC-MS was also used in conjunction with

LAESI to verify compounds. Chapter 4 further examines the use of this technique by imaging

Arabidopsis thaliana leaves. Both wild type *Arabidopsis thaliana* leaves and *atg5* mutant leaves

were imaged. Chapter 5 summarizes the conclusions from the above studies and presents further

implications of this work.

References

1) Ifa, D.R., Gumaelius, L.M., Eberlin, L.S., Manicke, N.E., Cooks, R.G. Forensic analysis of inks by imaging desorption electrospray ionization (DESI) mass spectrometry. *Analyst*, **2007**, 132**:** 461-467**.**

2) Domon, B., Aebersold, R., Mass Spectrometry and Protein Analysis. *Science*, **2006,** 312: 212-216**.**

3) Stoeckli, M., Chaurand, P., Hallahan, D.E., Caprioli, R.M. Imaging mass spectrometry: A new technology for the analysis of protein expression in mammalian tissues. *Nature Medicine,* 2001, 7: 493 – 496.

4) Bruins, A. et al. Mass spectrometry with ion sources operating at atmospheric pressure. *Mass Spectrometry Reviews*, **1991**, 10: 53-77.

5) Taylor, G. Disintegration of water drops in an electric field. *P. R. Soc. London,* **1964**, 280: 383-397.

6) Peterkop, R. K. Theory of ionization of atoms by electron impact, Translation by Aronson, E.; Hummer, D. G., Ed.; Colorado Associated University Press: Boulder, CO, **1977**.

7) Lee, Y. J., Perdian, D. C., Song, Z., Yeung, E. S., & Nikolau, B. J. Use of mass spectrometry for imaging metabolites in plants. *The Plant Journal*, **2012,** 70(1): 81-95.

8) McEwen,C.N., McKay, R.G., Larsen, B.S. Analysis of Solids, Liquids, and Biological Tissues Using Solids Probe Introduction at Atmospheric Pressure on Commercial LC/MS Instruments. *Anal. Chem*, **2005**, 77:7826-7831.

9) Pacholski, M.L., Winograd N. Imaging with mass spectrometry. *Chem Rev*., **1999**, 99: 2977.

10) McDonnell L.A., Heeren R.M.A., Imaging mass spectrometry. *Mass Spectrom Rev*., **2007**, 26:606–643.

11) Nemes, P., Vertes, A., Laser ablation electrospray ionization for atmospheric pressure, in vivo, and imaging mass spectrometry. *Anal Chem* , **2007**, 79: 8098.

12) Stoeckli, M., Chaurand, P., Hallahan, D.E., Caprioli, R.M. Imaging mass spectrometry: A new technology for the analysis of protein expression in mammalian tissues. *Nature Medicine*, **2001**, 7: 493 – 496.

13) Eberlin, L.S., Dill, A.L., Golby A.J., Ligon, K.L., Wiseman J.M., Cooks, R.G., Agar, N.Y. R. Discrimination of Human Astrocytoma Subtypes by Lipid Analysis Using Desorption Electrospray Ionization Imaging Mass Spectrometry. *Angewandte Chemie,* **2010**, 49(34): 5953-5956.

14) Drexler, D.M., Garrett, T.J., Cantone, J.L., Diters, R.L., Mitroka, J.G., Prieto Conaway, M.C., Adams, Admas, S.P., Yost, R.A., Sanders, M. Utility of imaging mass spectrometry (IMS) by matrix-assisted laser desorption ionization (MALDI) on an ion trap mass spectrometer in the analysis of drugs and metabolites in biological tissues. *Journal of Pharmacological and Toxicological Methods,* **2007**, 55(3): 279-288.

15) Cornett, D.S., Frappier, S.L., Caprioli, R.M., MALDI-FTICR Imaging Mass Spectrometry of Drugs and Metabolites in Tissue. ***Anal. Chem.***, **2008**, *80* (14): 5648–5653.

16) Vismeh, R., Waldon, D.J., Teffera, Y.,Zhao, Z., Localization and Quantification of Drugs in Animal Tissues by Use of Desorption Electrospray Ionization Mass Spectrometry Imaging. *Anal. Chem.*, **2012**, *84* (12): 5439–5445.

17) Bjarnholt, N., Li, B., D'Alvise, J., Janfelt, C. Mass spectrometry imaging of plant metabolites–principles and possibilities. *Nat. Prod. Rep*, **2014**, 31:818-837.

18) Hanhineva, K., Rogachev, I., Kokko, H., Mintz-Oron, S., Venger, I., Kärenlampi, S., Aharoni, A. Non-targeted analysis of spatial metabolite composition in strawberry (Fragaria× ananassa) flowers. *Phytochemistry*, **2008**, 69: 2463.

19) Dreisewerd, K. *Chem. Rev.,* **2003**, 103: 395–426.

20) Karas, M., Gluckmann, M., Schafer, J. *J. Mass Spectrom.*, **2000**, 35: 1–12.

21) Adriaens, A., van Ham, R., van Vaeck, L. in: J.C. Vickerman, D. Briggs (Eds.), ToFSIMS: Surface Analysis by Mass Spectrometry, *IM Publications and Surface Spectra Limited, Chichester, Manchester*, **2001**, 195.

22) Delcorte, A. in: J.C. Vickerman, D. Briggs (Eds.), ToF-SIMS: Surface Analysis by Mass Spectrometry, *IM Publications and Surface Spectra Limited*, Chichester, Manchester, **2001**, 161.

23) Urbassek, H.M. in: J.C. Vickerman, D. Briggs (Eds.), ToF-SIMS: Surface Analysis by Mass Spectrometry, *IM Publications and Surface Spectra Limited*, Chichester, **2001**, 139.

24) Carado, A, Passarelli, M.K., Kozole, J., Wingate, J.E., Winograd, N., Loboda, A.V. C-60 secondary ion mass spectrometry with a hybrid quadrupole orthogonal time-of-flight mass spectrometer. *Anal Chem,* **2008,** 80: 7921–7929.

25) Wu. C., Dill, A., Eberlin, L., Cooks, R.G., Ifa, D., Mass spectrometry imaging under ambient conditions. *Mass Spectrometry Reviews,* **2013**, 32: 218–243.

26) Campbell, D., Ferreira, C., Eberlin, L., Cooks, R.G. *Anal. Bioanal. Chem.*, **2012**, 404: 389–398.

27) Shrestha, B. Patt, J.M., Vertes, A. *Anal. Chem*., **2011**, 83: 2947–2955.

28) Nemes, P., Barton, A.A., Vertes, A. *Anal. Chem.*, **2009**, 81: 6668–6675.

29) Roempp, A., Schaefer, K. C., Guenther, S., Wang, Z., Köstler, M., Leisner, A., Paschke, C., Schramm, T., Spengler, B. High-resolution atmospheric pressure infrared laser desorption/ionization mass spectrometry imaging of biological tissue. *Anal and Bioanal Chem.,* **2013,** 405(22): 6959-6968.

30) Berisha, A., Dold, S., Guenther, S., Desbenoit, N., Takats, Z., Spengler, B., Roempp, **A.** A comprehensive high-resolution mass spectrometry approach for characterization of metabolites by combination of ambient ionization, chromatography and imaging methods. *Rapid Comm in Mass Spec.,* **2014,** 28(16): 1779-1791.

31) Shiea, J., Huang, M.Z., Su, H.J.H, Lee, C.Y., Yuan, C.H., Beech, I., Sunner, J. Electrospray-assisted laser desorption ionization mass spectrometry for direct ambient analysis of solids, *Rapid Commun. Mass Spectrom*. **2005**, 19: 3701.

32) Kao, Y.Y., Cheng, S.C., Cheng, C.N., Shiea, J., Ho, H.O. Detection of trace ink compounds in erased handwritings using electrospray assisted laser desorption ionization mass spectrometry, *J. Mass Spectrom*., **2014**, 49: 445.

33) Sampson, J.S., Hawkridge, A.M., Muddiman, D.C. Generation and detection of multiply-charged peptides and proteins by matrix-assisted laser desorption electrospray ionization (MALDESI) Fourier transform ion cyclotron mass spectrometry, *J. Amer. Soc. Mass Spectrom*. **2006**, 17: 1712.

34) Robichaud, C., Barry, J.A., Muddiman, D.C. IR-MALDESI mass spectrometry imaging of biological tissue sections using ice as a matrix, *J. Amer. Soc. Mass Spectrom.*, **2014**, 25: 319.

35) Bokhart, M.T., Rosen, E., Thompson, C., Syles, C., Kashuba, A.D., Muddiman, D.C. Quantitative Mass Spectrometry Imaging of Emtricitabine in Cervical Tissue Model using Matrix-Assisted Laser Desorption Electrospray Ionization. *Analytical and Bioanalytical Chemistry*, **2015**, 407(8): 2073-84.

36) Cochran, K., Barry, J.A., Robichaud, G., Muddiman, D.C. Analysis of trace fibers by IR-MALDESI imaging coupled with high resolving power. *Analytical and Bioanalytical Chemistry*, **2015**, 407(3): 813-820.

37) Sampson, J.S., Hawkridge, A.M., Muddiman, D.C. Direct Characterization of Intact Polypeptides by Matrix-Assisted Laser Desorption Electrospray Ionization (MALDESI) Quadrupole Fourier Transform Ion Cyclotron Resonance Mass Spectrometry. *Rapid Communications in Mass Spectrometry*, **2007**, 21 (7): 1150-1154.

38) Huang, M.Z., Cheng, S.C., Jiang, S.S., Chou, C.C., Cheng, C.N., Shiea, J., Popov, I.A., Nikolaev, E.N. Ambient molecular imaging of dry fungus surface by electrospray laser desorption ionization mass spectrometry. *Int. J. Mass Spectrom*. **2012**, 172: 325-327.

39) Nemes, P., Vertes, A. Laser ablation electrospray ionization for atmospheric pressure, in vivo, and imaging mass spectrometry. *Anal Chem,* **2007**, 79: 8098–8106.

40) Nemes, P., Barton, A.A., Li, Y., Vertes, A. Ambient molecular imaging and depth profiling of live tissue by infrared laser ablation electrospray ionization mass spectrometry. *Anal Chem,* **2008**, 80:4575–4582.

41) Nemes, P., Woods A.S., Vertes, A.Simultaneous Imaging of Small Metabolites and Lipids in Rat Brain Tissues at Atmospheric Pressure by Laser Ablation Electrospray Ionization Mass Spectrometry. *Anal. Chem*., **2010**, 82: 982-988.

42) Shrestha, B., Javonillo, R., Burns, J.R., Pirger, Z., Vertes, A. Comparative local analysis of metabolites, lipids and proteins in intact fish tissues by LAESI mass spectrometry. *Analyst*, **2013**, 138: 3444-3449.

43) Vaikkinen, A., Shrestha, B., Koivisto, J., Kostiainen, R., Vertes, A., Kauppila, T.J. Laser Ablation Atmospheric Pressure Photoionization Mass Spectrometry Imaging of Phytochemicals from Sage Leaves. *Rapid Commun. Mass Spectrom*., **2014**, 28: 2490-2496.

44) Li, H., Balan, P., Vertes, A. Molecular Imaging of Growth, Metabolism, and Antibiotic Inhibition in Bacterial Colonies by Laser Ablation Electrospray Ionization Mass Spectrometry. *Angew. Chem. Int. Ed.*, **2016**, 55: 15035 -15039.

45) Nielen M.W.F. Macroscopic and microscopic spatially-resolved analysis of food contaminants and constituents using laser-ablation electrospray ionization mass spectrometry imaging. *Analytical and Bioanalytical Chemistry,* **2014**, 406(27): 6805–6815.

46) Rompp, A., Spengler, B. Mass spectrometry imaging with high resolution in mass and space. *Histochem. Cell Biol*. **2013**, *139(6)*: 759.

47) Silfvast, W.T. Laser Fundamentals, 2ⁿᵈ ed., *Cambridge, University Press*, **2004**, 419.

48) Rezenom, Y.H., Dong, J., Murray, K.K. Infrared laser-assisted desorption electrospray ionization mass spectrometry. *Analys,t* **2008**, 133: 226.

49) Sampson, J.S., Murray, K.K., Muddiman, D.C. Intact and top-down characterization of biomolecules and direct analysis using infrared matrix-assisted laser desorption electrospray ionization coupled to FT-ICR mass spectrometry. *J. Amer. Soc. Mass Spectrom*. **2009**, 20: 667.

50) Hall, R.D. Plant metabolomics: from holistic hope, to hype, to hot topic. *NewPhytologist,* **2006** 169: 453.

Table

Table 1. Comparison of MALDI, SIMS, DESI, LAESI. These are typical values and may not reflect current and on-going research.

MSI Application	Ionization Source	Pressure	Spatial Resolution (μm)	m/z Range (Da)	Compounds
MALDI	UV or IR Laser Beam	Vacuum	10-100	<500,000	Large molecules (proteins)
SIMS	Ion Beam	Vacuum	0.2-3	< ~1,000	Small organic and inorganic compounds
DESI	Solvent Stream	Atmosphere	30-100	<66,000	Polar compounds/Volatile
LAESI	UV or IR Laser Beam	Atmosphere	200-300	<66,000	Polar compounds/Volatile

Figures
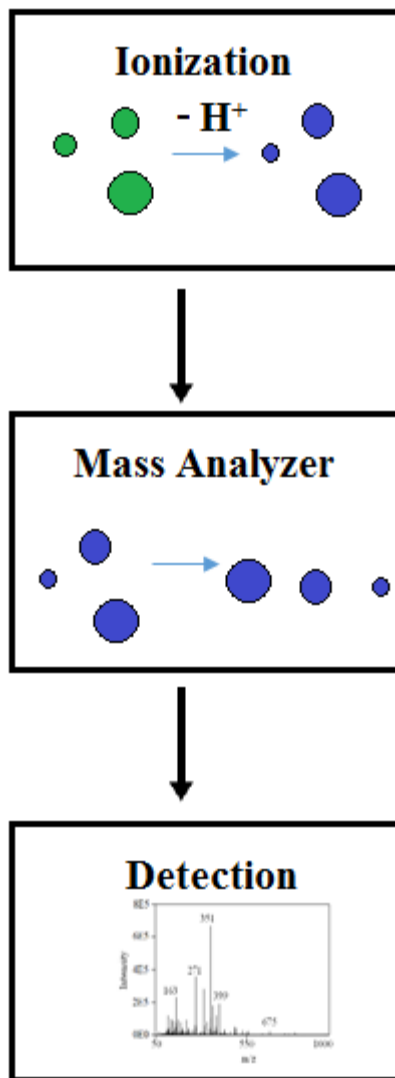
Figure 1. Typical MS run. The first step in any MS process is ionization of a sample. The newly formed ions continue further in the spectrometer to be mass analyzed and then detected, resulting in a mass spectrum.
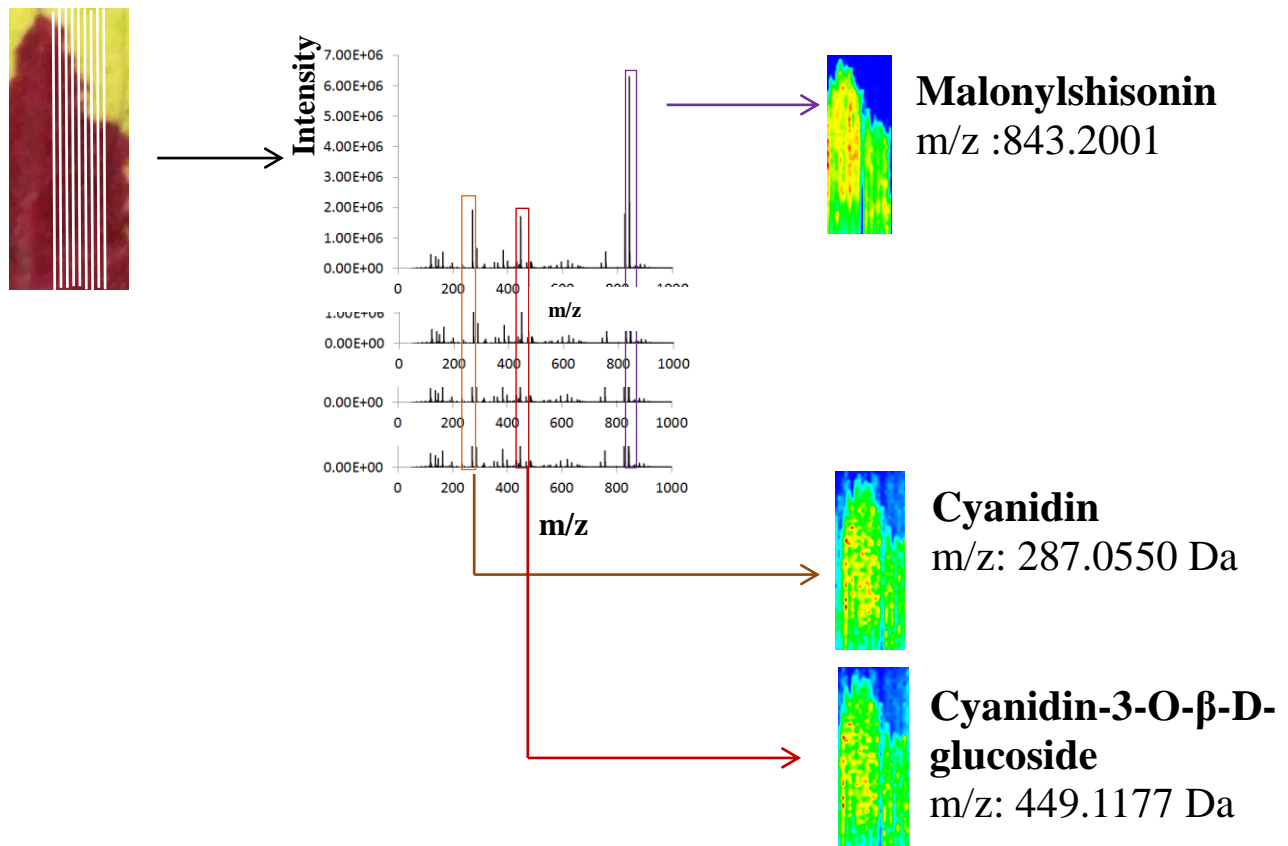
Figure 2. Basic principle of MSI. After a solid sample is ablated (upper left), a mass spectrum is produced for each individual ablation spot. This process is continued until an area is fully ablated, as shown by the white lines on the sample leaf. All the individual spectra are combined and images of certain ions can be made. The resultant images are unique to each individual ablation spot. For example, in the image for cyanidin (above, center), the ion is abundant (green/yellow) in the red portion of the leaf, but absent (as shown by the blue) in the green.
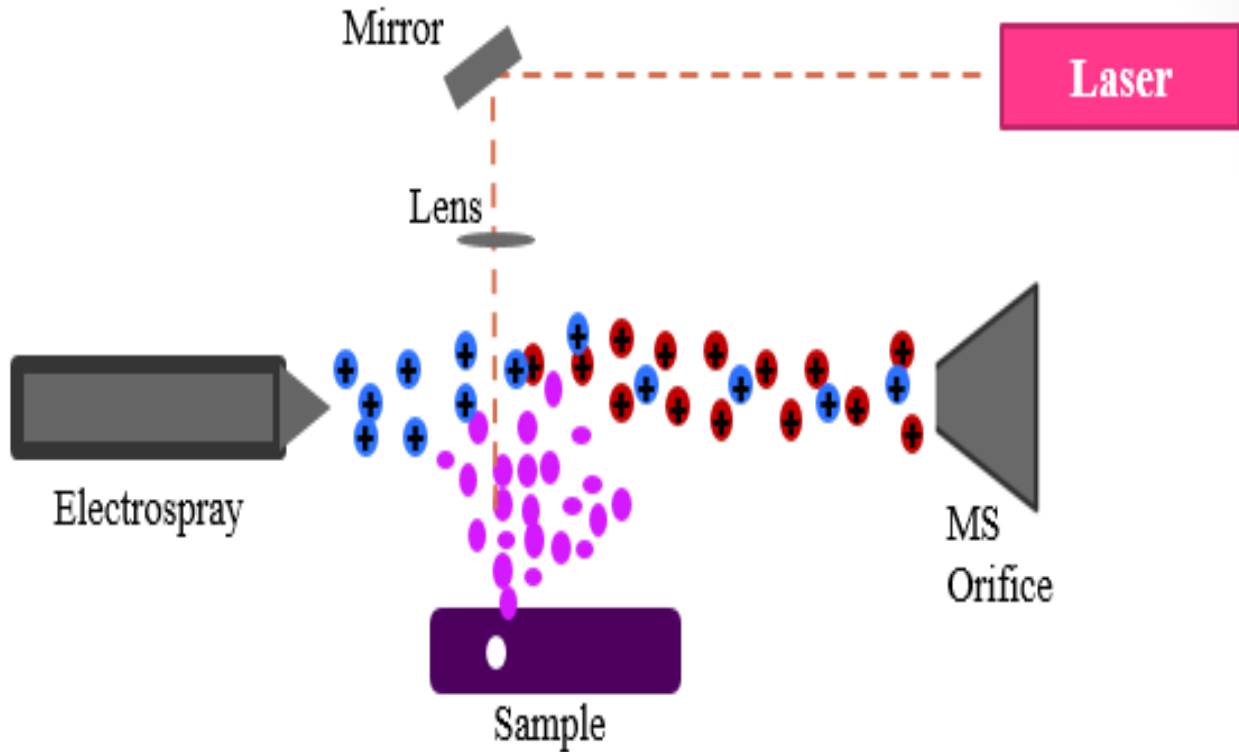
Figure 3. Typical LAESI set up. When a laser is fired, it focused onto a solid sample through a series of mirrors and lenses. When the laser hits the sample, a neutral plume is produced. In order to ionize this neutral plume, an external electrospray source is sprayed in the direction of the MS orifice. Once ionization occurs, ions of the sample and electrospray enters the mass spectrometer to be detected.
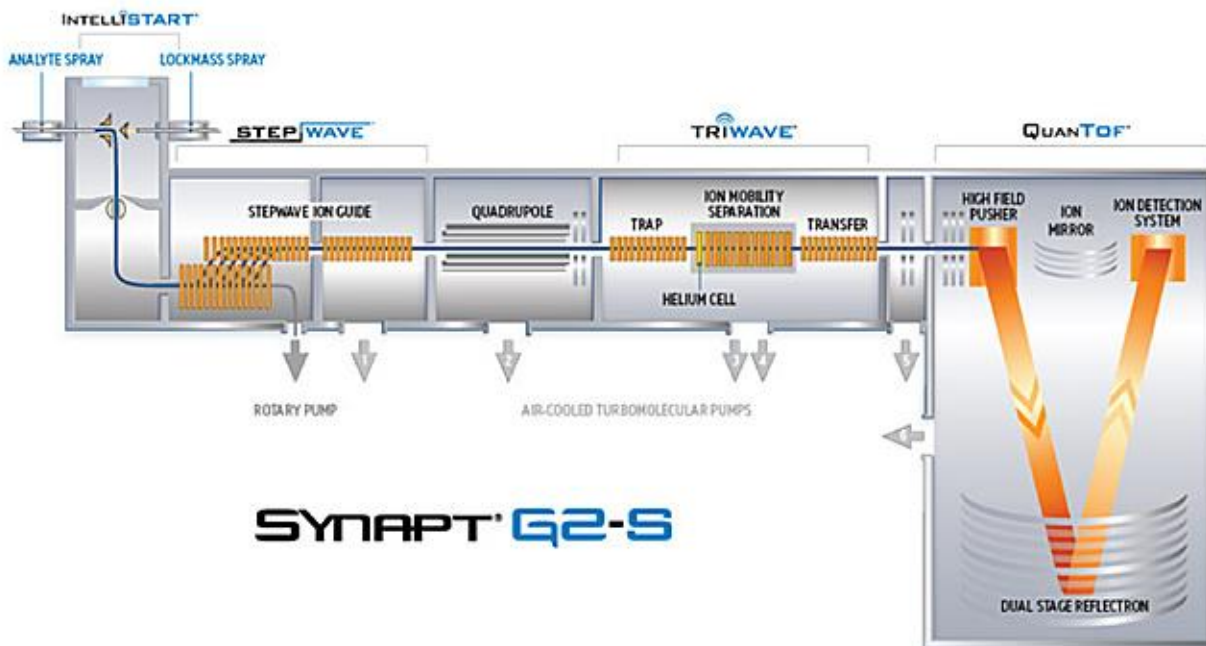
Figure 4. Water Synapt G2-S high resolution mass spectrometer. This instrument has tandem MS and ion mobility capabilities. The time of flight is operated in sensitivity (v-mode) for these experiments.

CHAPTER 2. MATRIX-FREE ATMOSPHERIC PRESSURE LASER ABLATION ELECTROSPRAY IONIZATION MASS SPECTROMETRY OF PLANT MATERIAL USING AN UNLTRAVIOLET LASER

Katherine-Jo Galayda[1,2,3], Patrick A. McVey[1,2,3], Timothy J. Anderson,[4] David P. Baldwin[5], Stanley J. Bajic[1] and R. S. Houk[1,2]

[1]*The Ames Laboratory, Iowa State University, Ames, Iowa, USA*

[2]*Department of Chemistry, Iowa State University, Ames, Iowa, USA*

[3]*These authors contributed equally to this work*

[4]*Exxon Mobil, Houston TX 77520 USA*

[5]*Special Technologies Laboratory, Santa Barbara, California, USA*

Abstract

Laser ablation electrospray ionization (LAESI) is a way to analyze materials without an added matrix coating. Most previous work on LAESI has been done with infrared lasers that are absorbed by the ambient water in the solid sample. In this work, an ultraviolet laser was tested to see if it could achieve better spatial resolution. The diffraction-limited spot size is smaller for a shorter wavelength laser, so UV laser could potentially yield better spatial resolution. A frequency tripled Nd:YAG laser at 355 nm which was focused to a 125 μm spot size and used to ablate material directly from leaves. Positive or negative ions were generated from the ablated material by ESI and measured with an ion mobility time-of-flight mass spectrometer (TOF-MS). No matrix coating was used. Plant leaves readily absorbed the ablation laser at 355 nm.

Common metabolites were identified from peony, French marigold, geranium and hosta leaves by accurate mass and tandem MS measurements. Ion maps show spatial variations of several metabolites in different areas of the leaves, especially for variegated plants like hosta. Thus, it can be concluded that plant materials are amenable to UV-LAESI for metabolite identification and spatial profiling.

Introduction

Plant metabolomics is important for many studies, such as a) genotyping and phenotyping, b) comparing transgenic plants with their wild types, c) identifying biomarkers, and d) elucidating bioactive compounds with possible human medicinal uses. Metabolomics is also important in the production of renewable energy sources and breeding of improved food products.[1] Many different analytical methods are used to investigate metabolite composition from a variety of different plant species. These methods commonly include extraction, pre-concentration, and separation steps prior to analysis by mass spectrometry (MS), thus providing detailed and accurate compound identification. However, such pretreatment steps do not provide spatially-resolved information within the plant.

To this end, many recent plant metabolomics analytical developments have focused on techniques that provide fast and sensitive in-situ analysis to generate MS images of plant materials and structures. Most of these imaging experiments are done at reduced pressure and use an additive or matrix coated onto the plant surface prior to analysis, i.e., matrix-assisted laser desorption ionization (MALDI).[2] An important exception is described by Scatos' group[3] who achieve 10 μm spatial resolution for plants by reduced pressure LDI ablating at 337 nm without an added matrix.

As with most techniques, conventional reduced pressure MS imaging methods that use an applied matrix have both advantages and disadvantages. In general, sensitivity is better when the sample is ionized at reduced pressure, so small laser spots can be used for good spatial resolution. On the opposite side, analytes can become delocalized on the sample surface when the matrix is applied. Furthermore, as the matrix solvent dries, different size matrix crystals may form, affecting the area and amount of sample interrogated by the laser. The need to evacuate the sample also limits the ability to see volatile analytes and complicates time-resolved experiments or measurements on living plants.

In order to circumvent these issues, a number of workers have investigated schemes for laser desorption at atmospheric pressure. Enhancing sensitivity and managing the usual trade-off between sensitivity and spatial resolution are key points for instrumentation or application studies using atmospheric pressure ablation. Many such experiments still use an added matrix coating.[2,4,5] For example, Spengler's group[6] recently reported atmospheric pressure MALDI measurements of many analytes in licorice rhizome using a 337 nm laser and samples coated with 2,5-dihydroxybenzoic acid (DHB). In their instrumentation, the laser is focused coaxially with the ion extraction capillary, which provides excellent sensitivity and spatial resolution (as good as ~ 5 µm).[7]

An alternative approach is to couple a supplemental ionization source (usually electrospray ionization, ESI) with atmospheric pressure laser desorption or ablation to improve sensitivity. Shiea, Sunner and co-workers initially described electrospray laser desorption ionization (ELDI) experiments that employed a UV laser (337 nm).[8] Shiea's group has continued this work with an ultraviolet (UV) laser for a variety of sample types and potential applications.[9] Muddiman's group started with an added matrix and a UV laser[10] and has progressed to an

infrared (IR) laser with ice matrix.[11] The water in most biological samples serves as a convenient absorbing "matrix" when IR lasers are used, as also shown by Murray.[12,13] Vertes group[14,15] has reported extensive studies on a matrix-free method called laser ablation electrospray ionization mass spectrometry (LAESI-MS). An IR laser at 2.94 µm is used that is readily absorbed by the ambient water in the sample, so no matrix coating is necessary. The laser desorbs analytes which are then ionized by interaction with an ESI plume. A number of analytical development and application studies of LAESI have been reported, including ion mobility,[16,17] measurement of contaminants in food products,[18,19] identification of explosives,[20] and forensic drug analysis.[21] Halls group[22] also employs a 2.94 µm laser and has imaged *Phalaenopsis* leaves and determined major flavonoids, including anthocyanins. Atmospheric pressure photoionization (APPI) can be substituted for ESI for compounds not readily ionized by the latter technique.[23]

The bulk of the previous LAESI or LAAPPI work uses an IR ablation laser, often at wavelength 2.94 µm. Most of these experiments are done with very large spot sizes, e.g., 200 µm.[24] In the present work we show that an ultraviolet (UV) laser (355 nm) also works for LAESI, at least for plant samples. A UV laser can be focused to a smaller diffraction limited spot size than an IR laser.[25,26] Thus, the spatial resolution is potentially better with a UV laser. Of course utilization of smaller laser spots generally means less analyte is desorbed, so the instrument sensitivity and background also affect the achievable spatial resolution.

Of the other groups that have investigated ELDI or LAESI with a UV laser at atmospheric pressure,[8,27] there are no reports of imaging of metabolites in plants, the closest materials being fungus slices ablated at 337 nm.[28] In related papers specifically involving laser ablation of plants, Levis' group uses LAESI with an IR (800 nm wavelength) fs laser,[29,30] and

Harada et al. report analysis of ginger rhizome at 355 nm, but without supplementary ESI.[31] Sunner's group recently reports laser ablation and solvent capture by aspiration (LASCA) for plants with ablation at 2.94 μm.[32]

Thus, it appears that the combination of UV lasers with additional ESI and no added matrix has not been extensively investigated specifically for MS analysis and mass spectrometry imaging (MSI) of plants. No such papers are listed in the recent reviews by Bjarnholt et al.,[4] Spengler[33] and Muddiman's group.[34] For that matter, MSI by any means has been used much less extensively for plants than for animal or human medical applications, although interest in MS imaging of plants is growing rapidly.[33] In the present work, instrumentation and initial results, including images, are described for atmospheric pressure UV-LAESI on peony, French marigold, geranium and hosta leaves.

Experimental

Mass spectrometer

A Waters Synapt G2-S quadrupole time-of-flight mass spectrometer was used in these experiments. Ions were collected with the standard ESI source enclosure removed. The Synapt fluidic systems and high voltage connections were bypassed, utilizing a specialized adapter supplied by Waters. No other modifications were made to the mass spectrometer. Mass spectra were recorded from either m/z 100 to 1200 or m/z 100 to 2000. The TOF mass analyzer was operated in "sensitivity" mode, i.e., the ions made one pass through only the main reflectron. The mass resolution was m/Δm 10,000 (FWHM). In tandem MS experiments the quadrupole resolution was Δm/z ~ 3 Da, and the collision energy was nominally 10 eV. Data were acquired and analyzed using Waters MassLynx V4.1 (SCN851) software.

Laser and ion source

Samples were mounted on glass microscope slides with double-stick tape and trimmed to the shape of the slide, if necessary. No matrix or additional treatment was applied. The samples were placed 8 mm below the ESI axis (Fig.1) and attached to a computer controlled xyz-translation stage (Z825B, Thorlabs, Inc. Newton, NJ).   The sample slide was translated at a rate of 0.4 mm/s during ablation to provide spatial resolution and to ensure that a fresh sample area was interrogated during the experiment

The leaves were irradiated normal to the sample surface with the laser beam axis approximately 2 mm downstream from the ESI capillary tip (Fig. 1). The third harmonic (355 nm) output from a Nd:YAG laser (ULTRA, Big Sky Laser Tech, Inc., Bozeman, MT) was focused onto the sample by a single fused-silica plano-convex focusing lens (focal length 75 mm). The nominal spot size was ~125 µm at the sample. The laser was operated at 10 Hz, 5 ns pulse width, with a nominal energy of 250 µJ/pulse measured before the focusing lens.

The tip of the ESI capillary was positioned on the ion extraction axis approximately 10 mm from the sample cone inlet of the mass spectrometer (Fig. 1).   A mixture of methanol and water (1:1 v/v) was pumped through a 53 µm i.d. polyimide-coated capillary at 0.4 µl/min by a syringe pump (Model 22, Harvard Apparatus, South Natick, MA). In positive ion mode, a 0.1% solution of formic acid (purity $\geq$ 99.5%, Fischer Scientific) was sprayed by the ESI source. In negative ion mode, 0.1% ammonium hydroxide (purity $\geq$ 99.99%, Sigma-Aldrich) was sprayed. Additionally, leucine-enkephalin (0.1 ppm, Waters) was added to the electrospray solutions and used as the lockspray mass calibrant. The ESI voltage was + 2.3 kV for positive ions or -2.3 kV for negative ions. The inlet sample cone completed the electrospray circuit and was kept at 100 ^{0}C with a nitrogen curtain gas (~ 1 l/hr, Waters default value).

Data Handling

　　Mass spectra and ion maps were generated from total ion chromatograms (TICs) provided by Waters MassLynx software. For images the *.raw data files were first converted into mzML files using the Proteowizard Mass ConverterTool .[35] The mzML files were then converted into imzML files using imzMLConverter.[36] The imzML files were viewed in DatacubeExplorer.[37] The black and white images from DatacubeExplorer were interpolated with cubic-spline smoothing and converted to false-color images using GIMP 2.8.

Safety Considerations

Laser safety goggles specifically for UV beams were used whenever the beam was exposed. Care was taken to avoid contact with the ESI spray tip.

Results and Discussion

　　The set-up for the experiments discussed here is shown in Figure 1. The distances depicted in the figure represent the optimized positions for maximum signal when analyzing plant material. With the ESI voltage off, the mass spectrometer observed few or no ions from laser ablation or desorption alone, as seen previously by Shiea et al.[8] With the ESI voltage on and the laser beam blocked, only background ions from the spray solution were observed, as shown by the left section of the total ion chromatogram in Fig 2a. These ions include the lockspray-mass calibrant at m/z 556.27, protonated leucine-enkephalin $[M+H]^+$. This observation indicates that no desorption ESI (DESI) effect[38,39] is produced from the original plant surface with the ions used in our usual setup. With the electrospray and laser both active the total ion signal is much higher than with ESI alone (Fig. 2a right), and many peaks are seen from the plant sample (Fig. 2b).

Varying the distance from the sample surface to the sample-cone axis between 6 to 10 mm, while also refocusing the laser, did not have a large effect on the ion signal intensity. Thus, the sample itself does not have to be perfectly flat. At closer distances (~ 4 to 6 mm) the ESI signal decreased, likely due to the distortion of the electric field because of the presence of the nonconductive microscope slide and holder. When the sample was closer than 4 mm from the ESI - sample cone axis, a DESI effect was observed, i.e., ions were seen from the sample without the laser.

A typical freshly ablated trench is presented in Figure 3. The sides of the trench are clean with little or no sample damage outside the 125 μm laser spot size. In the images in a subsequent figure, photos of the ablated sample appear to show more damage and wider trenches, but these latter photos were taken several hours after the actual experiment, and the sample leaf dried and cracked along the ablated trenches in the interim. Figure 3 also shows that, with the sample moving at 0.4 mm/s, the trench does not penetrate the leaf completely. Thus, the adhesive used to mount the sample is not desorbed and ionized.

Peony

Figure 2 illustrates a typical acquisition for a peony leaf in positive-ion mode. Similar results were obtained for other plants and in negative ion mode. Changes in the TIC are shown as a function of time. The length of time for a single acquisition was two minutes. A single acquisition here corresponds to a single ablated line across the surface of the sample, resulting in a trench like that shown in Fig. 3 approximately 24 mm long.

In the TIC shown in Figure 2, when the laser starts ablating material from the sample at 1 min; the TIC greatly increases. Each point in the TIC in the 2nd minute corresponds to a

complete, spatially-resolved mass spectrum from a particular location on the leaf generated by UV-LAESI.

A representative positive-ion mass spectrum (integrated from one laser ablation trench, 50 points) from the peony leaf is shown in Fig. 2b (for a single point mass spectrum, refer to supplementary materials). The most abundant ion signals are observed at m/z 287.0535 and 449.1084. These peaks correspond to the singly-charged flavonoids kaempferol and kaempferol-3-glucoside, respectively (for structures of these metabolites, refer to S1).[40] Ion signals were measured up to approximately m/z 950 for the peony in positive ion mode. The identities of these higher mass ions are not clear; they may originate from the peony cuticle, which is harder and thicker than those of the other plants investigated in this study. Low abundance doubly-charged ions were observed at m/z 244.0344, 460.0985, and 692.1361 from this sample. No other multiply charged ions were detected.

Some of the more abundant peaks observed from the peony and their suggested assignments are listed in Table 1. Peak assignments for the other plant samples are also given there.[41,42] Tandem MS measurements in both positive and negative ion mode were used to help identify many analyte compounds.

French Marigold

In order to assess the effectiveness of studying metabolic processes in plant materials by UV- LAESI, the technique was applied to several common plants that have been studied previously by IR - LAESI. A positive-ion mass spectrum from a French marigold leaf is shown in Figure 4. Several high abundance metabolites are observed. These include peaks at m/z 287.0609, 303.0548, 433.1310, 633.1613, and 649.1422. These ion signals mainly correspond to the singly-charged flavonoid and flavonoid glucoside species of kaempferol and quercetin.

Positive and negative ion MS and tandem MS spectra were collected from the marigold leaves. Below m/z 600, all but one compound from our French marigold leaves were reported in a previous analysis performed by IR-LAESI.[14] In the present work, we observed more peaks above m/z 600, for several possible reasons. These are not the same marigold samples. They were not grown in the same location, for example. The diversity of metabolites in a particular plant genus depends on a number of factors (e.g., species, environment, and harvest time),[41,42] which also may account for some of the differences in the observed metabolites.

Some of the more abundant peaks and their suggested assignments are listed in Table 1. Since the main goal of this work is to assess this UV ablation technique for studying plant metabolites, comprehensive assignments of all peaks was not undertaken. The assignments listed in Table 1 are based on a combination of exact mass measurements, database search results, tandem MS spectral information, and comparison with previous results from the literature.

Geranium

To assess the capability for imaging metabolites by atmospheric pressure UV- LAESI, several variegated plants were investigated. Figure 5 shows the integrated mass spectrum acquired from the leaf of a geranium plant. This leaf had both green and purple regions. The mass spectrum in Fig. 5 is an average of mass spectra collected from one track across the entire length of the leaf encompassing all the hues found. The three most abundant ion signals are at m/z 153.0410, 287.0535, and 303.0532. The suggested assignments for these mass peaks are cysteine + Na^+, kaempferol + H^+, and quercetin + H^+, respectively. Some of the more intense peaks from both positive and negative ion acquisitions from the geranium and their suggested assignments are listed in Table 1.

The inset in Figure 5 shows two groups of cluster species. The first group of clusters from m/z ~ 900 through 1000, are separated by Δm/z 16 u and are likely from lipid-type moieties and similar isomers. The second group of clusters from m/z ~ 1400 through 1750 is 76 u apart, and has been identified in previous work[14] as predominantly doubly-charged clusters of geranial oil, which is commonly found in geraniums. These clusters are believed to be in the plant and not artifacts of the ionization process. Other low abundance doubly-charged ions are also observed at m/z 461, 477, 484, and 492.

Tandem and Ion Mobility MS

Typical tandem MS spectra are given in Fig. 6a and 6b for two abundant positive ions from geranium: glucose + Na^+ (m/z 203) and kaempferol + H^+ (m/z 287). An IMS plot of drift time vs. m/z is shown for geranium positive ions in Fig 6c. Doubly charged (2+) ions are readily distinguished from 1+ ions, as seen using LAESI ionization by Vertes' group,[17] and the expected broad stripes of different slopes corresponding to different compound classes are observed.[43] A number of isobars or near-isobars in have resolvable drift times.[17]

Hosta

Spatial images were generated for the various plant samples discussed above. An example of these MSI results is described below for a hosta leaf sample, which has variegated leaves with separate dark green and yellow sections. Figure 7 shows an integrated mass spectrum for one ablation track in the hosta leaf. Some of the more abundant peaks and their suggested assignments are listed in Table 1.

A post-ablation photograph and false-color ion maps for a selected portion of hosta leaf are shown in Figure 8. The broad, fuzzy horizontal lines observed in the photo (Fig. 8a) are the tracks left behind after the ablated leaf has been allowed to dry ~ 8 hours. During an actual

experiment the tracks are much sharper, like the one shown in Fig. 3. For the image shown in Figure 8 there are 11 ablation tracks 125 μm wide x 300 μm apart.

The ion-map for m/z 561.171 (Fig. 8b) shows that this unknown compound is concentrated in the veins and in the dark green portion of the hosta leaf. Conversely, the map for m/z 663.126 (kaempferol 5-methyl ether 3-galactoside-4'-glucoside + K^+) (Fig. 8c) shows that the concentrations of this metabolite are low in the vein areas of this leaf. The ion map for m/z 175.117 (arginine + H^+) (Fig. 8d) shows that this metabolite is mainly in the yellow portion of the leaf. While m/z 381.078 (sucrose + K^+) (Fig. 8e) is found throughout the leaf, it is much more abundant in the greener portions.

Conclusions

This work demonstrates the potential value of atmospheric-pressure UV-LAESI for the analysis of metabolites in plants. For the analysis of lower abundance compounds further developments are desired to improve sensitivity of the method. By increasing the sensitivity, the laser spot size can be decreased for improved spatial resolution, allowing for analysis of compounds at various growth or uptake stages in specific parts of the plant. Recent work with this device has generated reasonable spectra with spot sizes of 50 μm (data not shown).

This technique requires very little sample preparation and does not need an applied matrix to analyze plant materials. The UV laser penetrates a few micrometers into the sample, enough to desorb a variety of analytes. The experiment is not restricted to green plants; woods, nuts and corn kernels ablate readily and produce good spectra using this laser. Since the plant sample is kept at atmospheric pressure, time-resolved measurements on living plants are possible. These and other studies are underway in our laboratory.

Acknowledgments

References

1) R. D. Hall. Plant metabolomics: from holistic hope, to hype, to hot topic. *New Phytologist.* **2006***, 169*, 453.

2) J. Grassl, N. L. Taylor, A. H. Millar. Matrix-assisted laser desorption/ionization mass spectrometry imaging and its development for plant protein imaging. *Plant Methods* **2011**, *7*, 21 (online content).

3) D. Holscher, R. Shroff, K. Knop, M. Gottschaldt, A. Grecelius, B. Schneider, D. G. Heckel, U. S. Schubery, A. Scatos, Matrix-free UV-laser desorption/ionization (LDI) mass spectrometric imaging at the single cell level: distribution of secondary metabolites of *Arabidopsis thaliana* and *Hypericum* species. *Plant. J.* **2009**, *60*, 907.

4) N. Bjarnholt, B. Li, J. D'Alviseb, C. Janfelt. Mass spectrometry imaging of plant metabolites – principles and possibilities. *Nat. Prod. Rep*., **2014**, *31*, 818.

5) D. C. Perdian, G. M. Schieffer, R. S. Houk, Atmospheric pressure laser desorption ionization of plant metabolites and plant tissues using colloidal graphite, *Rapid Commun. Mass Spectrom*. **2010**, *24*, 397.

6) B. Li, D. R. Bhandari, C. Janfelt, A, Roempp, B. Spengler, Natural products in Glycyrrhiza glabra (licorice) rhizome imaged at the celleular level by atmospheric pressure matrix assisted laser desorption/ionization tandem mass spectrometry imaging, *Plant. J*. **2014**, *80*, 161.

7) M. Koestler, D. Kirsch, A. Hester, S. Guenther, B. Spengler, A high-resolution scanning microprobe matrix-assisted laser desorption/ionization mass spectrometer for imaging analysis on an ion trap/Fourier transform ion cyclotron resonance mass spectrometer, Rapid Commun. Mass Spectrom. 2008, 22, 3275.

8) J. Shiea, M. Z. Huang, H. J. H. Su, C. Y. Lee, C. H. Yuan, I. Beech, J. Sunner, Electrospray-assisted laser desorption ionization mass spectrometry for direct ambient analysis of solids, *Rapid Commun. Mass Spectrom*. **2005**, *19*, 3701.

9) Y.-Y. Kao, S.-C. Cheng, C.-N. Cheng, J. Shiea, H.-O Ho, Detection of trace ink compounds in erased handwritings using electrospray assisted laser desorption ionization mass spectrometry, *J. Mass Spectrom*. **2014**, *49*, 445.

10) J. S. Sampson, A. M. Hawkridge, D. C. Muddiman, Generation and detection of multiply-charged peptides and proteins by matrix-assisted laser desorption electrospray ionization (MALDESI) Fourier transform ion cyclotron mass spectrometry, *J. Amer. Soc. Mass Spectrom*. **2006**, *17*, 1712.

11) C. Robichaud, J. A. Barry, D. C. Muddiman, IR-MALDESI mass spectrometry imaging of biological tissue sections using ice as a matrix, J. Amer. Soc. Mass Spectrom. 2014, 25, 319.

12) Y. H. Rezenom, J. Dong, K. K. Murray, Infrared laser-assisted desorption electrospray ionization mass spectrometry, *Analyst* **2008**, *133*, 226.

13) J. S. Sampson, K. K. Murray, D. C. Muddiman, Intact and top-down characterization of biomolecules and direct analysis using infrared matrix-assisted laser desorption electrospray ionization coupled to FT-ICR mass spectrometry, *J. Amer. Soc. Mass Spectrom*. **2009**, *20*, 667.

14) P. Nemes, A. Vertes. Laser ablation electrospray ionization for atmospheric pressure, in vivo, and imaging mass spectrometry. *Anal. Chem*. **2007**, *79*, 8098.

15) A. Vertes, P. Nemes, B. Shrestha, A. A. Barton, Z. Chen, Y. Li. Molecular imaging by mid-IR laser ablation mass spectrometry. *Appl. Phys. A* **2008**, *93*, 885.

16) B. Shrestha, A. Vertes. High-throughput cell and tissue analysis and enhanced molecular coverage by laser ablation electrospray ionization mass spectrometry using ion mobility separation. *Anal. Chem*. **2014**, *86*, 4308.

17) H. Li, B. K. Smith, L. Mark, P. Nemes, J. Nazarian, A. Vertes, Ambient molecular imaging by laser ablation electrospray ionization mass spectrometry with ion mobility separation, *Int. J. Mass Spectrom*. **2015**, *375*, 681.

18) J. Liu, B. Qui, H. Luo. Fingerprinting of yogurt products by laser desorption spray post-ionization mass spectrometry. *Rapid Commun. Mass Spectrom.* **2010**, *24*, 1365.

19) M. W. F. Nielen, T. A. van Beek. Macroscopic and microscopic spatially-resolved analysis of food contaminants and constituents using laser-ablation electrospray ionization mass spectrometry imaging. *Anal. Bioanal. Chem*. **2014**, *406*, 6805.

20) J. J. Brady, E. J. Judge, R. J. Levis. Identification of explosives and explosive formulations using laser electrospray mass spectrometry. *Rapid Commun. Mass Spectrom*. **2010**, *24*, 1659.

21) R. E. Deimler, T. T. Razunguzwa, B. R. Reschke, C. M. Walsh, M. J. Powell, G. P. Jackson. Direct analysis of drugs in forensic applications using laser ablation electrospray ionization-tandem mass spectrometry (LAESI-MS/MS). *Anal. Methods*, **2014**, *6*, 4810.

22) Etalo, D. W., De Vos, R. C., Joosten, M. H., & Hall, R. D. Spatially resolved plant metabolomics: some potentials and limitations of laser-ablation electrospray ionization mass spectrometry metabolite imaging. *Plant physiology*. **2015,** *169*(3): 1424-1435.

23) A. Vaikkinen, B. Shrestha, J. Koivisto, R. Kostiainen, A. Vertes, T. J. Kauppila. Laser Ablation Atmospheric Pressure Photoionization Mass Spectrometry Imaging of Phytochemicals from Sage Leaves. *Rapid Commun. Mass Spectrom.* **2014**, *28*, 2490.

24) D. W. Etalo, R. C. H. De Vos, M. H. A. J. Joosten, R. D. Hall. Spatially-resolved plant metabolomics: some potentials and limitations of laser ablation electrospray ionization mass spectrometry metabolite imaging. *Plant Physiol. Preview* **2015**, doi: 10.1104/pp.15.01176.

25) A. Roempp, B. Spengler. Mass spectrometry imaging with high resolution in mass and space. *Histochem. Cell Biol*. **2013**, *139(6)*, 759.

26) W. T. Silfvast, Laser Fundamentals, 2nd ed., Cambridge, University Press, 2004, p. 419.

27) M.-Z. Huang, H.-J. Hsu, C.-I. Wu, S.-Y. Lin, Y.-L. Ma, T.-L. Cheng, J. Shiea, Characterization of the chemical components on the surface of different solids with electrospray-assisted laser desorption ionization mass spectrometry. *Rapid Commun. Mass Spectrom*. **2007**, *21*, 1767
28) M.-Z. Huang, S.-C. Cheng, S.-S. Jiang, C.-C. Chou, C.-N. Cheng, J. Shiea, I. A Popov, E. N. Nikolaev, Ambient molecular imaging of dry fungus surface by electrospray laser desorption ionization mass spectrometry, *Int. J. Mass Spectrom*. **2012**, *325-327*, 172.

29) E. A. Judge, J. J. Brady, P. E. Barbano, R. J. Levis, Nonresonant femtosecond laser vaporization with electrospray postionization for ex vivo plant tissue typing using compressive linear classification, *Anal. Chem*. **2011**, **83**, 2145.

30) P. M. Flanigan IV, L. L. Radell, J. J. Brady, R. J. Levis, Differentiation of eight phenotypes and discovery of potential biomarkers for a single plant organ class using laser electrospray mass spectrometry and multivariate statistical analysis, *Anal. Chem*. **2012**, *84*, 6225.

31) T. Harada, A. Yuba-Kubo, Y. Sugiura, N. Zaima, T. Hayasdaka, N. Goto-Inoue, M. Wakui, M. Suematsu, K. Takeshita, K. Ogawa, Y. Yoshida, M. Setou, Visualization of volatile substances in different organelles with an atmospheric-pressure mass microscope, *Anal. Chem*. **2009**, *81*, 9153.

32) J. I. Brauer, I. B. Beech, J. Sunner, Mass spectrometric imaging using laser ablation and solvent capture by aspiration (LASCA), *J. Amer. Soc. Mass Spectrom*. **2015**, *26*, 1538.

33) B. Spengler, Mass spectrometry imaging of biomolecular information, *Anal. Chem.* **2014**, *87*, 64.

34) G. Robichaud, J. A. Barry, D. C. Muddiman, Atmospheric pressure mass spectrometry imaging, Encyclopedia of Analytical Chemistry, Wiley, 2014, p. 1. DOI:10.1002/9780470027318.a9399

35) M. C. Chambers, B. MacLean, R. Burke, D. Amode, D. L. Ruderman, S. Neumann, L. Gatto, B. Fischer, B. Pratt, J. Egertson, K. Hoff, D. Kessner, N. Tasman, N. Shulman, B. Frewen, T. A. Baker, M.-Y. Brusniak, C. Paulse, D. Creasy, L. Flashner, K. Kani, C. Moulding, S. L. Seymour, L. M. Nuwaysir, B. Lefebvre, F. Kuhlmann, J. Roark, P. Rainer, S. Detlev, T. Hemenway, A. Huhmer, J. Langridge, B. Connolly, T. Chadick, K. Holly, J. Eckels, E. W. Deutsch, R. L. Moritz, J. E. Katz, D. B. Agus, M. MacCoss, D. L. Tabb, P. Mallick, A cross-platform toolkit for mass spectrometry and proteomics. *Nature Biotechnology* **2012**, *30*, 918.

36) I. M. Race, I. B. Styles, J. Bunch. Inclusive sharing of mass spectrometry imaging data requires a converter for all. *J. Proteomics* **2012**, *75*, 5111.

37) I. Klinkert, K. Chughtai, S.R. Ellis, R.M.A. Heeren. Methods for full resolution data exploration and visualization for large 2D and 3D mass spectrometry imaging datasets. *Int. J. Mass Spectrom.* **2014**, *362*, 40.

38) F. M. Green, T. L. Salter, I. S. Gilmore, P. Stokes and G. O'Connor. The effect of electrospray solvent composition on desorption electrospray ionisation (DESI) efficiency and spatial resolution. *Analyst*, **2010**, *135*, 731.

39) D. R. Ifa, C. Wu, Z. Ouyang, R. G. Cooks. Desorption electrospray ionization and other ambient ionization methods: current progress and preview. *Analyst* **2010**, *135*, 669.

40) F. Sanchez-Rabaneda, O. Jauregui, R. M. Lamuela-Raventos, F. Viladomat, J. Bastida, C. Codina. Qualitative analysis of phenolic compounds in apple pomace using liquid chromatography coupled to mass spectrometry in tandem mode. *Rapid. Commun. Mass Spectrom.* **2004**, *18*, 553.

41) E. Urbanczyk-Wochniak, C. Baxter, A. Kolbe, J. Kopka, L. J. Sweetlove, A. R. Fernie. Profiling of diurnal patterns of metabolite and transcript abundance in potato (Solanum tuberosum) leaves. *Planta* **2005**, *221*, 891.

42) H. K. Kim, R. Verpoorte. Sample preparation for plant metabolomics. *Phytochem. Anal*. **2010**, *21*, 4.

43) J. C. May, J. A. McLean, The conformational landscape of biomolecules in ion mobility – mass spectrometry, in Ion mobility mass spectrometry theory and applications, C. L. Wilkins, S. Trimpin, Eds., CRC Press, Boca Raton, FL, Chap. 16 Figs. 16.4 and 16.

Table

Table I. Metabolites identified in peony, French marigold, geranium, and hosta by UV-LAESI under atmospheric pressure.

Plant	Suggested Assignent	Mean Measured (Da)	Accurate Mass (Da)	ΔDa (10^{-3})	Δ (ppm)		Measured Product Ions (m/z)
Peony	Kaempferol	287.0535	287.0555	-2	-6.97	$[M+H]^+$	258, 213, 165, 153
	Isorhamnetin	317.062	317.0661	-4.1	-12.93	$[M+H]^+$	
	Kaempferol-3-glucoside	449.1084	449.109	-0.6	-1.34	$[M+H]^+$	287
	Kaempferol-7-glucoside	471.0906	471.0903	0.3	0.64	$[M+Na]^+$	287
	Quercetin 3-O-glucoside or Quercetin 7-O-glucoside	487.0751	487.0853	-10.1	-20.94	$[M+Na]^+$	
	p-Hydrobenzoic acid	137.0245	137.0239	0.6	4.38	$[M-H]^-$	
	Kaempferol 3-O-arabinoside	417.0837	417.0822	1.5	3.60	$[M-H]^-$	
	Luteolin 7-O-glucoside	447.0995	447.0927	6.8	15.21	$[M-H]^-$	285
	Kaempferol 3-O-galloyl glucoside	599.1116	599.1037	7.9	13.19	$[M-H]^-$	
Marigold	Kaempferol	287.0609	287.0555	5.4	18.81	$[M+H]^+$	258, 213, 165, 153
	Quercetin	303.0548	303.0504	4.4	14.52	$[M+H]^+$	285, 257, 229, 165, 153
	Kaempferol-3-rhamnoside	433.1183	433.1134	4.9	11.31	$[M+H]^+$	287
	Kaempferol-3-glucoside or quercetin-3-rhamnoside	449.1084	449.109	-0.6	-1.34	$[M+H]^+$	303, 287
	Quercetin 3-O-glucoside or Quercetin 7-O-glucoside	487.0891	487.0853	3.8	7.80	$[M+Na]^+$	325, 303, 287, 177, 147
	Kaempferol 3-O-arabinoside	603.1431				$[M+H]^+$	
	Quercetin 3-O-galloylglucoside	617.1606				$[M+H]^+$	325, 287, 147
	Quercetin 3-O-arabinoside	433.0787	433.0771	1.6	3.69	$[M-H]^-$	
	Luteolin 7-O-glucoside	447.0995	447.0927	6.8	15.21	$[M-H]^-$	285

Table 1. Continued.

Plant	Suggested Assignent	Mean Measured	Accurate Mass	ΔDa (10⁻³)	Δ (ppm)		Measured Product Ions
	Quercetin 3-O-glucoside or Quercetin 7-O-glucoside	463.0906	463.0877	2.9	6.26	[M-H]⁻	301
	Kaempferol 3-O-glucoside-7-O-rhamnoside	593.16	593.1507	9.3	15.68	[M-H]⁻	447
	Kaempferol 3,7-di-O-glucoside	609.1509	609.1456	5.3	8.70	[M-H]⁻	447, 285
	Quercetin 3,7-di-O-glucoside	625.1469	625.1405	6.4	10.24	[M-H]⁻	
Geranium	Glucose	203.0602	203.053	7.2	35.46	[M+Na]⁺	
	Kaempferol	287.0535	287.0555	-2	-6.97	[M+H]⁺	
	Quercetin	303.0532	303.0504	2.8	9.24	[M+H]⁺	
	Quercetin-O-α-L-arabinofuranoside	435.0921	435.0927	-0.6	-1.38	[M+H]⁺	
	Quercetin-O-glucoside	465.1059	465.1033	2.6	5.59	[M+H]⁺	
	Kaempferol arabinoside	417.0863	417.0822	4.1	9.83	[M-H]⁻	285
	Quercetin arabinoside	433.0812	433.0771	4.1	9.47	[M-H]⁻	301
	Kaempferol 3-glucoside	447.0927	447.0927	0	0.00	[M-H]⁻	
	Quercetin 3-glucoside	463.0929	463.0877	5.2	11.23	[M-H]⁻	301
	Myricetin glycoside	479.0875	479.0826	4.9	10.23	[M-H]⁻	317
	Kaempferol galloylgalactoside or Kaempferol galloylglucoside	599.1019	599.1037	-1.8	-3.00	[M-H]⁻	
	Quercetin 3-(2-galloyl)galactoside or Quercetin 3-(2-galloyl)glucoside	615.1069	615.0986	8.3	13.49	[M-H]⁻	
	Trigalloyl quinic acid	647.094	647.0884	5.6	8.65	[M-H]⁻	
	Hexagalloylglucose	1091.131	1091.1213	9.8	8.98	[M-H]⁻	
	Heptagalloylglucose	1243.14	1243.1323	7.7	6.19	[M-H]⁻	
	Octagalloylglucose	1395.137	1395.1432	-6.6	-4.73	[M-H]⁻	*
	Nonagalloylglucose	1547.157	1547.1542	2.4	1.55	[M-H]⁻	*
	Decagalloylglucose	1699.159	1699.1652	-6.5	-3.83	[M-H]⁻	*
Hosta	Arginine	175.1165	175.1195	-3	-17.13	[M+H]⁺	157, 139
	Sucrose	381.0782	381.0799	-1.7	-4.46	[M+K]⁺	381

Table 1. Continued.

| Plant	Suggested Assignment	Mean Measured	Accurate Mass	ΔDa (10^{-3})	Δ (ppm)		Measured Product Ions
	Kaempferol 5-methyl ether 3-galactoside-4'-glucoside	663.1257	663.1327	-7	-10.56	[M+K]$^{+}$	
	Kaempferol 7-O-(6-trans-caffeoyl)-beta-glucopyranosyl-(1->3)-alpha-rhamnopyranoside-3-O-beta-glucopyranoside	957.2174	957.2067	10.7	11.18	[M+K]$^{+}$	671. 525,509, 363, 287
	Citric Acid	191.0194	191.0197	-0.3	-1.57	[M-H]$^{-}$	
	Sucrose	341.1103	341.1089	1.4	4.10	[M-H]$^{-}$	179, 161, 149
	Kaempferol diglucoside	609.1463	609.1456	0.7	1.15	[M-H]$^{-}$	489, 447, 429, 285
	Kaempferol 3-O-diglucoside-7-O-glucoside	771.1934	771.1983	-4.9	-6.35	[M-H]$^{-}$	609, 591, 429, 285

Figures
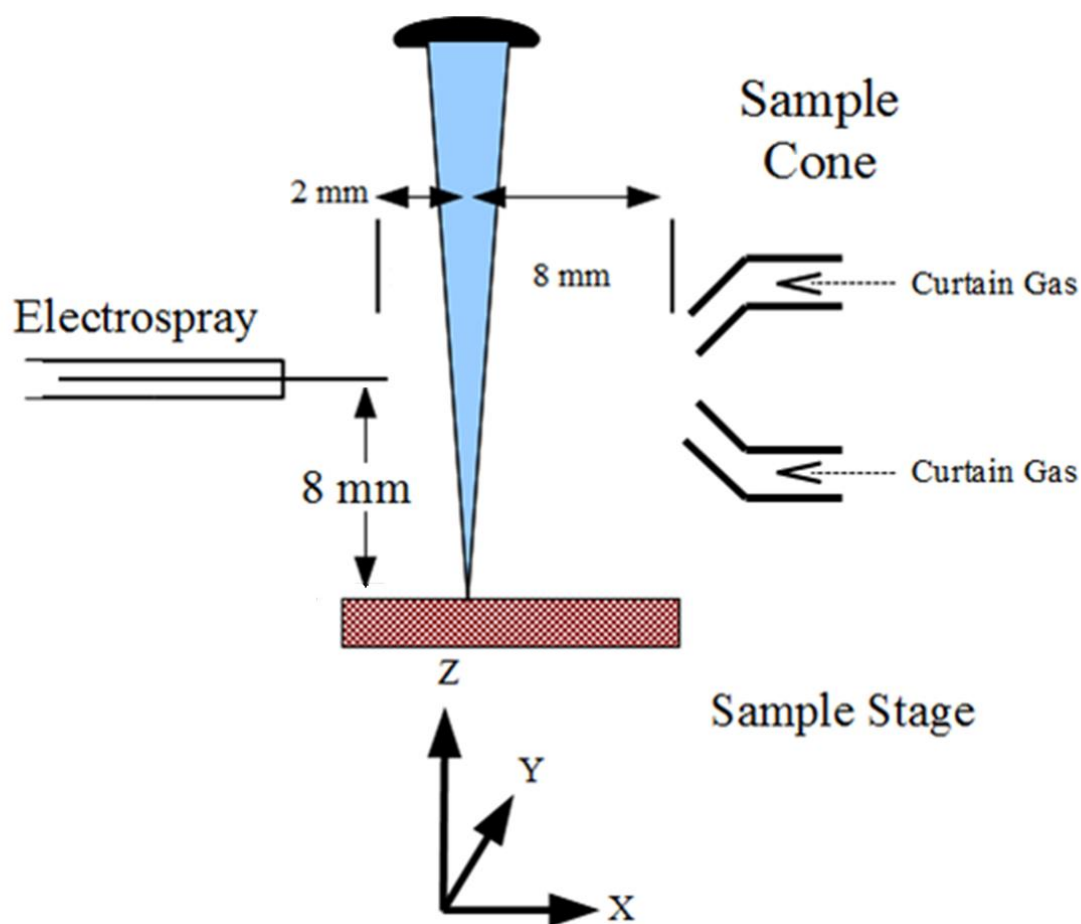
Figure 1. Experimental setup for UV- LAESI. The dimensions noted in the figure produced optimal signal intensities. The sample stage was a glass microscope slide with the plant sample taped to the top side.
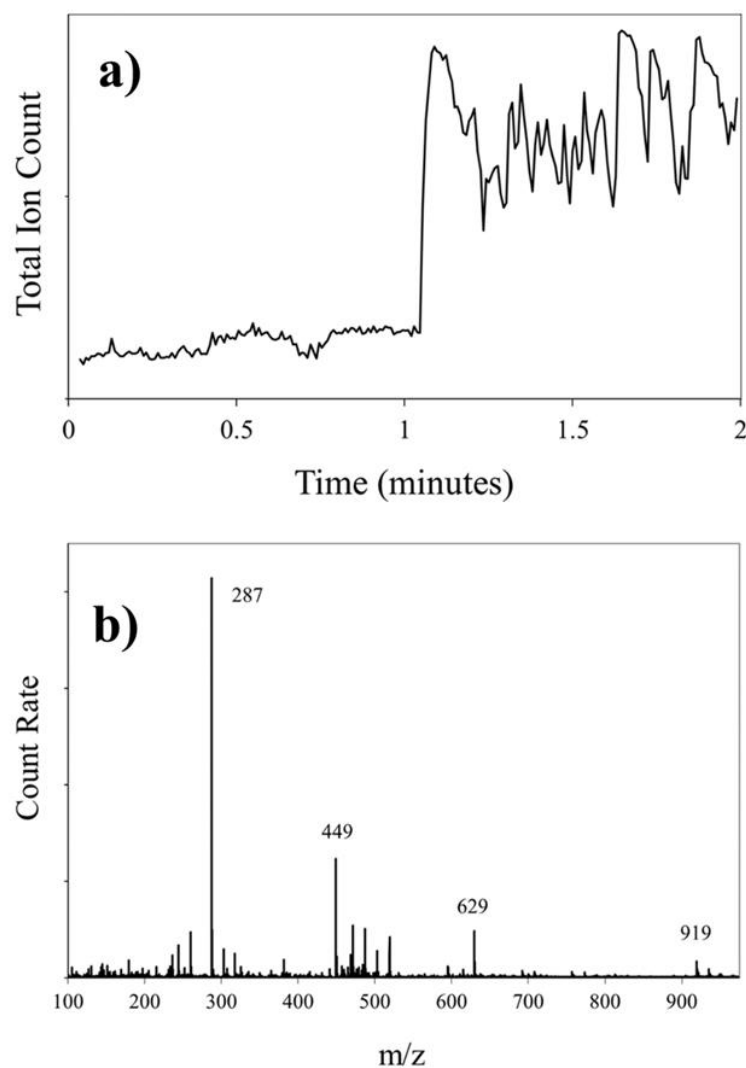
Figure 2. Typical chromatogram and spectra for a UV-LAESI acquisition. **A)** Typical total ion chromatogram recorded from one ablation track during ambient-pressure UV-LAESI acquisition. During the first minute of the acquisition, the laser is blocked and the TIC is solely due the ions generated from the electrospray. The laser is unblocked during the second minute of the acquisition and the TIC is a combination of ions from the ESI and the ions produced by electrospray ionization of ablated material. **B)** Integrated positive ion mass spectrum obtained from a peony leaf acquired by atmospheric-pressure UV-LAESI. This spectrum was integrated from the TIC in the latter part of Fig. 4a. The ESI background (time < 1 min) has been subtracted from the LAESI spectrum (time > 1 min).
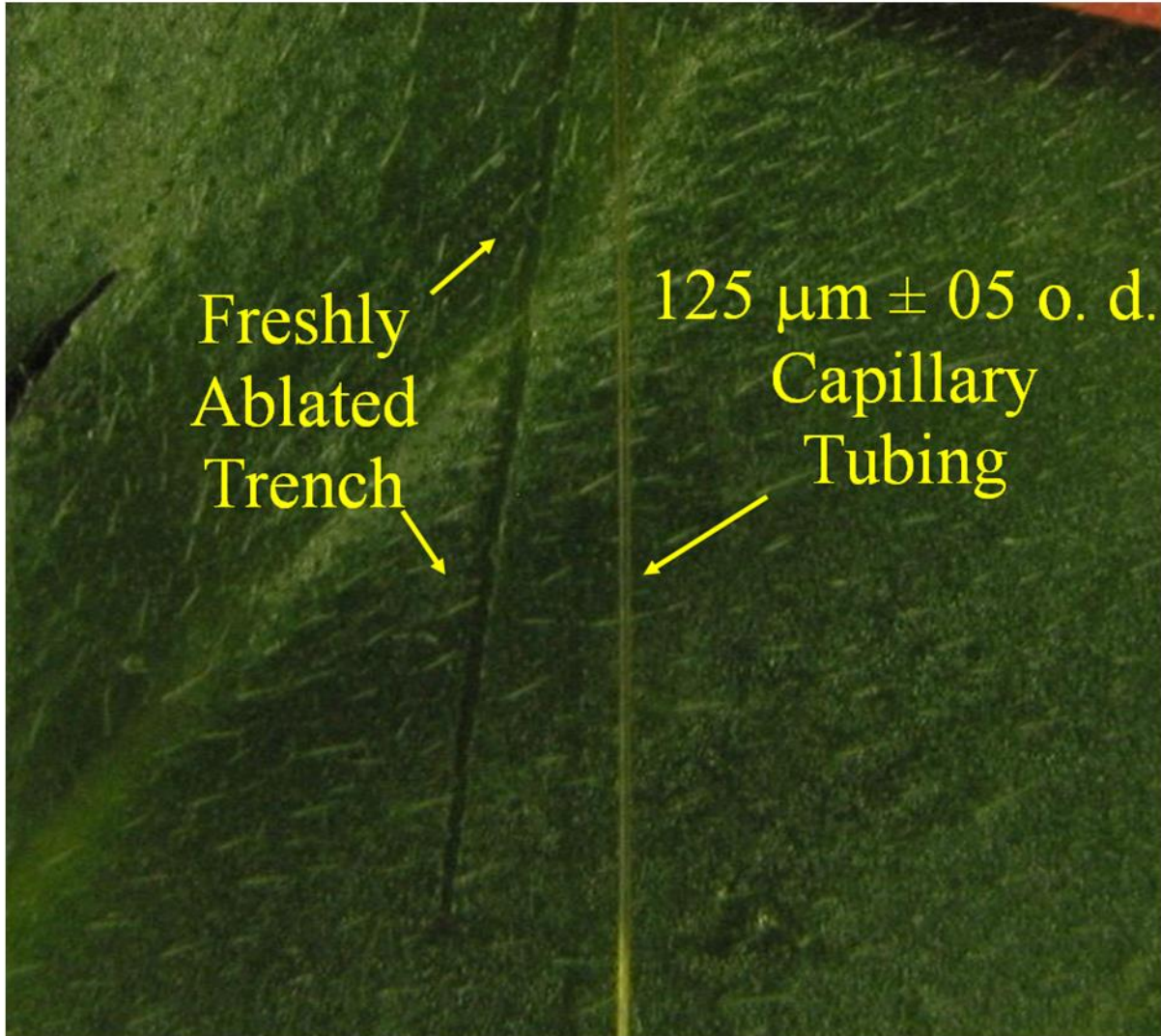
Figure 3. Photo showing nominal size of ablation trench produced on a translated French marigold leaf by the UV laser. This picture was taken a few seconds after an ablation run, before the sample dried and cracked
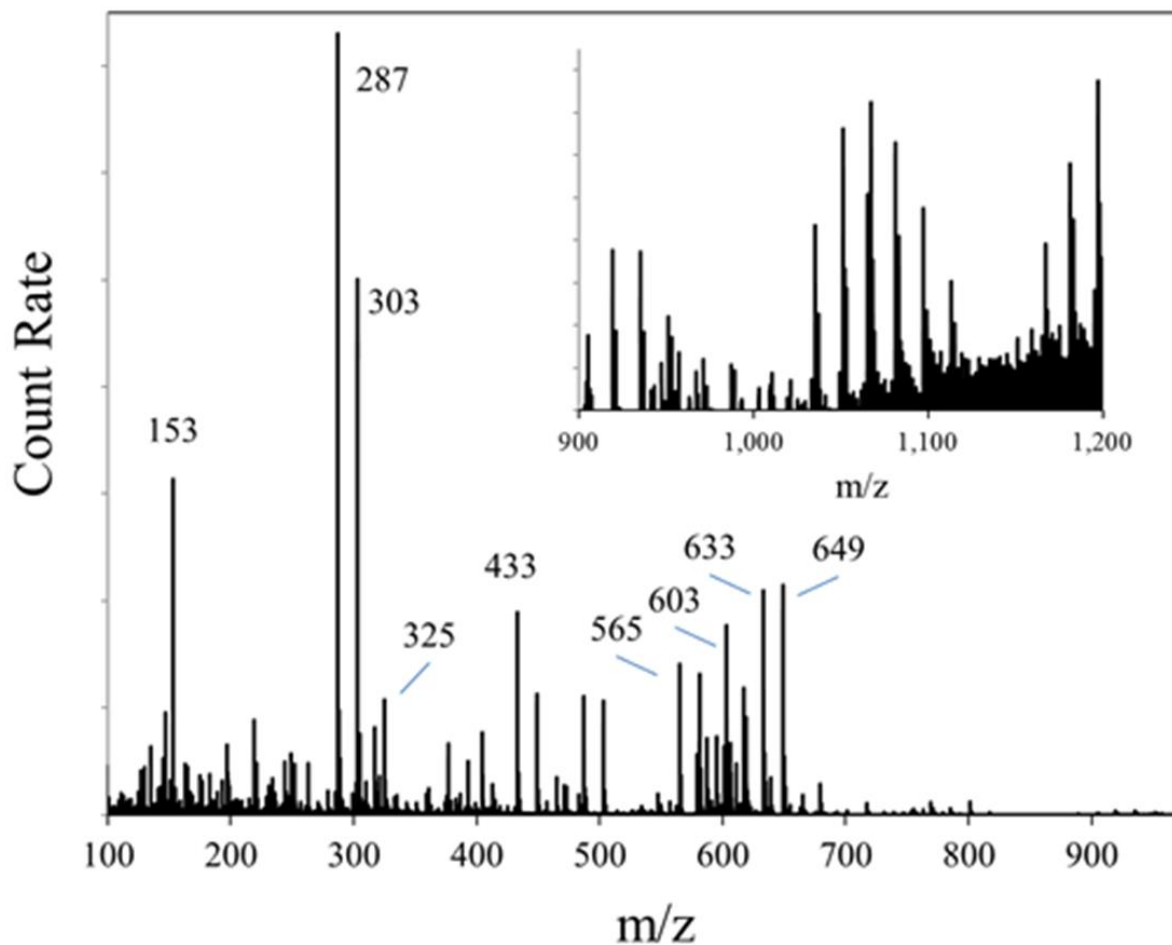
Figure 4. Integrated positive ion mass spectrum obtained from one ablation track in a French marigold leaf acquired by atmospheric-pressure UV-LAESI. The inset (~ 90x zoom) shows a range of clusters at higher m/z. The ESI background has been subtracted from this LAESI spectrum.
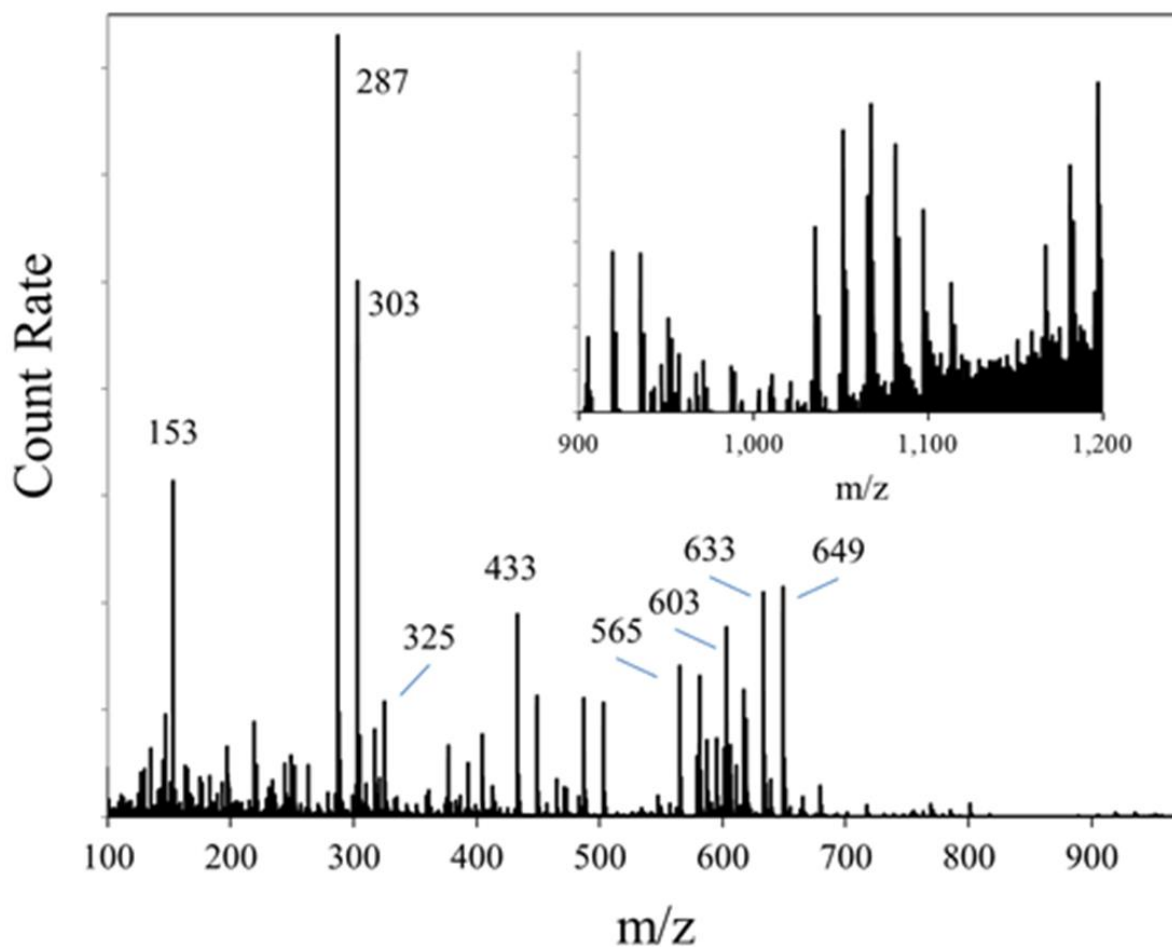
Figure 5. Integrated positive-ion mass spectrum obtained from a geranium leaf acquired by atmospheric-pressure UV-LAESI. The inset (~28x zoom) shows a range of cluster peaks at higher m/z. The electrospray background has been subtracted from this LAESI spectrum.
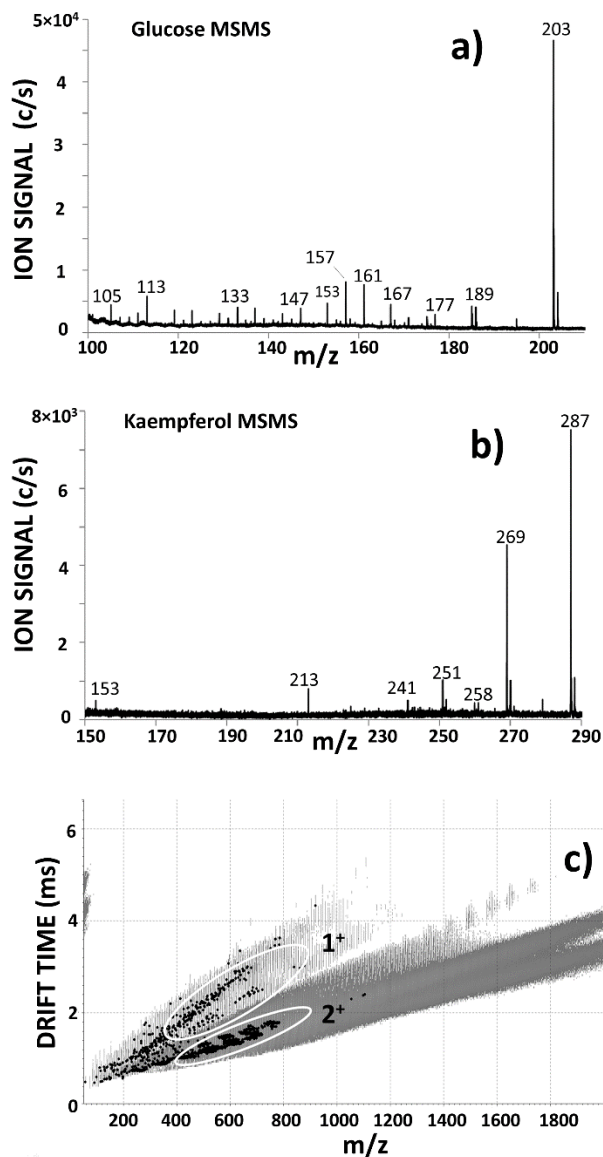
Figure 6. Typical tandem MS and IMS results for positive ions from geranium: a) tandem MS spectrum of glucose + Na$^+$, b) tandem MS spectrum of kaempferol + H$^+$, c) IMS plot of drift time vs. m/z values. Note separation of 2+ from 1+ ions, and diagonal swaths corresponding to different classes of compounds.
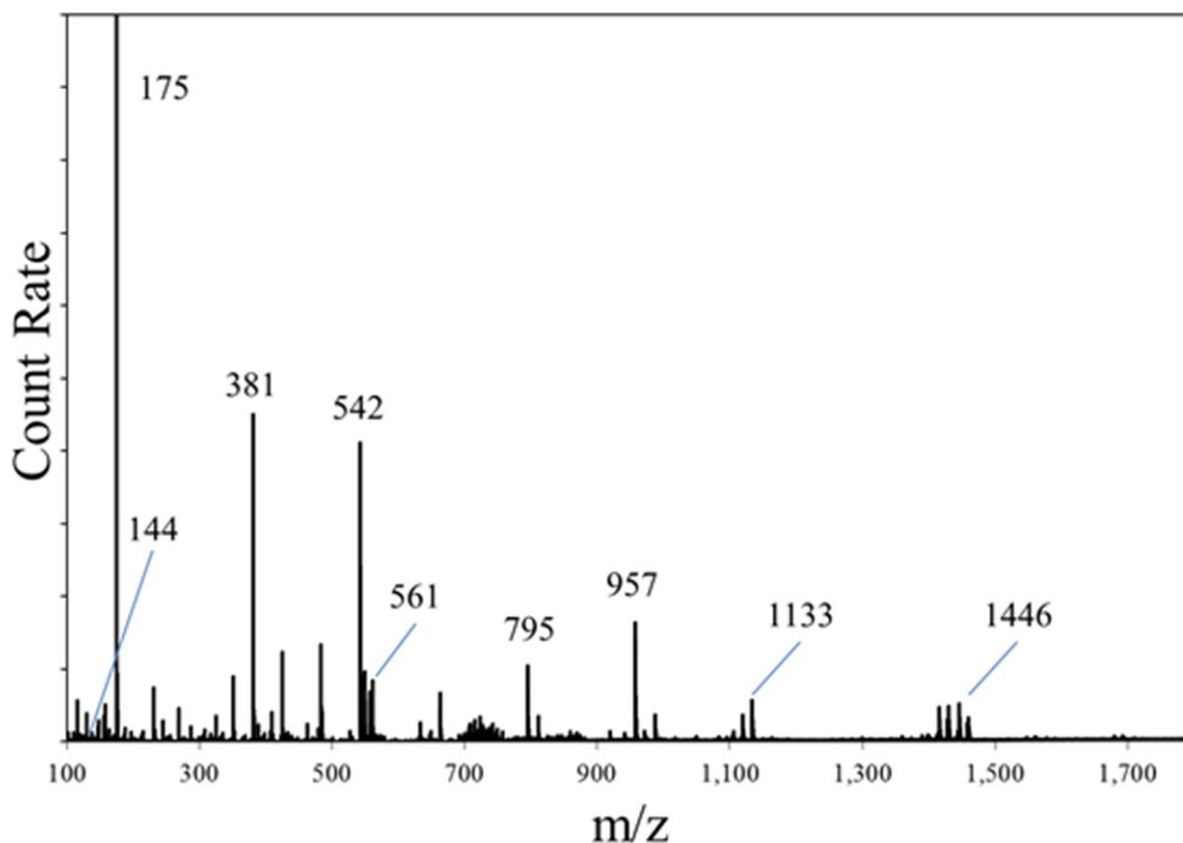
Figure 7. Integrated positive ion mass spectrum obtained from a hosta leaf acquired by atmospheric-pressure UV-LAESI. The m/z 175 peak at m/z 175 (arginine + H$^+$) is much more intense and extends above the figure boundary. This mass spectrum is an average of both the yellow and green areas seen in Fig. 8 acquired in one ablation track. The ESI background has been subtracted from this LAESI spectrum.
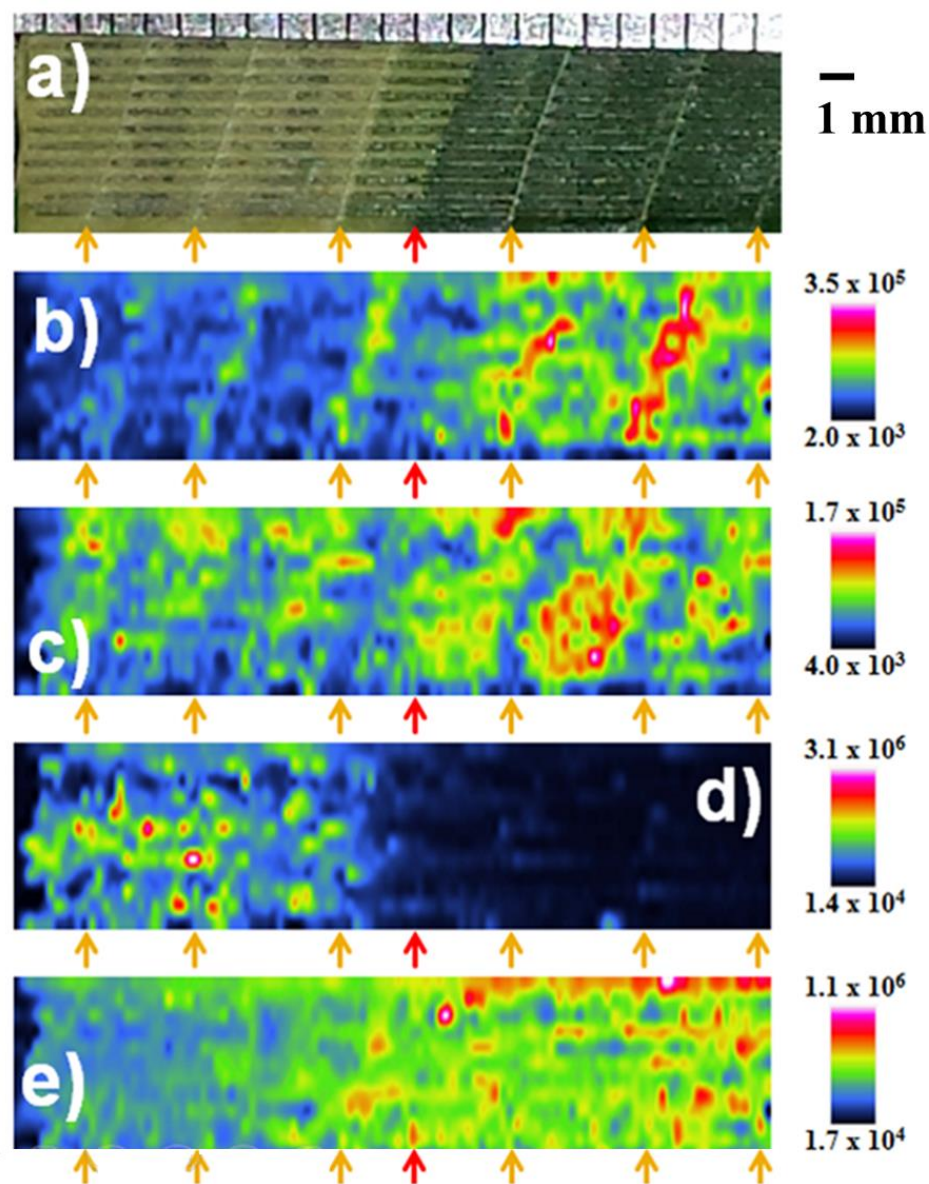
Figure 8. Images for positive ions from hosta leaf.   a) Optical photograph long after ablation. The veins are ~ 3 mm apart. False color ion maps of hosta at b) m/z 561.171, assignment uncertain, c) m/z 663.126, kaempferol-methyl ether-galactoside-glucoside + $^{39}K^+$, d) m/z 175.117, arginine + H^+, and e) m/z 381.078, sucrose + $^{39}K^+$. The orange arrows at the bottom of each ion image corresponds to the observed veins in the photo in a). The red arrow corresponds to the position of the leaf where it distinctly changes from yellow to green.
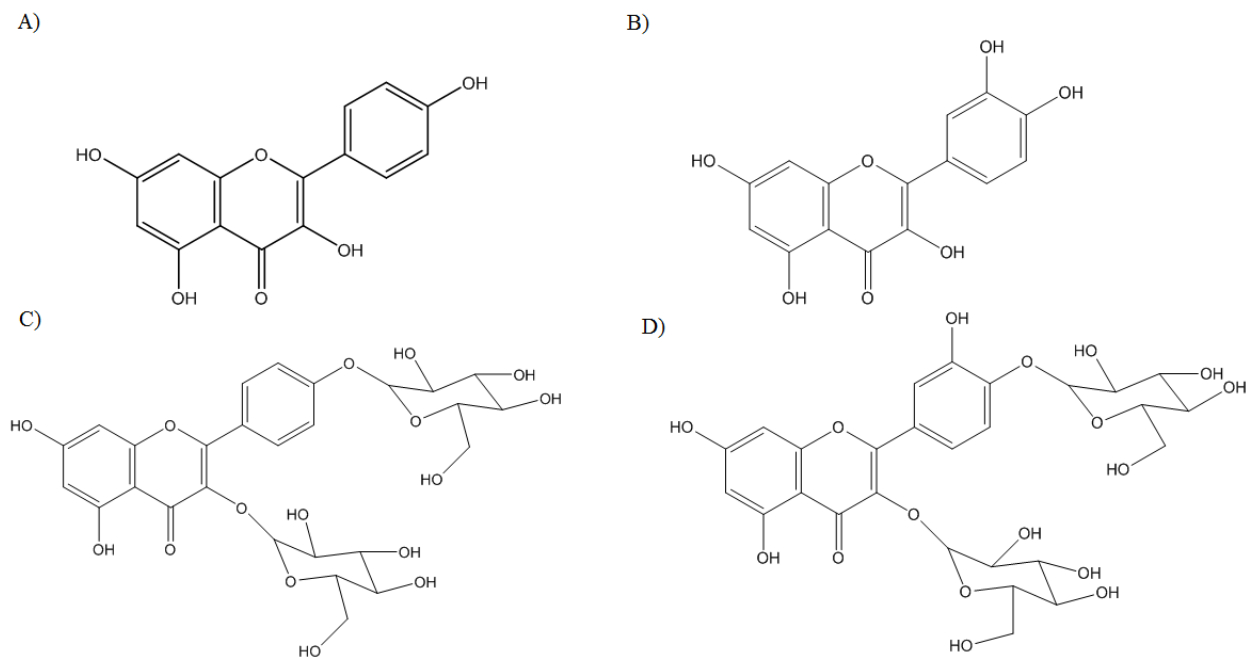
Figure S1. Structures of common metabolites present in a variety of plant material. A) Kaempferol, B) quercetin, C) kaempferol diglucoside (depicted here as kaempferol 3,4-diglucoside, and c) quercetin diglucoside (depicted here as quercetin 3,4-diglucoside)

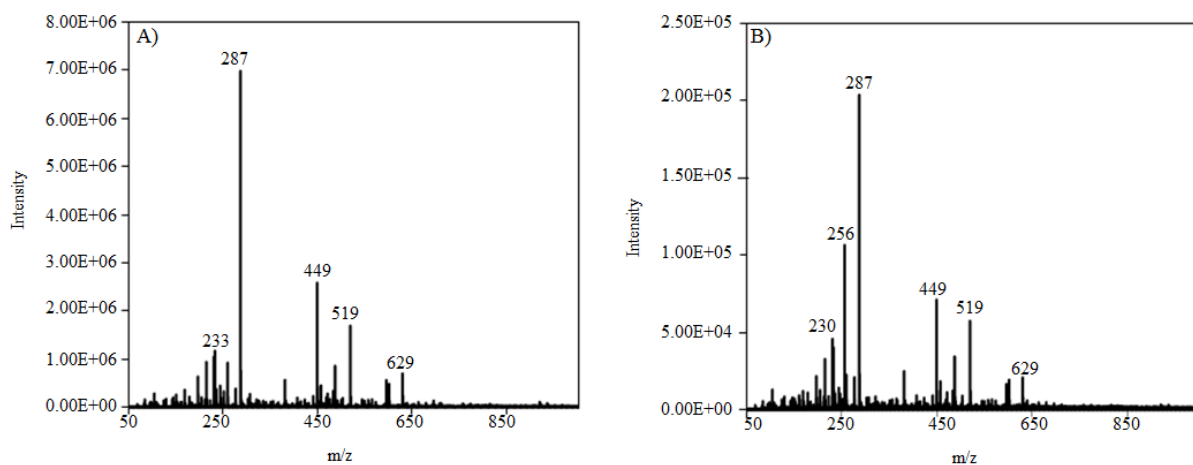**Figure S2.** Background subtracted spectra vs. not subtracted spectra of a peony leaf. A) Integrated positive mass spectrum by ambient-pressure UV-LAESI and B) single point positive mass spectrum by ambient-pressure UV-LAESI at time 1.21 minutes. The intensity of the single point mass spectrum is lower than the overall mass spectra. M/Z 256, shown in B), is a background ion typically not seen in the integrated spectra.
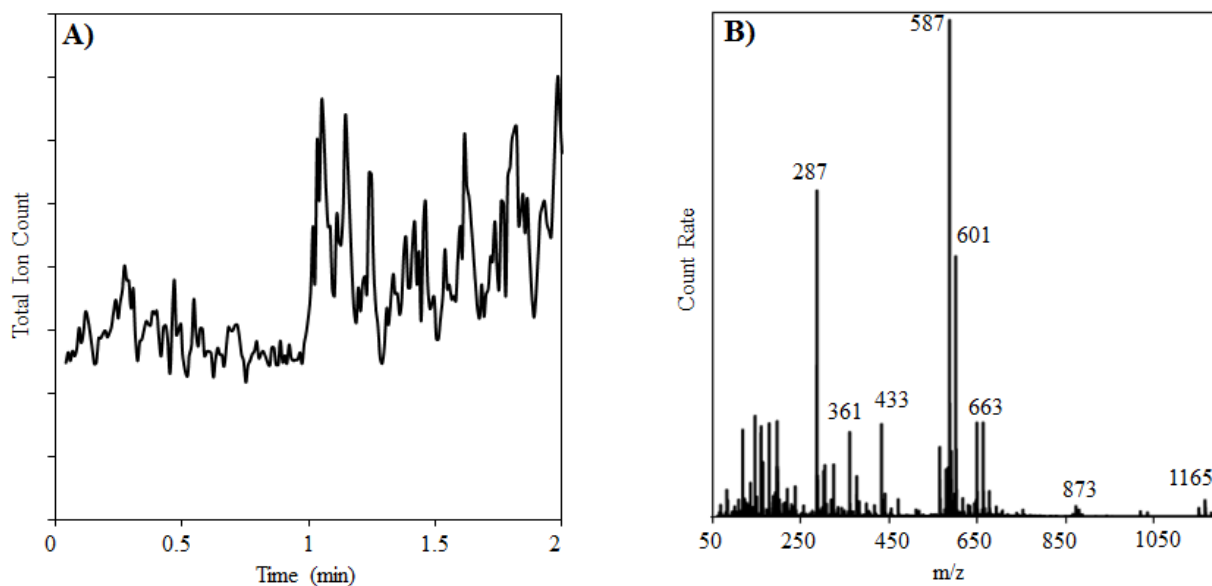
Figure S3. Experiments conducted with a 50 um laser spot size. A) Total ion chromatogram recorded from one ablation track of a marigold leaf during ambient-pressure UV-LAESI. The total ion count is 3.4×10^7. B) Integrated positive ion mass spectrum from a marigold leaf acquired by atmospheric-pressure UV-LAESI. ESI background has been subtracted from the LAESI spectrum.
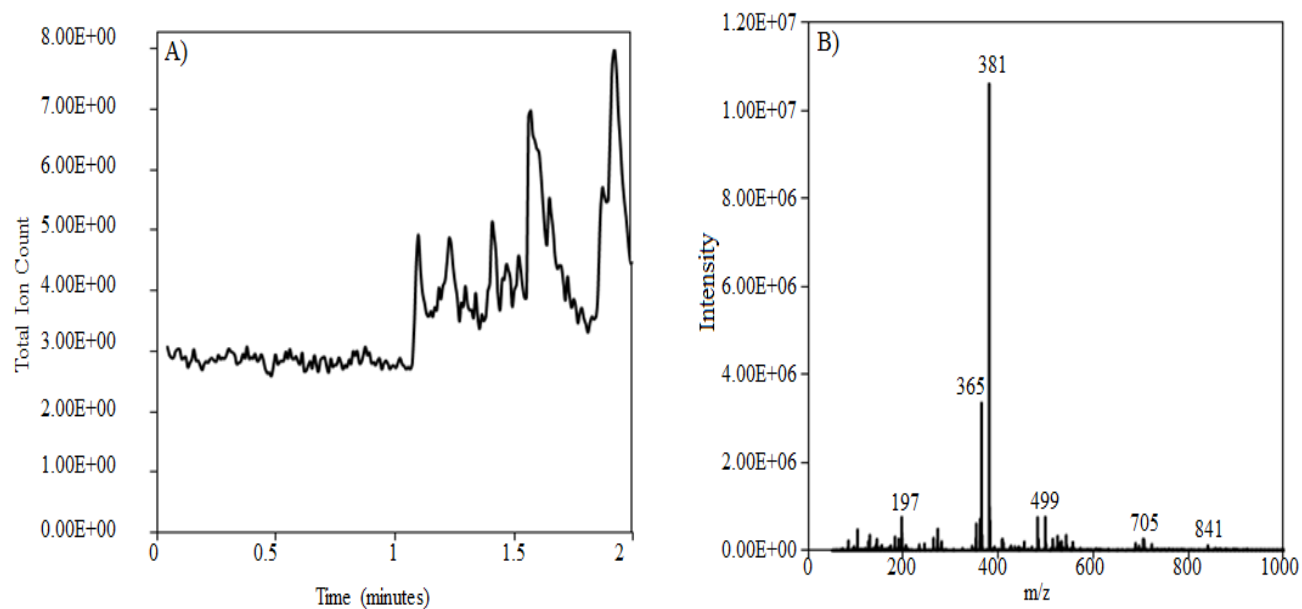
Figure S4. Total ion chromatogram and integrated positive mass spectrum obtained from a hazelnut by UV-LAESI. A) Chromatogram. During the first minute the laser is blocked and the TIC is solely due to ions from the electrospray. During the second minute, the laser is unblocked and the TIC are ions from both the electrospray and the ablated sample. B) Positive mass spectrum. The ESI background has been subtracted. The two most dominant ions in the spectrum are the Na^+ and K^+ adducts of sucrose

Figure S5. Images for positive ions in sweet corn. The depicted area is approximately 6mm × 10mm. A) Optical photograph taken long after ablation. B-D) False color ion maps for sweet corn at m/z 130 (id unknown), m/z 145 (id unknown), and m/z 365 (sodiated sucrose).

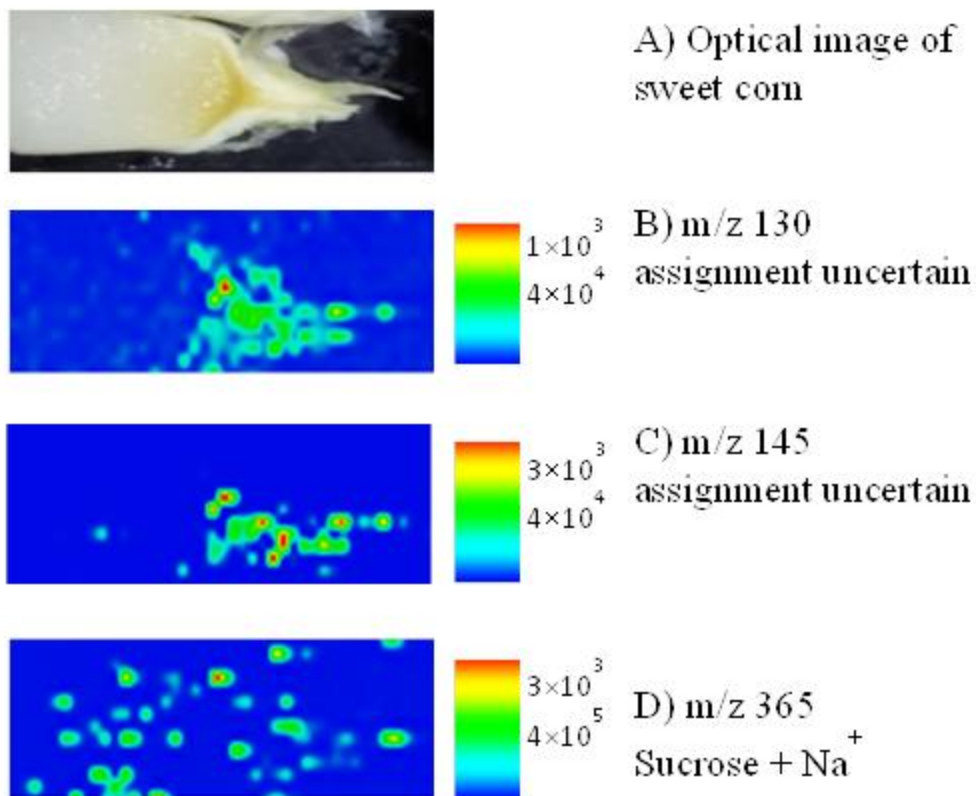# CHAPTER 3. ANTHOCYANIN IMAGING IN *SOLENOSTEMON SCUTELLARIODES* (COLEUS) LEAVES USING ULTRAVIOLET LASER ABLATION ELECTROSPRAY IONIZATION MASS SPECTROMETRY

Galayda, K.J[1,2]., Xie, B.[1,2,3], Alexander, L.[1.3], McVey, P.A.[1,2], Nikolau, B.[1,3] and Houk, R.S.[1,2]

[1]*The Ames Laboratory, Iowa State University, Ames, Iowa, 50011,USA*

[2]*Department of Chemistry, Iowa State University, Ames, Iowa, 50011, USA*

[3]*Department of Biochemistry/Biophysics & Molecular Biology, Iowa State University, Ames, Iowa, 5011, USA*

Abstract

A common horticultural plant *Solenostemon scutellariodes* (coleus) has diverse foliage colors and is ideal for studying the biological role of flavonoid compounds. Prior research has determined how these variations in leaf color are altered by varying light sources. However little research has been done to determine the types of flavonoid compounds present in coleus leaves. In this study, laser ablation electrospray ionization (LAESI) mass spectrometry imaging (MSI) was used to determine a specific class of flavonoids- anthocyanins, which were additionally, confirmed using liquid chromatography mass spectrometry (LC-MS). Two varieties of *Solenostemon scutellariodes* (coleus) were used for the study. Broad Street is anthocyanin-rich (dark burgundy/red leaf edged in green), while Wizard Jade is anthocyanin-poor (a leaf with creamy white center and green outer margin). Broad Street Coleus was found to be abundant in malonylshisonin. In contrast, Wizard Jade Coleus showed lower levels of this anthocyanin.

Mass spectrometry imaging (MSI) showed that the biosynthesis of malonylshisonin in Broad Street Coleus progressed from cyanidin to cyanidin-3-O-β-D-glucoside to cyanidin-3-(p-coumaroyl)-glucoside to shisonin and finally to malonylshisonin. LAESI was proven to be a sensitive technique in identifying small amounts of shisonin and malonylshisonin in specific spatial regions of Wizard Jade Coleus leaves. Spatial resolution is important when compounds are heterogeneously distributed. The use of LAESI-MSI can prove a useful source to study biological processes as it requires little sample preparation.

Introduction

Anthocyanins are part of a larger class of secondary metabolites called flavonoids. They are commonly found in leaves and act as a stress protector especially against ultraviolet (UV) damage, since anthocyanins readily absorb UV light. Anthocyanins induce the characteristic blue, red, or purple pigment in various plant tissues. Common anthocyanins include cyanidin, pelargonidin, and delphinidin, which all have a cyclic backbone structure that is positively charged. This positive charge allows anthocyanins to have unique biological roles, which vary depending on the plant species and the location of anthocyanins in the plant itself.[1] When anthocyanins are found primarily in seeds, their colors attract animals, thus aiding in seed dispersal. Alternatively, in leaves they can protect the plant against stressors like harsh weather conditions, heavy metal contamination, and UV radiation, the latter being the most commonly studied.[1-10] When a leaf is subjected to UV radiation, particularly UVB light (280-320 nm), proteins, DNA, and cell membranes can be altered or destroyed.[11] Thus, the anthocyanins accumulated in epidermal cells can protect leaves by acting as a barrier due to their strong UV absorbance.[12,13]

While the protective role of anthocyanins is the same across plant species, anthocyanin synthesis can vary depending on the plant.[14] The precursors of all anthocyanin syntheses are malonyl-COA and p-coumaroyl-COA; the latter is shown in Figure 1. These two compounds eventually form tetrahydroxychalcone, which is converted to naringenin, then dihydrokaempferol (DHK). DHK is hydroxylated to become dihydroquercetin (DHQ) or dihydromyricetin (DHM). DHK, DHQ, and DHM are reduced to leucoanthocyanidins, pelargonidin, cyanidin, and delphinidin as common byproducts, depending on the plant. For example, petunias do not produce pelargonidin but can produce delphinidin, whereas maize can produce delphinidin but not pelargonidin.

Solenostemon scutellariodes (coleus), a horticulturally attractive plant with highly ornamental foliage, has been used in many studies involving the influence of light intensity on foliage color and growth.[15] As a member of the *Lamiaceae* (mint) family, coleus plants accumulate anthocyanins in the outer epidermal region of their leaves. Most studies involving anthocyanins in coleus involve manipulating the amount of UV and visible light the leaf receives.[16-18] For example, a study by Nguyen et al., noted changes in pigmentation when various coleus species were subjected to high intensity light.[16] There seems to be little information, however, on the actual anthocyanin compounds present in coleus.

Mass spectrometry imaging (MSI) can be used to study this question. MSI is an emerging tool in the plant field. It has recently shown its capabilities not only in spatial localization of metabolites but also in providing new insights into biological pathways.[19] Several ionization techniques are used in MSI, including matrix assisted laser desorption ionization (MALDI), desorption electrospray ionization (DESI), and laser ablation electrospray ionization (LAESI).[20-

[22] It should be noted in the literature LAESI is closely related to matrix assisted laser desorption electrospray ionization (MALDESI) and electrospray laser desorption ionization (ELDI).[22]

Previous studies involving plant metabolite identification through various MSI techniques, including reduced and atmospheric pressure laser desorption ionization, have been conducted on peonies, marigolds, Arabidopsis, and rice leaves.[21,23-25] While each technique offers its own advantages and disadvantages, LAESI has become useful for metabolite identification in both plant and biological samples over recent years. One the biggest advantage of this type of analysis is the ease of sample preparation (i.e. no matrix coating). An experiment conducted by Nemes et al[20] using IR-LAESI (2.94 μm), found ion abundances in petite French marigold seedlings were ~10^2-10^4 enhanced compared to atmospheric pressure IR-MALDI.

A typical LAESI experiment is shown in Figure 2. A sample leaf is prepped for analysis, and undergoes ablation from the laser. The ablation results in the formation of a neutral plume from the sample, which is then ionized by a charged electrospray stream. The newly formed ions enter the mass spectrometer and the m/z ratio is measured for all the ions present, resulting in a mass spectrum. To obtain an image, several hundred spectra are gathered together to be processed. A mass spectrometry image can now be produced for every compound found in the sample. In our setup, a UV laser (355 nm) was used partly because anthocyanins efficiently absorb UV light.[12,13]

To date, there have been no attempts to image anthocyanins in coleus. We believe that MSI can allow further insight into anthocyanin synthesis. In this study, two varieties of coleus were imaged, Broad Street (dark burgundy/red leaf edged in green; an anthocyanin rich variety) and Wizard Jade (creamy white center and green outer margin; an anthocyanin poor variety). LAESI was performed on both types of leaves to identify the anthocyanins present and their

spatial localization in the leaf. Additionally, extractions and liquid chromatography (LC-MS) were performed for validation and quantification.

Experimental

Plant Maintenance and Light Conditions

Solenostemon scuttellarioides – Broad Street and Wizard Jade were purchased from a local greenhouse (Earl May, Ankeny, Iowa). All plants were transferred to LC1 Sunshine Mix soil (Sun Gro Horticulture, Bellevue, WA), watered weekly in a growth room at 22 °C under continuous illumination (2568 Lux or photosynthetic photon flux density 100 µmol of photons $m^{-2} sec^{-1}$). Leaves (three biological replicates) were harvested and taken for each experimental platform: MS imaging, optical imaging and/or anthocyanin analysis through LC-MS.

Tissue Sectioning and Microscopy

Fresh leaf tissues were hand-sectioned along the longitudinal axis of the leaves using a vibratome at 70-100 µm for spatial imaging. Each section was immediately visualized using a BX-40 microscope equipped with an Axioplan software. It should be noted that MS was not done on these sections.

Anthocyanin Extraction and LC-MS

For anthocyanin analysis, harvested leaves were immediately flash-frozen using liquid nitrogen, dried using a vacuum lyophilizer and pulverized using a Mixer Mill 301(Retsch GmbH, Germany) in 2 mL Eppendorf tubes prior to extraction. The anthocyanin extractions were extracted as described by Wu e. al[26] in 1.5 ml tubes containing 5 mg of lyophilized tissues. Briefly, 300 µL of methanol/ water/ acetic acid (85:10:0.5; v/v) was added to lyophilized samples and sonicated for one hour in dark at 4˚C and then further incubated in the same

conditions (dark, 4°C) for an additional two hours. The samples were then centrifuged for five minutes at 13,000 rpm and the liquid phase (supernatant/upper layer) was filtered twice using 13 mm x 0.45µm Teflon Syringe filters (Supelco, PA).

An Atlantis T3 column (2.1×150mm, 3µm, Waters, Milford, MA) was used for separation. Elution was performed using mobile phase A (5% formic acid in LC-MS grade water) and mobile phase B (5% Formic acid in methanol). The flow rate was kept at a 0.2mL/min. When a 5 µL of sample was injected, a gradient was used as follows: 0-6 min, 0-20% B; 6-40 min, 20-50% B; 40-44 min, 50-50% B; 44-48 min, 50%-100% B; 48-52 min, 100-100% B; 52-56 min, 100-0% B.

Chromatographic separations were performed with an 1100 series HPLC (Agilent Technologies). This was attached to an Agilent 6210 MSD time-of-flight mass spectrometer with an electrospray ionization (ESI) source. The ESI capillary voltage was +3.0 kV, nitrogen gas temperature was set to 350 ˚C, drying gas flow rate was 11 L/min, nebulizer gas pressure was 35 psi, skimmer was 65 V, and OCT RF was 250 V. Mass data from mass range 100-2000 were collected and analyzed using Agilent DataAnalysis.

Individual anthocyanin peak areas were generated using the QuantAnalysis, and then were used to quantitatively compare the different level of each anthocyanins expressed. The tentative structure identification for each anthocyanin was interpreted through MS/MS performed with various collision energy (25-35 eV).

Sample Preparation for LAESI-MSI

Leaves were cut from the plant using scissors and placed in a petri dish over a damp filter paper to prevent drying until ready for ablation. Both the petri dish and the scissors were washed in acetone prior to handling. No additional treatment or matrix was applied. Once the samples

were ready to be ablated, they were mounted onto glass microscope slides with double sided tape and placed on a xyz- translation stage (Z825B, Thorlabs, Inc. Newton, NJ). The samples were positioned 8 mm below the electrospray axis and translated at a rate 0.4 mm/s.

LAESI Source

A 53 µm i.d. polyimide-coated capillary was positioned with the tip approximately 10 mm from the cone inlet of the mass spectrometer. A mixture of methanol and water (1:1 v/v) with a 0.1% formic acid solution (purity $\geq$ 99.5%, Fischer Scientific) was pumped through the capillary by a syringe pump (Model 22, Harvard Apparatus, South Natick, MA) at a rate of 0.6 µl/min. Leucine-enkaphalin (0.1 ppm, Waters) was added to the electrospray solution as a lockspray mass calibrant. The ESI voltage was +2.7 kV.

A 355 nm Nd:YAG ultraviolet laser (ULTRA, Big Sky Laser Tech, Inc., Bozeman, MT) was used. Typical laser pulses of 250 μJ/pulse energy were focused to ~125 μm spot size by a 75 mm fused-silica plano-convex focusing lens. The laser was operated at 10 Hz with a 5 ns pulse width.

LAESI Mass Spectrometer

A Waters Synapt G2-S quadrupole time-of-flight mass spectrometer was used in these experiments. The mass spectrometer was modified by removing the ESI source enclosure. To bypass any electrical connections from this enclosure an adaptor, provided by Waters, was used. During a normal MS acquisition, the quadrupole collision energy was kept at a preset voltage of 30 eV. During tandem MS, the collision energy was nominally 20 to 30 eV. The TOF mass analyzer was operated in sensitivity mode, with a mass resolution of approximately m/Δm 10,000 (FWHM). Mass spectra were recorded from 50 to 2000 m/z. The time-of-flight extraction events were not synchronized to the laser pulses.

LAESI Data Processing

Mass spectra were generated from total ion chromatograms using MassLynx V4.1 (SCN851) software provided by Waters. Peak assignments from these chromatograms were based on accurate mass measurements, tandem MS analysis, and database searches including METLIN[27], KEGG[28], and MetCyc[29]. These databases were last accessed on September 20, 2016. To generate images, MassLynx *.raw data files were converted into mzML files using the Proteowizard Mass ConverterTool[30]. The mzML files were then converted into imzML files using imzMLConverter[31]. The imzML files were then made into black and white images in DatacubeExplorer[32] which were then converted to false-color images in GIMP 2.8.

Safety Considerations

Laser safety goggles specifically for UV beams were used whenever the beam was exposed. Care was taken to avoid contact with the ESI spray tip.

Results and Discussion

Leaf color variations

Foliage color differences between Wizard Jade and Broad Street were visualized at a magnification of 10x using 100 μm thick hand-sections (Fig. 3). Both coleus cultivars showed no anthocyanin accumulation on the lower epidermal layers of the leaf. The green pigments accumulated in chloroplast cells of the mesophyll and palisade layers imparting the differences in leaf color. In Broad Street coleus anthocyanins accumulated only in the upper epidermal layers of the leaf, no anthocyanins were found in Wizard Jade.

Anthocyanin Identification by LC-MS and LC-MS/MS

Identification and peak assignment of anthocyanins were primarily based on the molecular weight, MSMS fragmentation and references.[26] The chromatogram from the red

portion of Broad Street is shown in Figure 4. Table 1 gives tentative assignments for five major anthocyanins and their corresponding MSMS fragments. It should be noted that exact linkages among these structures were not able to be identified because the corresponding standards were not available for comparison.

Similar anthocyanin extraction and LCMS detection were performed on the creamy white area of Wizard Jade. As indicated in Figure 4, anthocyanins detected from the red portion of Broad Street were not detected in Wizard Jade. This is typical as the extracted solution from wizard jade is yellow and believed to not contain anthocyanins.

LAESI-MSI of Broad Street and Wizard Jade

A representative background subtracted positive-ion mass spectrum (integrated from one laser ablation trench over the course of 50 s) from Broad Street coleus is shown in Fig. 6a. The most abundant ion signals that were observed included peaks representing the anthocyanins, cyanidin and malonylshisonin at m/z 287.0550 and 843.1984. Other observable anthocyanins included apigenen (m/z 271.0615), Cyanidin-3-(p-coumaroyl)-glucoside (m/z 595.1451), and Cyanidin 3-(6''-p-coumarylglucoside)-5-4'', 6''-dimalonylglucoside (m/z 929.1982). Other anthocyanins and their suggested assignments are listed in Table 2. Linkage positions were based on literature, and were measured in present work.[14]

Figure 6b shows a representative background subtracted positive-ion mass spectrum (integrated from one laser ablation trench over the course of 50 seconds) from Wizard Jade coleus. This spectrum is very from that of Broad Street. The most abundant ions observed included caffeic acid $-H_2O +H^+$ at m/z 163, kaempferol at m/z 287.0570, and unknown ions at m/z 351 and 399. Lower abundance ions showed the presence of carotenoids and lipids and are listed in table 2. The integrated mass spectra did not show the presence of anthocyanins.

For both variety of leaves, tandem MS measurements were taken and compared to databases. Collision energies ranged from 15-30 eV. Representative spectra can be found in the supplementary materials. Furthermore, tandem MS measurements of Broad Street coleus were compared to the LC-MS/MS data.

Anthocyanin Imaging in Broad Street Coleus and the Malonylshisonin Pathway

Figure 7 shows the pre-ablation optical image and false-color ion maps for anthocyanins in Broad Street coleus. For the images shown, there are 35 ablation tracks 125 μm wide × 250 μm apart. Each ablation track took 50 s at a speed of 0.5 mm/s.

As expected, anthocyanins were concentrated in the red area of the leaf, particularly in the areas around the veins. This is understandable as veins transport anthocyanins to various parts of the leaves, and a small reserve of anthocyanins is stored in the veins for times of stress.[33,34] The only anthocyanin spatial images which appear to have some accumulation in the green area are those for cyanidin (m/z 287.0550) and cyanidin-3-O-β-D-glucoside (m/z 449.1084). These ions are isomers of the flavonoids kaempferol and kaempferol-3-O-β-D-glucoside. Tandem MS measurements were taken of both ions in the green and red portions of Broad Street coleus. Representative tandem MS spectra of the isomers cyanidin and kaempferol is show in Figure 8a. These results show that cyanidin was present in the red portion, while kaempferol was present in the green portion, shown by tandem MS measurements on a new Broad street leaf (figure 8b). MS/MS was taken of a single line in the green portion while a separate line was ablated in the red portion. Collision energies were 20 eV.

Malonylshisonin was the most abundant anthocyanin present in Broad Street coleus. It has been studied previously in *Perilla ocimoides* leaves and has a structure of *3-0-(6-0-(E)-p-coumaryl-p- D-glucopyranosyl)-5-0-(6-0-malonyl-p- D-gluco pyranosyl)cyanidin*.[35] It is the

final product of the super pathway of malonylshisonin biosynthesis, which is common in plants and higher organisms (Fig. 9).[36-38] The pathway begins with cyanidin (287.0555 Da) which becomes cyanidin-3-O-β-D-glucoside (449.1084 Da). The pathway than splits into either cyanidin-3,5-di-O-β-D-glucoside (611.1612 Da) or cyanidin-3-(p-coumaroyl)-glucoside (595.1451 Da). The pathway then converges to form shisonin (757.1980 Da) and eventually malonylshisonin (843.1984 Da).

Using mass spectrometry imaging, we were able to determine that malonylshisonin is formed in Broad Street coleus through cyanidin-3-(p-coumaroyl)-glucoside. The ion, cyanidin-3,5-di-O-β-D-glucoside, was not present in the mass spectrum, thus this pathway was not used. To verify that this ion can be seen with our instrument, another variegated hybrid of coleus, Mosaic, was tested. Cyanidin-3,5-di-O-β-D-glucoside (m/z 611.1513) was present in mosaic and its image is shown in Figure 10**.**

Anthocyanin Imaging in Wizard Jade Coleus

Upon initial review of the LC-MS and spatially integrated LAESI-MS data, no anthocyanins were found in Wizard Jade coleus. However, when images were processed, shisonin and malonylshisonin were present in a small portion of the leaf and at very low intensities (Fig. 11). Upon further inspection, only a single time resolved mass spectrum at 1.35 min in a 2 minute acquisition showed these ions. Figure 12 shows the time resolved mass spectrum from abaltion trench 27. Shisonin and malonylshisonin were present in the stem of the leaf which we believe are there to protect the leaf from damage, much like the reserves found in the veins of Broad Street coleus.[33,34] The spatial resolution of LAESI-MS allowed measurement of these low –abundance compounds, which were not found by chemical extraction techniques,

like LC-MS. MS images were made for other compounds found in Wizard Jade (such as carotenes) and can be found in supplementary materials.

Conclusions

Studies have reported that anthocyanins are water soluble pigments that contribute to the red coloration in coleus plants. These pigments are synthesized in the cytoplasm and actively transported and accumulate in the vacuoles of epidermal or mesophyll cells. To determine anthocyanin variations in both Broad Street and Wizard Jade coleus leaves laser ablation electrospray ionization was used. The use of an ultraviolet laser in this experiment helped any anthocyanins present in the samples to easily be absorbed and detected in the mass spectrometer. Several anthocyanin species were identified in Broad Street, but more surprisingly, anthocyanins were detected in Wizard Jade, a green and yellow variety of coleus. Two interesting compounds, shisonin and malonylshisonin, were found only in a few localized areas of the leaves and could not be observed by spatially-integrated methods.

When LAESI is coupled with mass spectrometry imaging, we were also able to determine the steps in the malonylshisonin biosynthesis pathway. Since there is little sample preparation, LAESI MSI is a quicker, sensitive option than assays or other forms of mass spectrometry to investigate biological processes in plants. Our results showed that Broad Street coleus favored unique steps in the malonylshisonin biosynthesis pathway and demonstrated the sensitivity of LAESI in detection of small abundant molecules in coleus Jade.

Acknowledgments

References

1) Holton, T.A., Cornish, E.C., Genetics and Biochemistry of Anthocyanin Biosynthesis. *The Plant Cell.* **1995**, 7: 1071-1083.

2) Burns K.C., Dalen J.L., Foliage color contrasts and adaptive fruit color variation in a bird-dispersed plant community. *Oikos*. **2002**, 96(3):463–469.

3) Chalker-Scott L., Environmental significance of anthocyanins in plant stress responses. *Photochem Photobiol*. **1999**, 70(1):1–9.

4) McKown R, Kuroki G, Warren G. Cold responses ofArabidopsis mutants impaired in freezing tolerance. JExpBot. 1996;47(305):1919–1925.

5) Nozzolillo C, Isabelle P, Andersen OM, Abou-Zaid M. Anthocyanins of Jack Pine *(Pinus banksiana)* seedlings. *Can J Bot*. **2002**, 80(7):796–801.

6) Mendez M., Gwynn-Jones D., Manetas Y., Enhanced UV-B radiation under field conditions increases anthocyanin and reduces the risk of photoinhibition but does not affect growth in the carnivorous plant *Pinguicula vulgaris*. *New Phytol*. **1999**, 144(2): 275–282.

7) Solecka D., Kacperska A., Phenylpropanoid deficiency affects the course of plant acclimation to cold. *Physiol Plant*. **2003**, 119(2):253–262.

8) Hale K.L., McGrath S.P., Lombi E., et al., Molybdenum sequestration in Brassica species. A role for anthocyanins?. *Plant Physiol*. **2001**, 126(4):1391–1402.

9) Hale K.L., Tufan H.A., Pickering I.J., et al., Anthocyanins facilitate tungsten accumulation in Brassica. *Physiol Plant*. **2002**, 116(3):351–358.

10) Krupa Z., Baranowska M., Orzol D,. Can anthocyanins be considered as heavy metal stress indicator in higher plants?. *Acta Physiol Plantarum*. **1996**, (18): 147–151.

11) Jansen, M.A.K., Gaba, V., Greenberg, B.M., Higher plants and UV-B radiation: Balancing damage, repair and acclimation. *Trends Plant Sci*. **1998**, (3): 131-135.

12) Stapleton, A.E., Ultraviolet radiation and plants: Burning questions. *Plant Cel.l* 1992, (4): 1353-1358.

13) Markham K.R., Techniques of Flavonoid Identification. *London, UK: Academic Press.* **1982**.

14) Holton, T., Cornish, E., Genetics and Biochemistry of Anthocyanin Biosynthesis. *The Plant Cell*. **1995**, (7): 1071-1083.

15) Nishimura T., Ohyama K., Goto E., Inagaki N., Morota T., Ultraviolet B radiation suppressed the growth and anthocyanin production of Perilla plants grown under controlled environments with artificial light. *Acta Hortic*. 2008, 797: 425–429.

16) Nguyen P., Valeriano D., The role of light on foliage colour development in coleus (Solenostemon scutellarioides (L.) Codd). *Plant Physiology and Biochemistry.* **2009**, 47: 934–945.

17) Burger J., Edwards G., Photosynthetic Efficiency, and Photodamage by UV and Visible Radiation, in Red versus Green Leaf Coleus Varieties . *Plant Cell Physiol*. **1996**, 37(3): 395-399.

18) Chalker-Scott, L., Do Anthocyanins Function as Osmoregulators in Leaf Tissues? *Advances in Botanical Research.* **2002**, 37: 103–106.

19) Lee Y. J., Perdian D. C., Song Z., Yeung E. S., Nikolau B. J., Use of mass spectrometry for imaging metabolites in plants. *The Plant Journal*. **2012**, 70: 81–95.

20) Nemes P., Vertes A., Laser ablation electrospray ionization for atmospheric pressure, in vivo, and imaging mass spectrometry. *Anal. Chem*. **2007**, 79: 8098.

21) Robichaud G., Barry J., Muddiman D., IR-MALDESI mass spectrometry imaging of biological tissue sections using ice as a matrix. *J Am Soc Mass Spectrom*. 2014, 25:319–328.

22) Boughton B.A., Thinagaran D., Sarabia D., Bacic A., Roessner, U., Mass spectrometry imaging for plant biology: a review. *Phytochem Rev.* **2016**, 15:445–488.

23) Lee Y. J., Perdian D. C., Song Z., Yeung E. S., Nikolau, B. J. Use of mass spectrometry for imaging metabolites in plants. *The Plant Journal*. 2012, 70: 81–95.

24) Klein A., Yagnik G., Hohenstein J., Zhiyuan J., Zi J., Reichert M., MacIntosh G., Yang B.,   Peters R., Vela J., Lee Y-L., Investigation of the Chemical Interface in the Soybean–Aphid and Rice–Bacteria Interactions Using MALDI-Mass Spectrometry Imaging. *Anal. Chem.* **2015**, 87 (10): 5294–5301.

25) Shroff R., Schramm K., Jeschke V., Nemes P., Vertes A., Gershenzon J., Svatos A., Quantification of plant surface metabolites by MALDI mass spectrometry imaging: glucosinolates on *Arabidopsis thaliana* leaves. *The Plant Journal.* **2015**. 81: 961-972.

26) Wu, X., Gu, L., Prior, R. L. & Mckay, S. Characterization of Anthocyanins and Proanthocyanidins in Some Cultivars of Ribes, Aronia, and Sambucus and Their Antioxidant Capacity. *Journal of Agricultural and Food Chemistry.* **2004.** 52: 7846–7856.

27) Smith C.A., O'Maille G., Want E.J., Qin C., Trauger S.A., Brandon T.R., Custodio D.E., Abagyan R., Siuzdak G., METLIN: a metabolite mass spectral database. *Ther Drug Monit* [Internet]. **2005**, 27 :747-51. https://metlin.scripps.edu/

28) Kegg Pathway database search. http://www.genome.jp/kegg/pathway.html

29) MetaCyc Compound Search. https://metacyc.org/cpd-search.shtml

30) Chambers M.C., MacLean, B., Burke R., Amode D., Ruderman D.L., Neumann S., Gatto L.,Fischer B., .Pratt B., Egertson J., Hoff K., Kessner D., Tasman N., Shulman N., Frewen B., Baker T.A., BrusniakM.-Y., Paulse C., Creasy D., Flashner L., Kani K., Moulding C., Seymour S.L., Nuwaysir L.M., Lefebvre B., Kuhlmann F., Roark J., Rainer P., Detlev S., Hemenway T., Huhmer A., Langridge J., Connolly B., Chadick T., Holly K., Eckels J., Deutsch E.W., Moritz R.L, Katz J.E., Agus D.B., MacCoss M., Tabb D.L., Mallick P., A cross-platform toolkit for mass spectrometry and proteomics. *Nature Biotechnology.* **2012**, 30:918.

31) Race I.M., Styles I.B., Bunch J., Inclusive sharing of mass spectrometry imaging data requires a converter for all. *J. Proteomics.* **2012**, *75*: 5111.

32) Klinkert I., Chughtai K., Ellis S.R., Heeren R.M.A., Methods for full resolution data exploration and visualization for large 2D and 3D mass spectrometry imaging datasets. *Int. J. Mass Spectrom.* **2014**, 362: 40.

33) Hughes N. M., Neufeld H. S., Burkey, K. O., Functional role of anthocyanins in high-light winter leaves of the evergreen herb *Galax urceolata*. *New Phytologist.* **2005**, 168: 575–587.

34) Steyn W. J., Wand S. J. E., Holcroft D. M. Jacobs G., Anthocyanins in vegetative tissues: a proposed unified function in photoprotection. *New Phytologist.* **2002**, 155: 349–361.

35) Kondo T., Tamura H., Yoshida K., Goto T., Structure of Malonylshisonin, a Genuine Pigment in Purple Leaves of Perilla ocimoides L. var. crispa Benth. *Agric. Bioi. Chern.* **1989**, 53 (3):797-800.

36)Fujiwara H., Tanaka Y., Fukui Y., Ashikari T., Yamaguchi M., Kusumi T., Purification and characterization of anthocyanin 3-aromatic acyltransferase from Perilla frutescens**. *Plant Science*. **1998,** 137: 87-94.

37)Yonekura-Sakakibara K., Tanaka Y., Fukuchi-Mizutani M., Fujiwara H., Fukui Y., Ashikari T., Murakami Y., Yamaguchi M., Kusumi T., Molecular and biochemical characterization of a novel hydroxycinnamoyl-CoA: anthocyanin 3-O-glucoside-6"-O-acyltransferase from Perilla frutescens. *Plant Cell Physiol.* **2000**, 41(4): 495-502.

 38) Yamazaki M., Gong Z., Fukuchi-Mizutani M., Fukui Y., Tanaka Y., Kusumi T, Saito K., Molecular cloning and biochemical characterization of a novel anthocyanin 5-O-glucosyltransferase by mRNA differential display for plant forms regarding anthocyanin**. *J Biol Chem*. **1999**, 274(11): 7405-11.

Tables

Table 1. Metabolites identified in Broad Street and Wizard jade coleus by LC-MS

Peak	$[M]^+$ (m/z)	MS/MS fragments (m/z)	Proposed Anthocyanin Structure
3	757.3	287.0,449.0,595.1	Cyanidin 3-O-(6-O-p-coumaroyl)glucoside-5-O-glucoside
6	857.3	287.0, 549.1, 595.1	Cyanidin-3-rutinoside-5-succinyl-glucoside
7	857.3	287.0 595.2,649.1	Cyanidin-3-rutinoside-5-succinyl-glucoside
8	843.3	287.0, 535.0, 595.1, 799.1	Cyanidin-3-3-O-(6-O-p-coumaroyl)glucoside-5-malonyl-glucoside
9	957.3	287.0, 595.2, 649.1	Cyanidin-3-rutinoside-5-(succinyl)(succinyl)-glucoside
10	957.4	287.0, 595.2, 649.1	Cyanidin-3-rutinoside-5-(succinyl)(succinyl)-glucoside
11	943.3	287.0, 595.2, 635.1	Cyanidin-3-rutinoside-5-malonyl-succinyl-glucoside

Table 2. Metabolites identified in Broad Street and Wizard jade coleus by UV-LAESI under atmospheric pressure. Carotenes in Jade coleus are suggested due to mass defect of ~0.4xxx.

| Plant	Suggested Assignment	Mean Measured (Da)	Accurate Mass (Da)	Δppm	Measured Product Ions
Broadstreet	Caffeic Acid	163.0364	163.0395	19	145,135,117,89
	Apigenin	271.0615	271.0606	3	212,194,153
	Cyanidin	287.0550	287.0550	0	
	Rosmarinate	383.0751	383.0737	3	271,221,163
	Cyanidin 3-O-(6-O-p-coumaroyl) glucoside	595.1451	595.1446	0.8	287
	Shisonin	757.1926	757.1974	6	595, 449, 287, 147
	Malonylshisonin	843.1984	843.1978	0.7	595, 535, 287
	Cyanidin 3-(6"-p-coumarylglucoside)-5-4", 6"-dimalonylglucoside	929.1982	929.1982	0	843,621, 595, 287
Jade	Caffeic Acid	163.0364	163.0395	19	145,135,117,89
	Apigenin	271.0636	271.0606	11	212,194,153
	Kaempferol	287.0557	287.0550	2	
	ID Unknown	351.1137	--	--	333,191,163
	Rosmarinate	383.0751	383.0737	3	271,221,163
	ID Unknown	399.0544	--	--	383, 353, 296, 163
	ID Unknown-possible carotene	651.4186	--	--	637, 581
	ID Unknown-possible carotene	813.4608	--	--	271, 163
	ID Unknown-possible carotene	911.6208	--	--	271, 163
	ID Unknown-possible carotene	975.4839	--	--	637

Figures
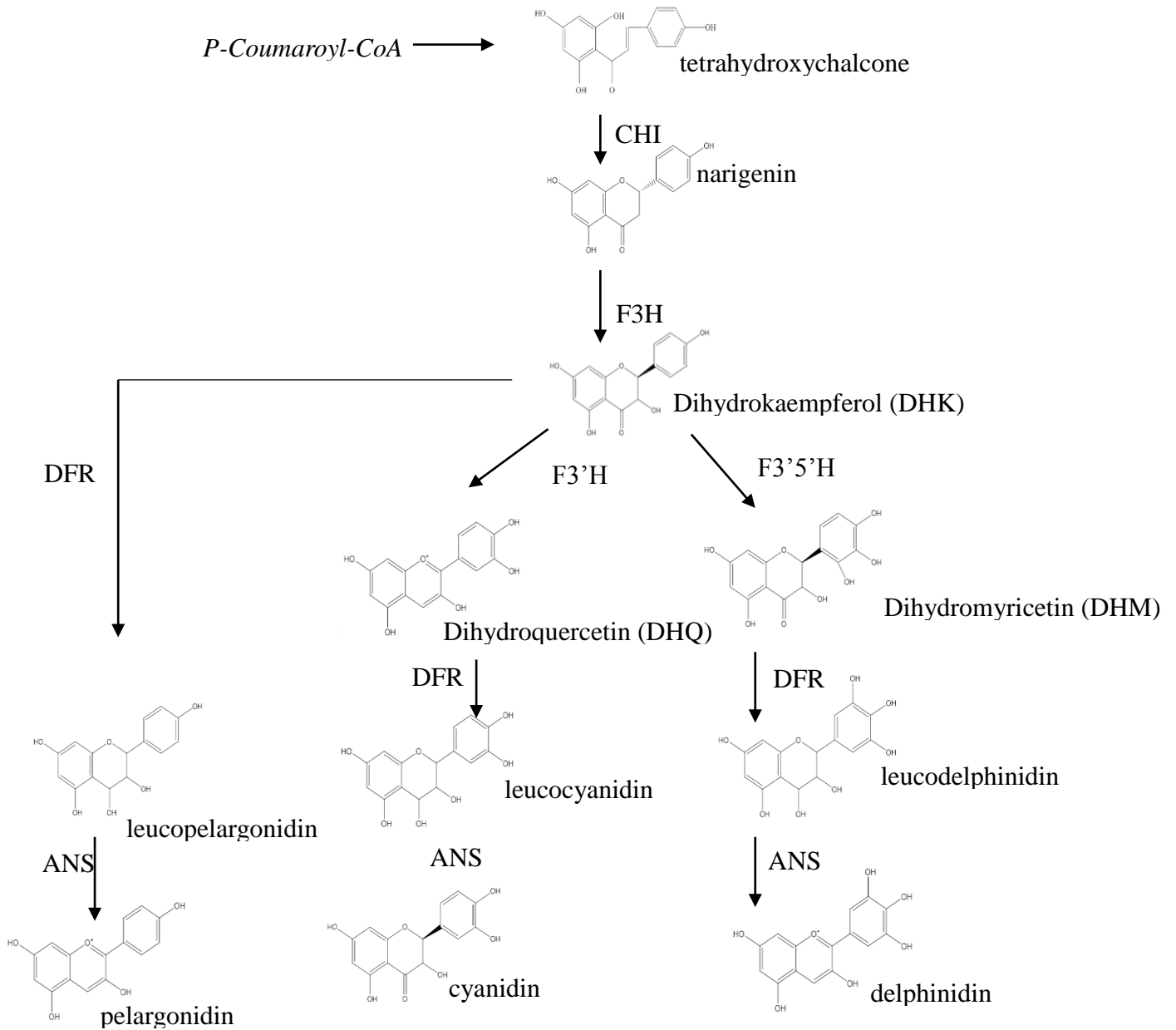
Figure 1. Anthocyanin biosynthesis. F3H is flavonone 3-hydroxylase, F3'H is flavonoid 3'-hydroxylase, F3'5'H is flavonoid 3'5'-hydroxylase, DFR is dihydroflavonol 4-reductase, and ANS is anthocyanidin synthase
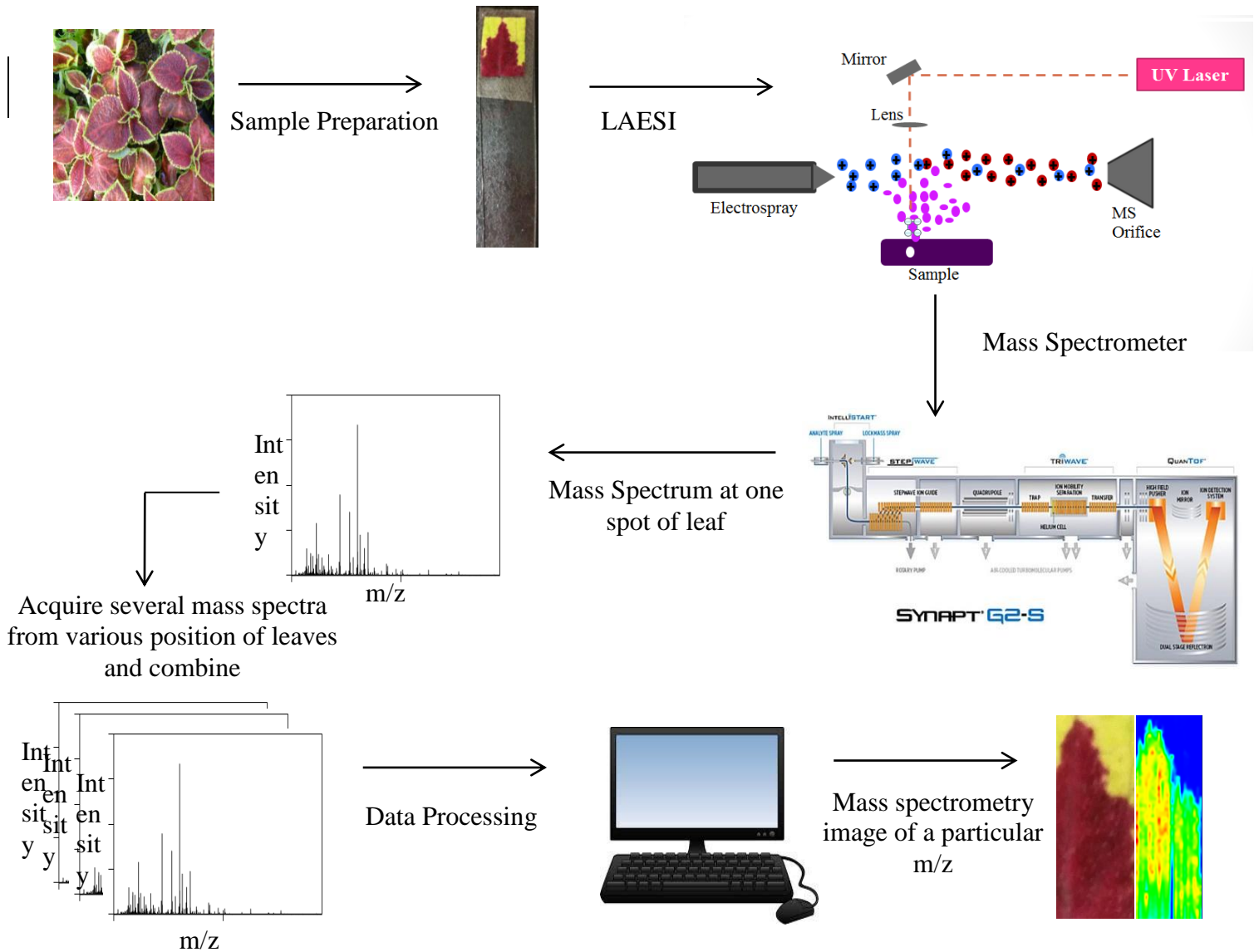
Figure 2. Typical LAESI-MSI experiment**.** Once the leaves are picked, they are put attached to a glass slide by double sided tape. The sample is ablated by a UV laser and an external electrospray source turns the ablated sample into ions. These ions can enter the mass spectrometer and an individual mass spectrum is produced. Over the course of an imaging run, every time the laser hits the sample, a mass spectrum is produced. Every individual spectrum is combined and data processed. Images can now be created for all m/z.
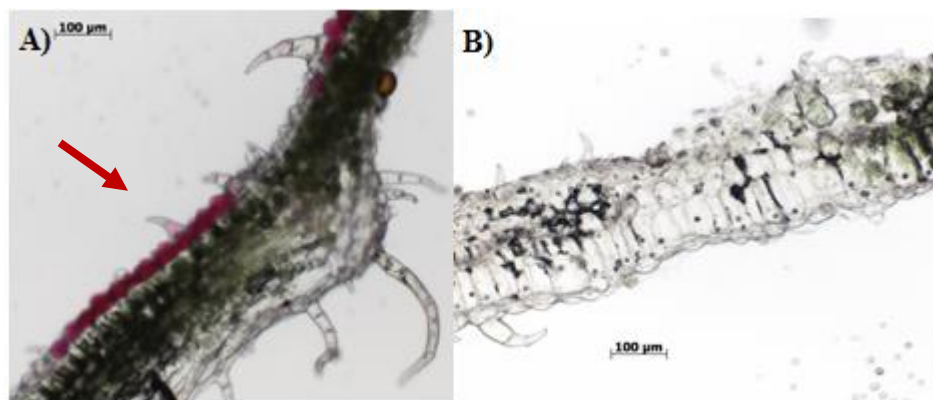
Figure 3. Tissue sectioning of coleus leaves at 100 µm thickness and a magnification of 10X. A) Tissue section of broadstreet coleus. Anthocyanins (red spots, indicated by red arrow) are accumulated on the upper epidermal layer of the leaf. B) Tissue section of Jade coleus. No anthocyanins are present, although there is a greater accumulation of chlorophyll than Broadstreet coleus.
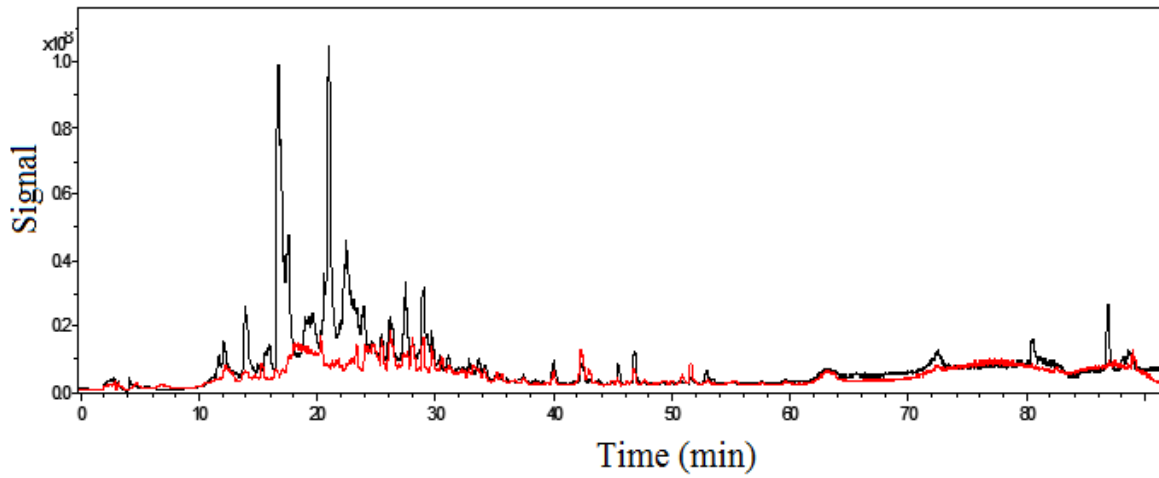
Figure 4. LC-MS comparison of Broadstreet coleus (black) and wizard jade (red). No anthocyanins were found in wizard jade.
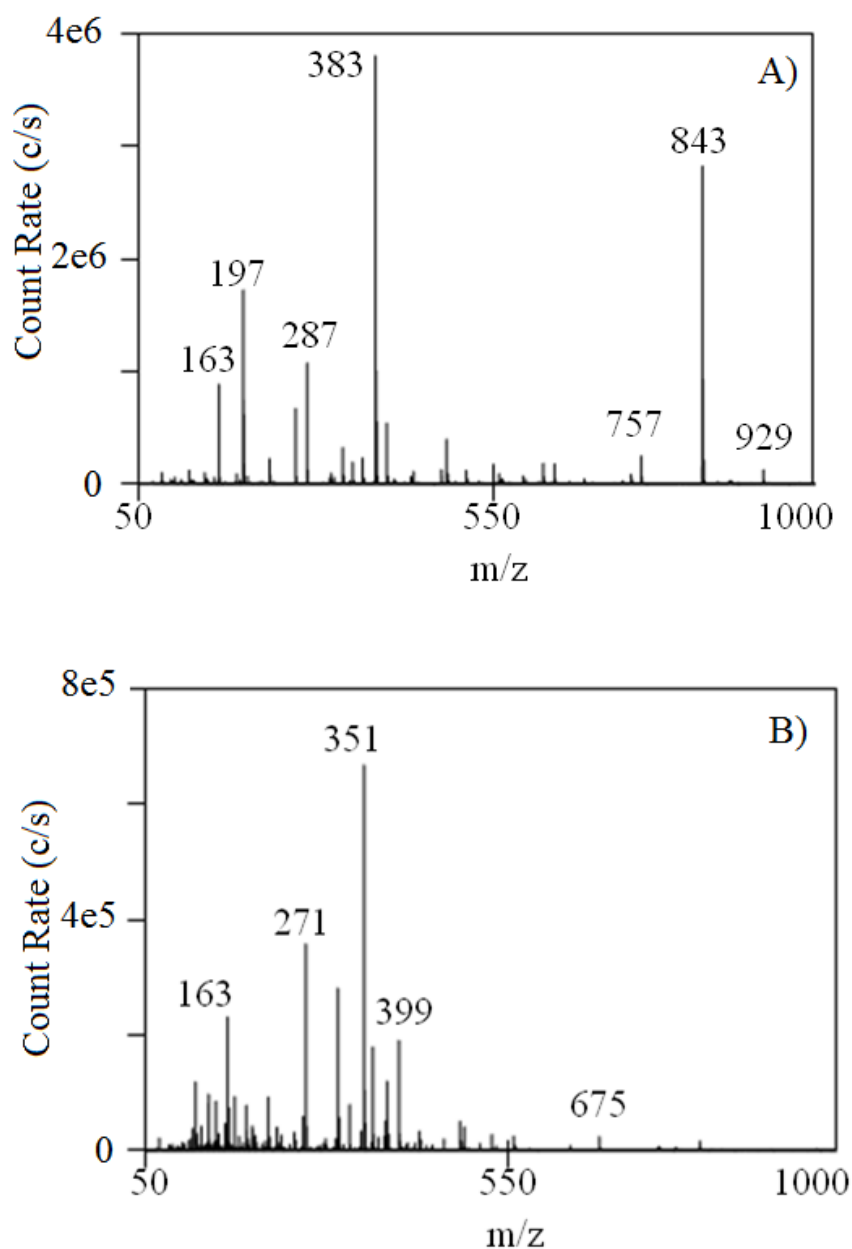
Figure 5. Integrated positive ion mass spectrum obtained from one ablation track in A) Broad Street coleus and B) Wizard Jade coleus. The ESI background has been subtracted from these LAESI spectra.
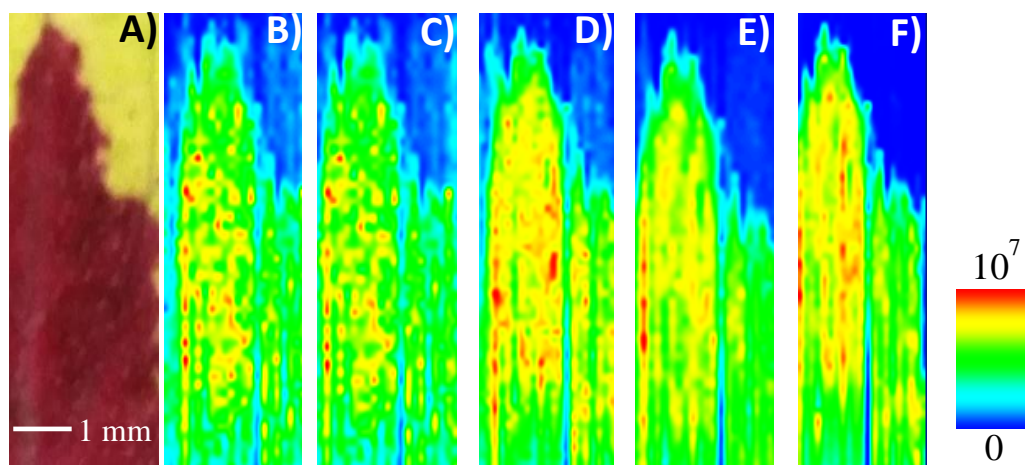
Figure 6. Images for positive ions from broadstreet coleus.   a) Optical photograph before ablation. False color ion maps of broadstreet at b) m/z 287.0535, cyanidin, c) m/z 449.1177, Cyanidin-3-O-β-D-glucoside, d) m/z 595.1498, Cyanidin-3-(p-coumaroyl) glucoside, e) m/z 757.1926, shisonin, and f) m/z 843.2001, malonylshisonin.

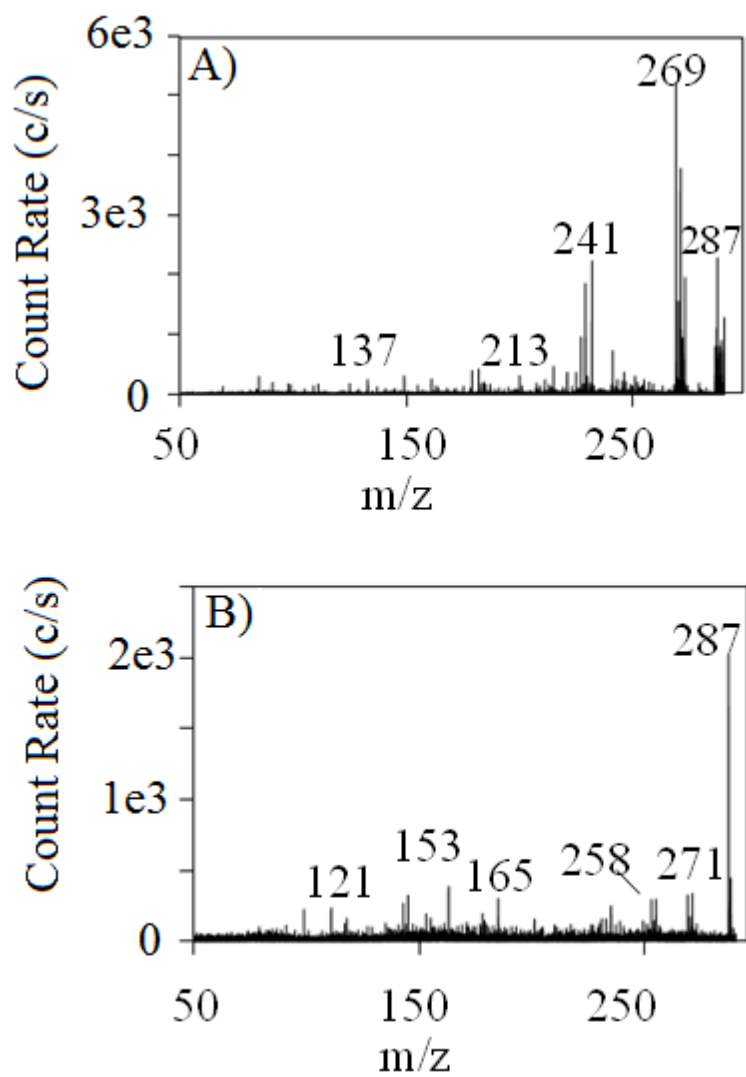**Figure 7.** Typical tandem MS results for isomeric positive ions from broadstreet: A) tandem MS of spectrum of cyanidin and, B) tandem MS spectrum of kaempferol. The collision energies for these experiments were 30 eV.

Cyanidin ($C_{15}H_9O_6$)
Accurate Mass: 287.0555

Cyanidin-3-O-β-D-glucoside
Accurate Mass: 449.1084 Da

Cyanidin-3,5-di-O-β-D-glucoside
Accurate Mass: 611.1612 Da

Cyanidin-3-(p-coumaroyl)-glucoside
Accurate Mass: 595.1451 Da

Shisonin
Accurate Mass: 757. 1980 Da
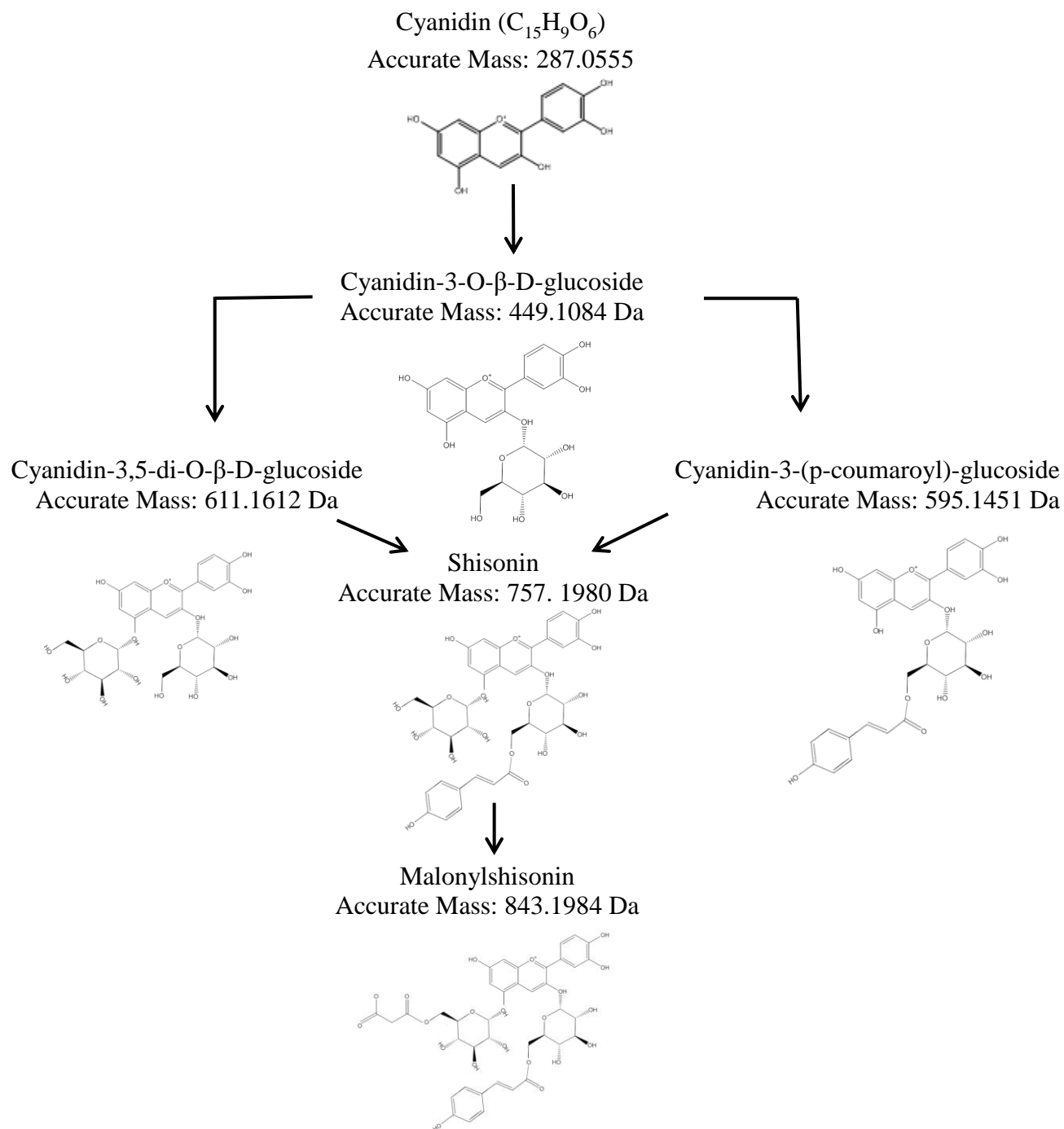
Malonylshisonin
Accurate Mass: 843.1984 Da

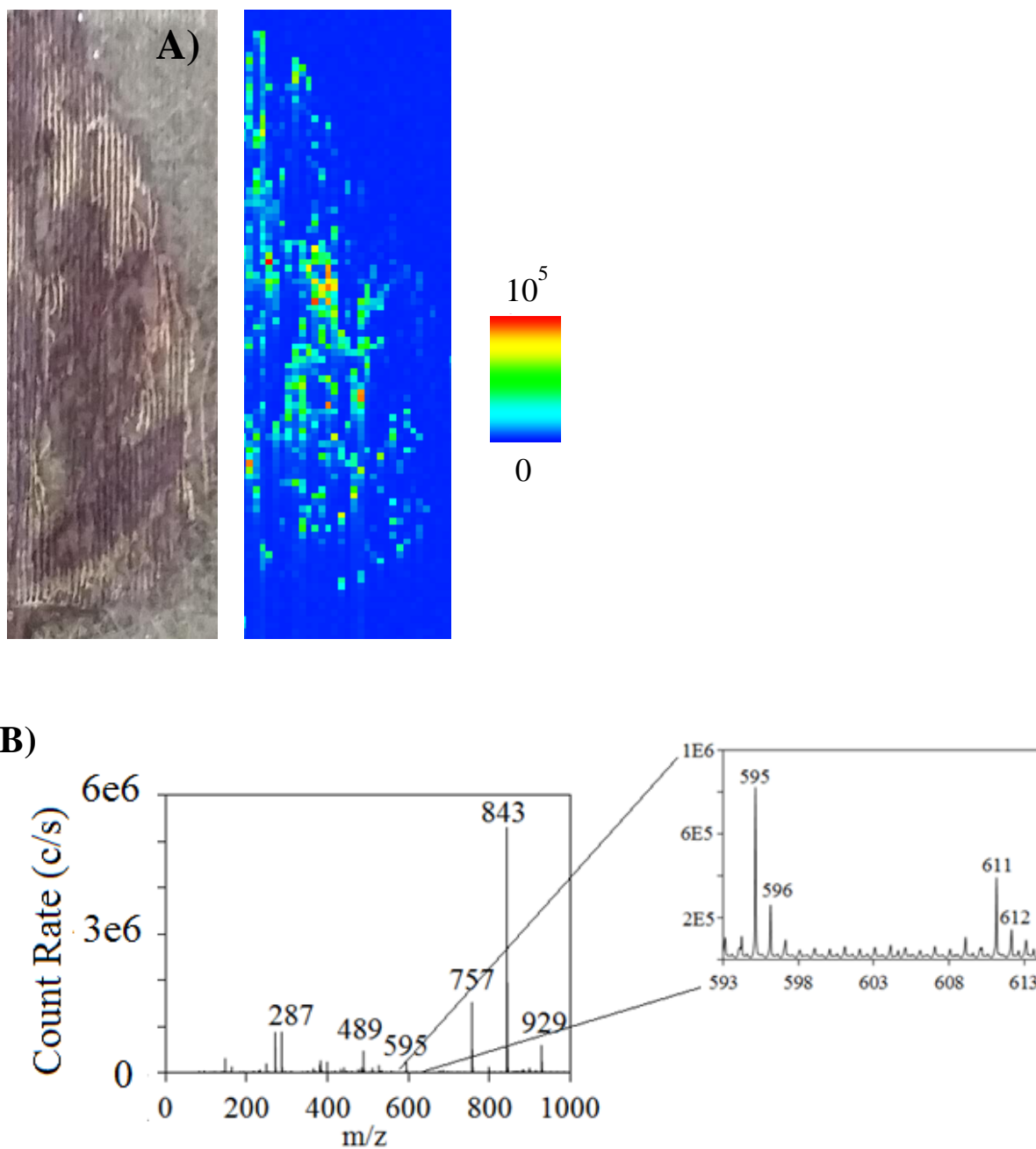**Figure 8.** The biosynthetic pathway of malonylshisonin from cyanidin.

Figure 9. Mosaic coleus. A) image for cyanidin-di-glucoside (m/z 611.1513 Da). B) Integrated positive ion mass spectrum obtained from one ablation track in mosaic coleus acquired by atmospheric-pressure UV-LAESI. The ESI background has been subtracted from this LAESI spectrum. Inset shows the presence of cyanidin-di-glucoside at m/z 611.1513.
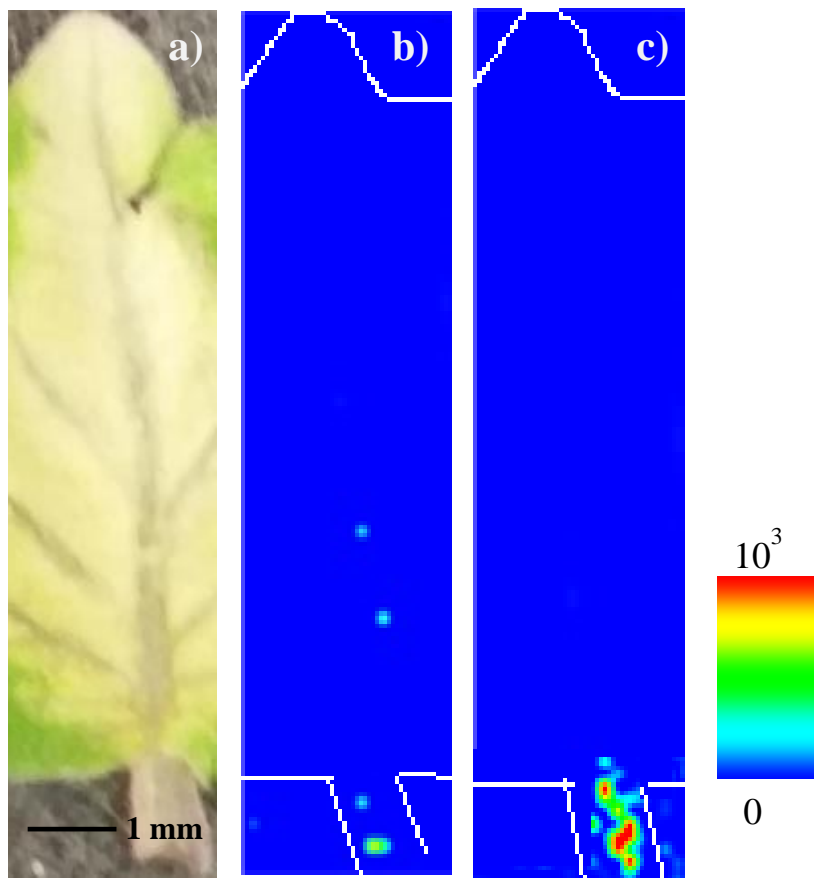
Figure 12. Images for positive anthocyanin images from jade coleus: a) optical photograph of jade coleus prior to ablation. False color ion maps of jade at b) m/z 757.1986, shisonin, and, c) m/z 843.1920, malonylshisonin.
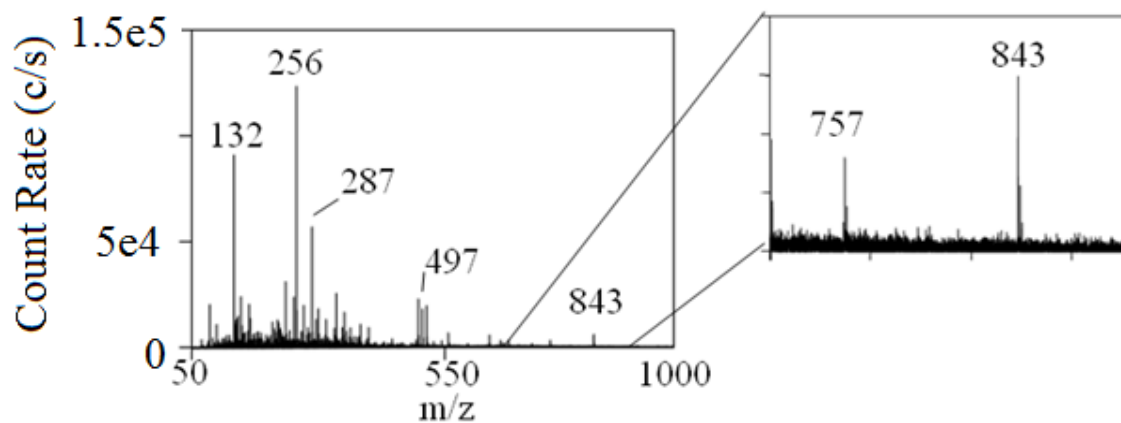
Figure 13. Time resolved mass spectrum of jade coleus taken at 1.36 minutes during a 2 minute acquisition. Inset (~5X zoomed) show the presence of shisonin (m/z 757.1986) and malonylshisonin (m/z 843.1920). This spectrum is not background subtracted.
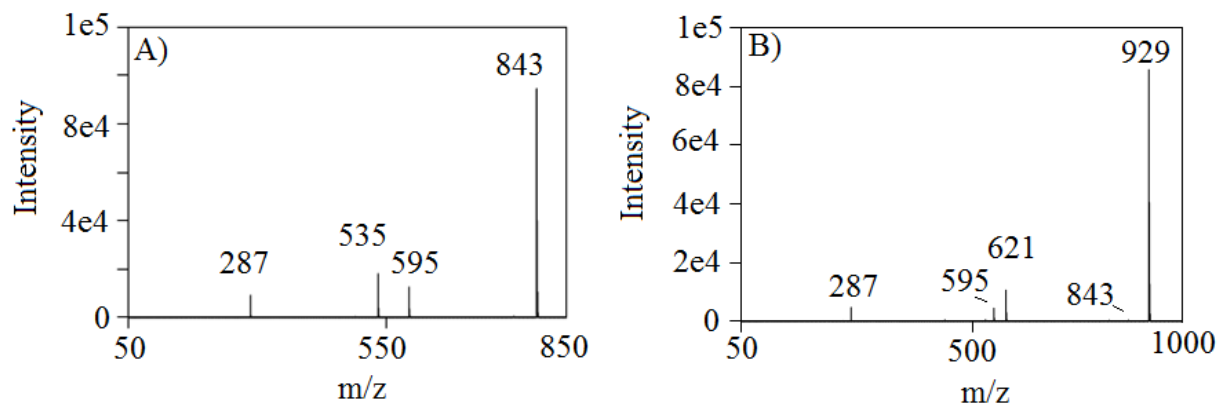
Figure S1. MS/MS of the red section of broadstreet coleus taken by ambient-pressure UV-LAESI for A) m/z 843, malonylshisonin, and B) m/z 929, Cyanidin 3-(6"-p-coumarylglucoside)-5-4", 6"-dimalonylglucoside. The collision energy for both was 15 eV.
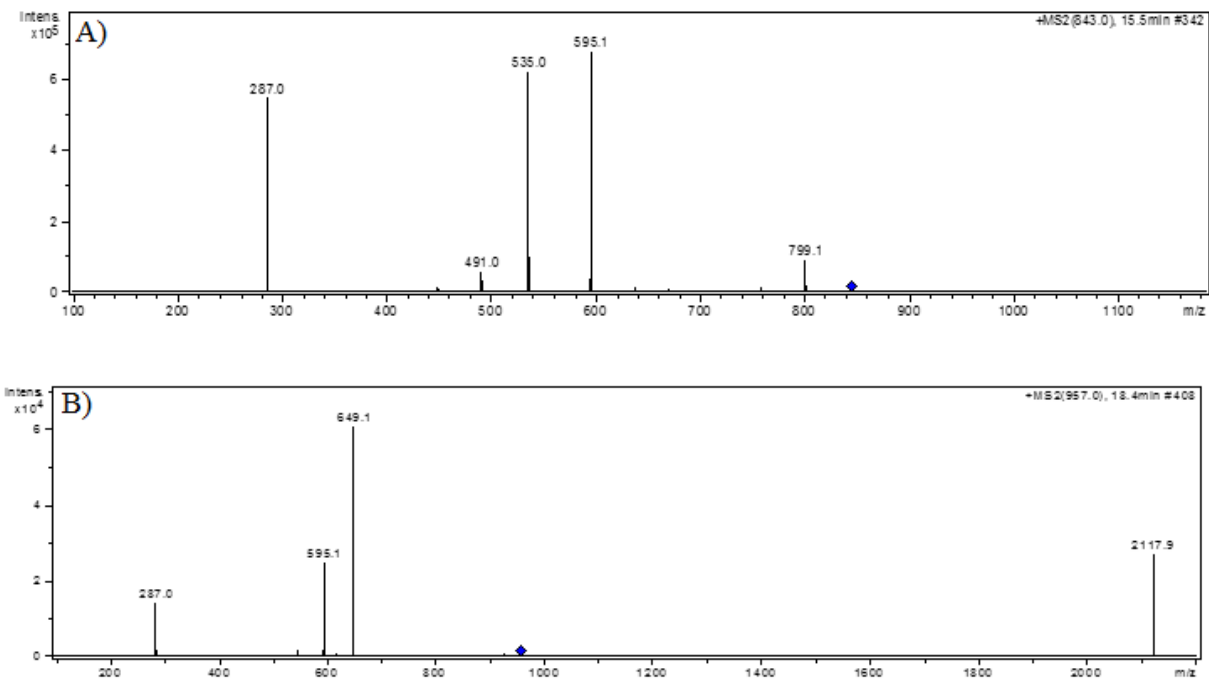
Figure S3. MS/MS of the red section of broadstreet coleus taken by LC-MS. A) m/z 843, malonylshisonin, and B) m/z 929, Cyanidin 3-(6''-p-coumarylglucoside)-5-4'', 6''-dimalonylglucoside. The results are similar to those taken by UV-LAESI

Figure S3. Optical and positive images in Jade coleus leaves taken by ambient-pressure UV-LAESI. Due to the mass defect, it is assumed that the images represent lipids, although the actual IDs are unknown.

CHAPTER 4. DETERMINING LIPID CHANGES DURING AUTOPHAGY IN *ARABIDOPSIS THALIANA* PLANTS USING MASS SPECTROMETRY IMAGING

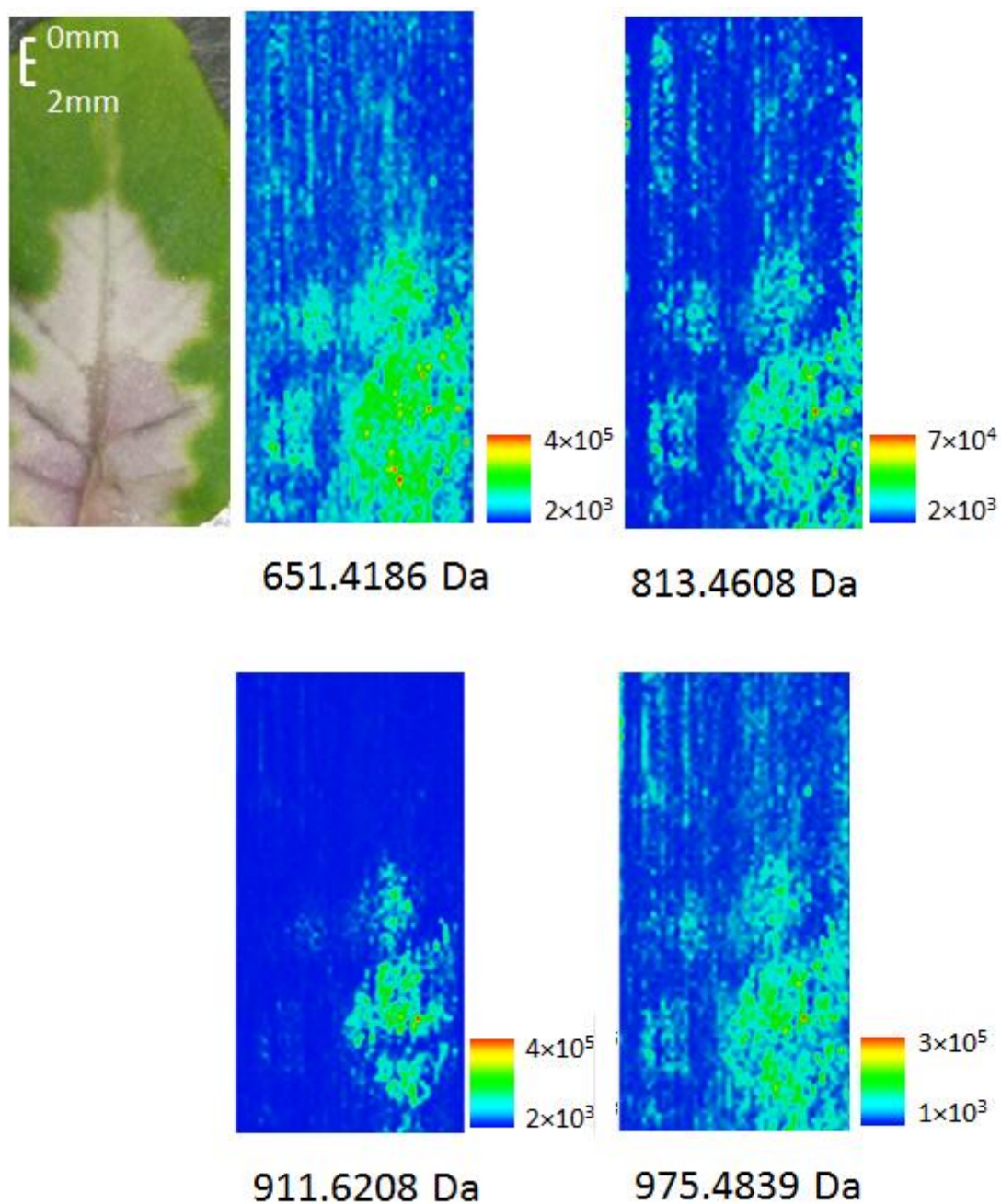Galayda, K.J.[1,2], Ding, G.[3], Mugume, Y. [4], McVey, P.A.[1,2], Bassham, D.[4] , Nikolau, B.[1,3] and Houk, R.S.[1,2]

[1]*The Ames Laboratory, Iowa State University, Ames, Iowa, 5011, USA*

[2]*Department of Chemistry, Iowa State University, Ames, Iowa, 5011, USA*

[3]*Department of Biochemistry/Biophysics & Molecular Biology, Iowa State University, Ames, Iowa, 5011,USA*

[4]*Department of Genetics. Development & Cell Biology, Iowa State University, Ames, Iowa, 5011, USA*

Abstract

Ultraviolet laser ablation electrospray ionization (UV-LAESI) was used to study differences in wild type and mutant *atg5 Arabidopsis thaliana* leaves when subjected to autophagy. To induce autophagy, nitrogen starvation was used. Both roots and leaves were imaged. In roots, the lipids PE(34:2), PE(36:2), PI(34:2), and PI(36:2) were present in wild type, but in the *atg5* mutant they were at lower, undetectable levels. This is consistent with previous lipidomic data. In leaves, the lipids PC(34:2), PI(34:2), PE(34:2), and PE(34:3) show higher abundance in nitrogen rich conditions in both wild type and *atg5*. This observation suggests that autophagy conditions hinder the synthesis of these lipids. In autophagy conditions, PC(34:3) and PI(34:3) in *atg5* appear to be higher than in nitrogen rich conditions. These data are also consistent with on-going research being conducted in a collaborative project with our lab. UV-

LAESI mass spectrometry imaging requires little sample preparation and is a relatively fast technique and could offer an alternative in understanding autophagy in plants.

Introduction

Lipids are hydrophobic molecules which serve many important functions, such as energy storage and light absorption. They also contribute to the structure of membranes.[1-4] There are several types of lipids including certain fats and oils, waxes, glycolipids, and phospholipids. While each have their own role in living organisms, particularly in plants, phospholipids are perhaps the most important.[5-6]

Phospolipids are one of the main structural components of membranes. They aid in plant growth and help with cellular responses to environmental changes and stressors.[7,8] There are several classes of phospholipids including phosphtatidylcholines (PC), phosphtatidylethanolamines (PE), and phosphatidylinositol (PI), each serving a specific purpose. For example, PC is the most abundant of the phospholipids and serves as the bulk structural component of membranes, which helps plants grow.[9,10] PE is the second most abundant whereas PI is found in small amounts in plants.[11,12]

Since lipids are essential for plants, an important concept to study is autophagy and how lipids affect the process. Autophagy protects cells during times of stress (starvation etc.) and contributes nutrients and other materials to promote cellular remodeling when needed.[13-15] Lipids can aid the autophagy process by controlling certain fundamental aspects such as a) acting as membrane-bound signalers to mediate membrane deformation in times of duress,[16] and b) controlling membrane dynamics by affecting physio-chemical properties of lipid bilayers.[17]

Arabidopsis thaliana is commonly used to understand these phenomena. It is a small flowering plant that has a small genome compared to other flora. Much is known of the genome; free-access websites, such as arabidopsis.com, give detailed information on the lipids that are present in the plant. There have been numerous studies on this subject including one by Contento[13] et al., where a fluorescent dye monodansylcadaverine (MDC) and a green fluorescent labelled protein (GFP)-AtATG8e was used to visualize autophagy in *Arabidopsis.*

The majority of research investigating lipids and autophagy in *Arabidopsis* utilize analytical methods such as assays, gas chromatography (GC), and transmission electron microscopy (TEM).[18-20] While most of these processes give quantitative data , they are labor intensive involving dissection, fractionation, and/or extraction of the analyte (with the exception of TEM). Mass spectrometry imaging (MSI), a technique which requires less sample preparation and can obtain a complete data set from one entire sample, has proven to be a good complementary method.[21-23]

One of the main advantages of MSI is its high resolution spatial localization capabilities.[24] There are many variations of MSI including matrix assisted laser desorption (MALDI), desorption electrospray ionization (DESI), and laser ablation electrospray ionization (LAESI), each with its own advantages and disadvantages as described in a number of reviews.[24-28] In this experiment, LAESI, an atmospheric pressure technique, was used since there is virtually no sample preparation (i.e. no matrix coating), and it is sensitive enough to see many interesting compounds directly in plants.[29]

To date, there has been no attempt to use MSI to compare normal growth conditions to autophagy conditions. In this experiment, autophagy of wild type (WT) *Arabidopsis* and mutant *atg5 Arabidopsis*, an autophagy-related protein that is essential for autophagosome formation[30],

was investigated by LAESI MSI. Autophagy was induced by nitrogen starvation. Images from WT and *atg5* in nitrogen "rich" (+N, no autophagy) conditions were compared to those in nitrogen "poor" (-N, autophagy induced) conditions. Additionally, we compare these data to a lipidomic profile data set, which has been obtained previously. Results from MSI were compared to a lipidomic profile data set to see if MSI can be a good addition to lipid profiling.

<p style="text-align:center;">**Experimental**</p>

Plant Growth

The hydroponic method was used for growing seedlings.[31] Briefly, seeds were sterilized and kept in dark conditions for 48 hours. Seeds were then gathered and grown on mesh measuring about 3.5 cm × 4 cm. The mesh was placed on 0.5 MS Plates made of nutrient solid Murashige-Skoog medium with vitamins (MS) (MSP09; Caisson Labs), 1% sucrose, 2.4 mM 2-(*N*-morpholino)ethanesulfonic acid (MES) (pH 5.7), and 0.8% (w/v) phytoagar (PTP01; Caisson Labs). Seeds for mutant type *Arabidopsis thaliana* were grown by the Vierstra lab and growth conditions can be found elsewhere.[32] Two meshes were used per plate. After 5 days the seedlings were transferred by lifting the mesh carefully off the media. Care was used to avoid damage on the roots and to ensure sterile conditions. Seedlings were then transferred to one of two meshes in liquid media. The first was +N (no autophagy) which contained 0.5 mM nutrient liquid Murashige-Skoog medium with vitamins (MS) (MSP09; Caisson Labs), 1% sucrose, and 2.4 mM MES pH 5.7. The second mesh, -N (autophagy inducing) was 0.5 MS Nitrogen depleted media. Seedlings were supported such that only the roots were submerged in the liquid nutrient media (Figure 1). After 4 days seedlings were collected carefully for analyses.

Sample Preparation for LAESI-MSI

Arabidopsis thaliana leaves were prepared for analysis using two different methods, the typical sample preparation for UV-LAESI and a fracturing method. Leaves of the cotyledon (Figure 2) were used. For the typical UV-LAESI method, cotyledon leaves were cut from the roots using scissors and placed on a glass microscope slide fitted with double sided tape. No additional treatment or matrix was used.

The fracturing method has been described elsewhere[33] and is shown in Figure 3. Briefly, leaves were placed onto packing tape and evacuated (~150 mtorr) for ~1 hr. The tape was then folded in half so both sides of the leaves were covered in tape. A mallet was used to ensure no air bubbles were present. The tape was then carefully pulled apart leaving one surface on each side of the tape. Both sides were placed on a glass microscope slide to prepare for ablation.

Mutant and wild type *Arabidopsis* leaves were ablated on the same slide with one leaf grown under nitrogen rich conditions on one half of the slide and a separate, nitrogen poor leaf on the other (Figure 4).

WT and mutant *Arabidopsis* roots in +N conditions were also imaged. Roots were cut using acetone washed scissors and using tweezers placed onto double sided tape that was attached to a glass microscope slide. No further treatment was done.

LAESI Source

The LAESI ion source used in this experiment has been used in our lab previously and has been described in earlier chapters of this dissertation.[34] In the present work, we measured negative ions using the following conditions. An electrospray solution consisting of a 50/50 methanol water mixture with 0.1% ammonium hydroxide solution (Sigma Aldrich) was pumped through a 53 μm i.d. capillary through a syringe pump (Model 22, Harvard Apparatus, South

Natick, MA) at a rate of 0.6 μl/min. Leucine-enkaphaelin (0.1 ppm, Waters), a lockspray mass calibrant, was added to the electrospray solution. The ESI voltage was -2.9 kV.

A 355 nm Nd:YAG ultraviolet laser (ULTRA, Big Sky Laser Tech, Inc., Bozeman, MT) was used in this experiment and operated at 10 Hz with a 5 ns pulse width. Laser pulses were 250 μJ/pulse energy and were focused to ~125 μm spot size by a plano-convex focusing lens. Once samples were ready to be ablated, the slides were placed on a xyz translation stage (Z825B, Thorlabs, Inc. Newton, NJ) positioned 8 mm below the electrospray axis. Samples were translated at a rate of 0.2 mm/s. The combined ablation and translation processes yielded a set of parallel trenches ~125 μm wide × ~30 μm deep spaced 150 μm apart center to center.

Mass Spectrometer

A Waters Synapt G2-S quadrupole time-of-flight (TOF) mass spectrometer was used in these experiments. The ESI source enclosure was removed. An adaptor was used to bypass connections from this enclosure. The TOF mass analyzer was operated in sensitivity mode, one pass through the main reflectron, resolution m/Δm 10,000 FWHM. Mass spectra were recorded from m/z 50 to 1200. Each single line scan run took approximately 1.5 minutes. Experiments were repeated two times to assess reproducibility.

Data Handling

ESI background subtracted spectra were generated at specific sample positions from total ion chromatograms through MassLynx software. The .raw Waters data files were converted to MzML files by Proteowizard Mass Converter Tool software. An iMzML converter was used to turn combined MzML files into iMzML files to be compatible with MSiReader V0.06[35] in order to generate mass spectrometry images. All images had linear interpolation and "Jet" color map/false color appearance.

Results and Discussion

Fracturing Plant Leaf Metabolite Imaging

The fracturing method described and the normal sample preparation method were compared. This method was tested to see if there was a difference from metabolites on the surface of the leaves compared to those on the inside. A comparison of ion images in fracturing vs. normal conditions is shown in Figure 5. Amino acids were the most abundant ion signals ($>10^4$). Glutamic acid, phenylalanine, and either isoleucine or leucine were higher in nitrogen "rich" conditions for both wild type and *atg5*. No change was observed in cysteine. This agrees with previously published literature[36-38] where plants under nitrogen starvation showed a decrease in amino acid synthesis. Table 1 lists these and other amino acids.

While images for high abundance ions ($>10^4$) were comparable among both sample preparation methods, lower abundance ions ($<10^3$), such as lipids, could just barely be detected and could not be imaged using the fracturing method (data not shown). Since other mass spectrometry imaging techniques, such as matrix assisted laser desorption ionization (MALDI),[39] have used this method with success for imaging lipids, this is likely due to limitations of the UV-LAESI system. Since only half the leaf was ablated, the laser penetrated completely through the fractured leaf, a common occurrence in LAESI, which has a larger depth penetration (~20 μm) compared to MALDI (~5 μm). [40] Since less material enters the mass spectrometer compared to an intact leaf, low abundance ions may not be reaching the detector compared to higher abundance ions. Thus, the fracturing method should be used in LAESI only when high abundance ions are to be studied.

Lipid Imaging in Arabidopsis Roots

Arabidopsis roots in nitrogen rich conditions were also studied to see if there was a correlation between roots and cotyledon leaves. Figure 6 shows the pre-ablation optical image and negative mode false color maps for lipids in both WT and *atg5 Arabidopsis* roots. For the images of wild type roots, there are 22 ablation tracks 125 μm wide × 150 μm apart. Each ablation track took 30 s at a speed of 0.4 mm/s. For the *atg5* images, there were 25 ablation tracks 125 μm wide × 150 μm apart taking 30 s at a speed of 0.4 mm/s.

The lipids PE(34:2), PE(36:2), PI(34:2), and PI(36:2) were present in WT roots, but in the *atg5* mutant all but PE(34:2) were at lower, undetectable levels. The lipids at higher levels were present in a few isolated spots and not distributed throughout the roots. The results are consistent with extract based lipidomic analyses previously conducted.[41,42]

Lipid Imaging in Arabidopsis Cotyledon Leaves

Figure 7 shows WT and *atg5* pre-ablation optical images and negative mode false color ion maps for lipids in both nitrogen rich and nitrogen poor conditions. For the images shown, there are 35 ablation tracks 125 μm wide × 200 μm apart. Each ablation track took 50 s at a speed of 0.4 mm/s. Lipid identification was based on accurate mass and previous literature.[43-45] Lipids, with their suggested assignments, are listed in Table 2.

In both WT and *atg5*, the lipids PC(34:2), PI(34:2), PE(34:2), and PE(34:3) show higher abundance in nitrogen rich conditions, suggesting that autophagy conditions hinders the synthesis of these lipids. In *atg5* however, PC(34:3) and PI(34:3) are more abundant in nitrogen starvation conditions than in nitrogen rich conditions. These data are consistent with biological assay experiments conducted by the Nikolau lab.[46] Overall, it appears most lipids have higher

concentrations in +N conditions, though certain lipids (LPC (16:0), PC(32:3)) show reverse trends spatially averaged over the entire leaf, which are not presented here.

To assess whether MSI is be an alternative to costly and time consuming assays, representative logarithmic scale graphs (similar to those produced by the Nikolau lab) were made using Equation 1 below:

$$\text{Log}\left(\frac{-N}{+N}\right) = \log_2\left(\frac{\frac{\text{Ion Intensity - N}}{\text{Total Ion Current - N}}}{\frac{\text{Ion Intensity + N}}{\text{Total Ion Current + N}}}\right) \qquad\qquad \text{(eq. 1)}$$

To obtain these values, ion intensities from individual ions were divided by the total ion count of a particular MSI run. Ablation tracks for the entire leaf were averaged together and standard deviations calculated. The -N average intensities were then divided by the +N conditions of the same leaf and the log taken. Figure 8 shows the results for WT and *atg5*. Although these values are not absolute, and larger data sets will need to be used to draw firm conclusions, results agree with experiments conducted by the Nikolau group.[46] MSI can be a fast approach in determining differences in lipid content between mutant and wild type plants.

Conclusions

UV-LAESI was successfully used to image metabolites of wild and mutant type *Arabidopsis thaliana* leaves. Amino acids were the most abundant metabolites in both sample preparation methods (normal and fracturing methods), although when leaves were fractured, we were unable to see lower intensity ions such as lipids. In the normal sample preparation method however, lipids could be imaged. Both +N and -N leaves were tested to compare lipid content under autophagy conditions. We were able to see differences which agreed with previously

published literature and on-going research. Since these results are reproducible and little sample preparation is involved, LAESI MSI is a quick, sensitive option compared to assay or other forms of mass spectrometry based on analyte extractions to investigate biological processes. This study is part of a larger on-going lipidomic study which seeks to understand autophagy in *Arabidopsis thaliana* and provide an open source data base of lipid images to serve as a model for future experiments.

Acknowledgments

References

1) Walton TJ, Kolattukudy PE. Determination of the structures of cutin monomers by a novel depolymerization procedure and combined gas chromatography and mass spectrometry. *Biochemistry*. **1972**, 11(10):1885-96.

2) Kolattukudy, P.E., Walton, T.J. The biochemistry of plant cuticular lipids. *Biochemistry*. **1973**, 13: 119-175.

3) Tulloch, A. P. Chemistry of waxes of higher plants. *Chem and biochem of natural waxes*. **1976**. 235-287.

4) Hadley, N. F. Cuticular Lipids of Terrestrial Plants and Arthropods: A Comparison of Their Structure, Composition, and Waterproofing Function. *Biological Reviews*. **1981,** 56: 23–47.

5) Xue, H., Chen, X., Mei, Y. Function and regulation of phospholipid signaling in plants. *Biochem Journal*. **2009**, 421(2): 145-156.

6) Meijer, H. J., Munnik, T. Phospholipid-based signaling in plants. *Annu. Rev. Plant Biol*. **2003,** 54: 265–306.

7) Munnik, T., Irvine, R. F., Musgrave, A. Phospholipid signalling in plants. *Biochim. Biophys. Acta*. **1998,** 1389: 222–272.

8) Xue, H., Chen, X., Li, G. Involvement of phospholipid signaling in plant growth and hormone effects. *Curr. Opin. Plant Biol*. **2007,** 10: 483–489.

9) Cole, L.K., Vance, J.E., Vance, D.E. Phosphatidylcholine biosynthesis and lipoprotein metabolism. *Biochim. Biophys. Acta*. **2012, 1821**: 754-761.

10) Kanno, K., Wu, M.K.m Scapa, E.F., Roderick, S.L., Cohen, D.E., Structure and Function of Phosphatidylcholine Transfer Protein (PC-TP)/StarD2. *Biochim Biophys Acta*. **2007,** 1771(6): 654–662.

11) Federica, G., Smith, T.K. The Kennedy pathway—de novo synthesis of phosphatidylethanolamine and phosphatidylcholine. *IUBMB life.* **2010,** 62(6): 414-428.

12) Heilmann, M., Heilmann, I. Plant phosphoinositides—complex networks controlling growth and adaptation. *Biochimica et Biophysica Acta* **2015,** 1851: 759-769.

13) Contento, A. L., Xiong, Y., Bassham, D.C. Visualization of autophagy in Arabidopsis using the fluorescent dye monodansylcadaverine and a GFP-AtATG8e fusion protein. *The Plant Journal* **2005,** 42.4: 598-608.

14) Huang, W.P., Klionsky, D.J. Autophagy in yeast: a reviewof the molecular machinery. *Cell. Struct. Funct.* **2002,** 27: 409–420.

15) Dall'Armi, C., Devereaux, K.A., Di Paolo, G. The role of lipids in the control of autophagy. *Current Biology.* **2013,** 23.1: 33-45.

16) Zoncu, R., Efeyan, A., Sabatini, D.M. mTOR: from growth signal integration to cancer, diabetes and ageing*. Nat. Rev. Mol. Cell Biol*. **2011,** 12: 21–35.

17) Haucke, Volker, Di Paolo, G. Lipids and lipid modifications in the regulation of membrane traffic. *Current opinion in cell biology* **2007,** 19.4: 426-435.

18) Eisenhaber, B. Glycosylphosphatidylinositol lipid anchoring of plant proteins. Sensitive prediction from sequence-and genome-wide studies for Arabidopsis and rice. *Plant Phys.* **2003,** 133.4: 1691-1701.

19) Kosma, D. K. The impact of water deficiency on leaf cuticle lipids of Arabidopsis. *Plant Phys.* **2009,** 151.4: 1918-1929.

20) Boudsocq, M., Barbier-Brygoo, H., Laurière, C. Identification of nine sucrose nonfermenting 1-related protein kinases 2 activated by hyperosmotic and saline stresses in Arabidopsis thaliana. *Journal of Biological Chem.* **2004,** 279.40: 41758-41766.

21) Amstalden van Hove, E. R., Smith, D.F., Heeren, R.M. A concise review of mass spectrometry imaging. *J. Chromatogr. A.* **2010,** 1217: 3946.

22) Blanksby, S.J., Mitchell, T.W. Advances in Mass Spectrometry for Lipidomics. *Annual Review of Analytical Chemistry.* **2010,** 3: 433.

23) Veit, M., Pauli, G.F. Major Flavonoids from Arabidopsis thaliana Leaves. *J. Nat. Prod.* **1999,** 62: 1301.

24) Lee Y. J., Perdian D. C., Song Z., Yeung E. S., Nikolau B. J., Use of mass spectrometry for imaging metabolites in plants. *The Plant Journal.* **2012**, 70: 81–95.

25) Stoeckli, M., Chaurand, P., Hallahan, D.E., Caprioli, R.M. Imaging mass spectrometry: A new technology for the analysis of protein expression in mammalian tissues. *Nature Medicine*, **2001**, 7: 493 – 496.

26) Pacholski, M.L., Winograd N. Imaging with mass spectrometry. *Chem Rev.* **1999,** 99: 2977.

27) McDonnell, L.A., Heeren R.M.A., Imaging mass spectrometry. *Mass Spectrom Rev.* **2007,** 26:606–643.

28) Bjarnholt, N., Li, B., D'Alvise, J., Janfelt, C. Mass spectrometry imaging of plant metabolites–principles and possibilities. *Nat. Prod. Rep*, **2014**, 31:818-837.

29) Nemes P., Vertes A., Laser ablation electrospray ionization for atmospheric pressure, in vivo, and imaging mass spectrometry. *Anal. Chem.* **2007**, 79: 8098.

30) Le Bars, R. ATG5 defines a phagophore domain connected to the endoplasmic reticulum during autophagosome formation in plants. *Nature Commun.* **2014,** 5.

31) Doelling, J. H., Walker, J. M., Friedman, E. M., Thompson, A. R., & Vierstra, R. D. The APG8/12-activating enzyme APG7 is required for proper nutrient recycling and senescence in Arabidopsis thaliana. *Journal of Biological Chemistry*, **2002,** *277*(36): 33105-33114.

32) Thompson, A. R., Doelling, J. H., Suttangkakul, A., & Vierstra, R. D. Autophagic nutrient recycling in Arabidopsis directed by the ATG8 and ATG12 conjugation pathways. *Plant physiology*, **2005,** *138*(4): 2097-2110.

33) Klein, A. T., Yagnik, G. B., Hohenstein, J. D., Ji, Z., Zi, J., Reichert, M. D., Lee, Y. J. Investigation of the chemical interface in the soybean–aphid and rice–bacteria interactions using MALDI-mass spectrometry imaging. *Analytical chemistry*, **2015,** *87*(10): 5294-5301.

34) Galayda, K.J., McVey. P.A., Anderson, T.J., Baldwin, D.P., Bajic, S.J., Houk, R.S. Matrix-Free Atmospheric Pressure Laser Ablation Electrospray Ionization Mass Spectrometry of Plant Material Using an Ultraviolet Laser. *Journal of the American Society for Mass Spectrometry.* under review.

35) Robichaud, G., Garrard, K. P., Barry, J. A., & Muddiman, D. C. MSiReader: an open-source interface to view and analyze high resolving power MS imaging files on Matlab platform. *Journal of the American Society for Mass Spectrometry*, **2013,** 24(5): 718-721.

36) Frommer, W. B., Hummel, S., Unseld, M., & Ninnemann, O. Seed and vascular expression of a high-affinity transporter for cationic amino acids in Arabidopsis. *Proceedings of the National Academy of Sciences*. **1995,** *92*(26): 12036-12040.

37) Lam, H. M., Coschigano, K., Schultz, C., Melo-Oliveira, R., Tjaden, G., Oliveira, I., Coruzzi, G. Use of Arabidopsis mutants and genes to study amide amino acid biosynthesis. *The Plant Cell*, **1995,** *7*(7): 887.

38) Frommer, W. B., Hummel, S., Unseld, M., & Ninnemann, O. Seed and vascular expression of a high-affinity transporter for cationic amino acids in Arabidopsis. *Proceedings of the National Academy of Sciences*, **1995,** *92*(26): 12036-12040.

39) Dueñas, M. E., Klein, A. T., Alexander, L. E., Yandeau-Nelson, M. D., Nikolau, B. J., Lee, Y. J. High-Spatial Resolution Mass Spectrometry Imaging reveals the genetically programmed, developmental modification of the distribution of thylakoid membrane lipids among individual cells of the maize leaf. *The Plant Journal*. **2016.**

40) Nemes, P., Barton, A.A., Vertes, A. *Anal. Chem.*, **2009**, 81: 6668–6675.

41) Bao, Y., Mugume, Y., Bassham, D.C. Biochemical Methods to Monitor Autophagic Responses in Plants**.** *Methods Enzymology*. **2017,** 588: 497–513.

42) Floyd , ,B.E., Mugume, Y. , Morriss , S.C., MacIntosh, G.C., Bassham, D.C. Localization of RNS2 Ribonuclease to the Vacuole Is Required for Its Role in Cellular Homeostasis. *Planta*. **2016,** 245(4): 779-792.

43) Wallis, J.G., Browse, J. Mutants of *Arabidopsis* reveal many roles for membrane lipids. *Progress in Lipid Research.* **2002,** 41(3): 254–278.

44) Wolters-Arts, M., Lush, W.M., Mariani, C.. Lipids are required for directional pollen-tube growth. *Nature.* **1998,** 392: 818-821.

Tables

Table 1. Amino acids identified in *Arabidopsis* leaves by LAESI in negative mode

Plant	Suggested Assignment	m/z Measured (Da)	Accurate m/z (Da)	Δppm	Sample Preparation Method
Wild Type +N	Glutamic Acid	129.0429	129.0426	-2.3	Normal
	Phenylalanine	147.0679	147.0684	-3.3	Normal
	Isoleucine or Leucine	113.0852	113.0840	10	Normal
	Cysteine	103.0095	103.0091	3.8	Normal
	Glutamic Acid	129.0428	129.0426	1.5	Fracture
	Phenylalanine	147.0683	147.0684	1.3	Fracture
	Isoleucine or Leucine	113.0845	113.0840	4.4	Fracture
	Cysteine	103.0089	103.0091	-1.9	Fracture
Wild Type -N	Glutamic Acid	129.0429	129.0426	-2.3	Normal
	Phenylalanine	147.0679	147.0684	-3.3	Normal
	Isoleucine or Leucine	113.0852	113.0840	10	Normal
	Cysteine	103.0095	103.0091	3.8	Normal
	Glutamic Acid	129.0428	129.0426	1.5	Fracture
	Phenylalanine	147.0683	147.0684	1.3	Fracture
	Isoleucine or Leucine	113.0845	113.0840	4.4	Fracture
	Cysteine	103.0089	103.0091	-1.9	Fracture

Table 1. Continued

Plant	Suggested Assignment	m/z Measured (Da)	Accurate m/z(Da)	Δppm	Sample Preparation Method
atg5+N	Glutamic Acid	129.0422	129.0426	-3	Normal
	Phenylalanine	147.0691	147.0684	4.7	Normal
	Isoleucine or Leucine	113.0837	113.0840	-2.6	Normal
	Cysteine	103.0092	103.0091	0.9	Normal
	Glutamic Acid	129.0422	129.0426	-3	Normal
	Phenylalanine	147.0691	147.0684	4.7	Normal
	Isoleucine or Leucine	113.0837	113.0840	-2.6	Normal
	Cysteine	103.0092	103.0091	0.9	Normal
	Glutamic Acid	129.0421	129.0426	-3.8	Fracture
	Phenylalanine	147.0691	147.0684	4.7	Fracture
	Isoleucine or Leucine	113.0837	113.0840	-2.6	Fracture
	Cysteine	103.0094	103.0091	-2.9	Fracture

Table 2. Lipids identified in *Arabidopsis* leaves by LAESI in negative mode.

Plant	Suggested Assignment	m/z Measured (Da)	Accurate m/z (Da)	Δppm
Wild Type +N	PC (34:2)	756.5538	756.5549	-1.4
	PC (34:3)	754.5347	754.5392	-5.9
	PI (34:2)	833.5179	833.5185	-0.7
	PI (34:3)	831.5044	831.5023	2.5
	PE (34:2)	714.5070	714.5079	-1.2
	PE (34:3)	712.4981	712.4917	8
Wild Type -N	PC (34:2)	756.5558	756.5549	1.2
	PC (34:3)	754.5347	754.5392	-5.9
	PI (34:2)	833.5169	833.5185	-1.9
	PE (34:2)	714.5073	714.5079	-0.8
	PE (34:3)	712.4931	712.4917	-1.9
atg5+N	PC (34:2)	756.5578	756.5549	3.8
	PC (34:3)	754.5367	754.5392	-3.3
	PI (34:2)	833.5164	833.5185	-2.5
	PI (34:3)	831.5018	831.5023	-0.6
	PE (34:2)	714.5081	714.5079	0.2
	PE (34:3)	712.4965	712.4917	6.7

Table 2. Continued

Plant	Suggested Assignment	m/z Measured (Da)	Accurate m/z (Da)	Δppm
atg5-N	PC (34:3)	754.5387	754.5392	-0.6
	PI (34:2)	833.5183	833.5185	-2.3
	PI (34:3)	831.5014	831.5023	-1.1
	PE (34:2)	714.5083	714.5079	0.5
	PE (34:3)	712.4981	712.4917	6.7

Figures

Figure 1. Typical set up for growth of *Arabidopsis*. The leaves are above the mesh and not in the liquid; the roots are under the mesh, in the liquid.

Figure 2. Optical photograph of an intact *Arabidopsis* plant which shows the cotyledon leaves. These leaves are the first to sprout and were used in all experiments.
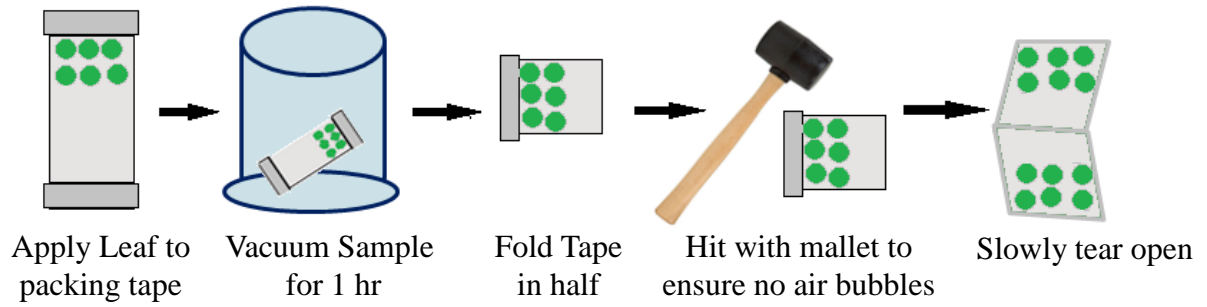
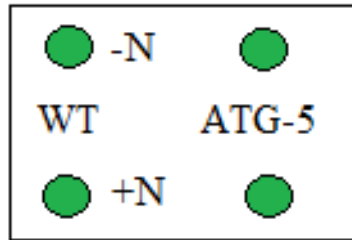Apply Leaf to packing tape   Vacuum Sample for 1 hr   Fold Tape in half   Hit with mallet to ensure no air bubbles   Slowly tear open

Figure 3. Fracturing method schematic.[32]

Figure 4. Typical placement of leaves onto glass microscope slides in anticipation for ablation.

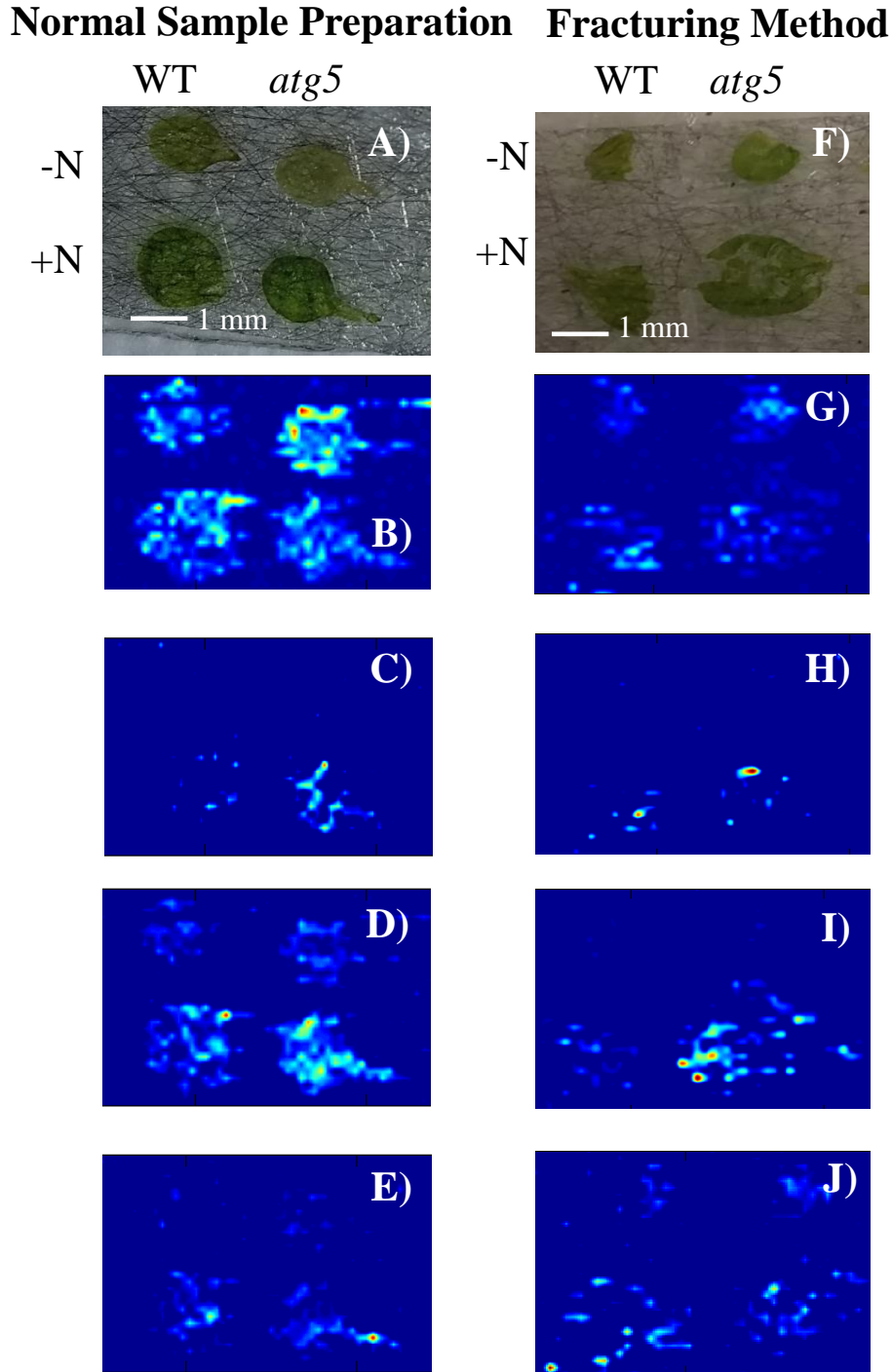**Normal Sample Preparation** **Fracturing Method**

Figure 5. Images for negative ions from *Arabidopsis* leaves. A) Optical photograph before ablation using normal sample preparation. False color ion maps at B) m/z 102.0012, cysteine C) m/z 112.0759, isoleucine or leucine D) m/z146.0648, phenylalanine E) m/z 128.0342, glutamic acid; F) Optical photograph before ablation using the fracturing method. False color ion maps at G) m/z 102.0015, cysteine; H) m/z 112.0768, isoleucine or leucine; I) m/z 146.0661, phenylalanine; and J) m/z 128.0350, glutamic acid.
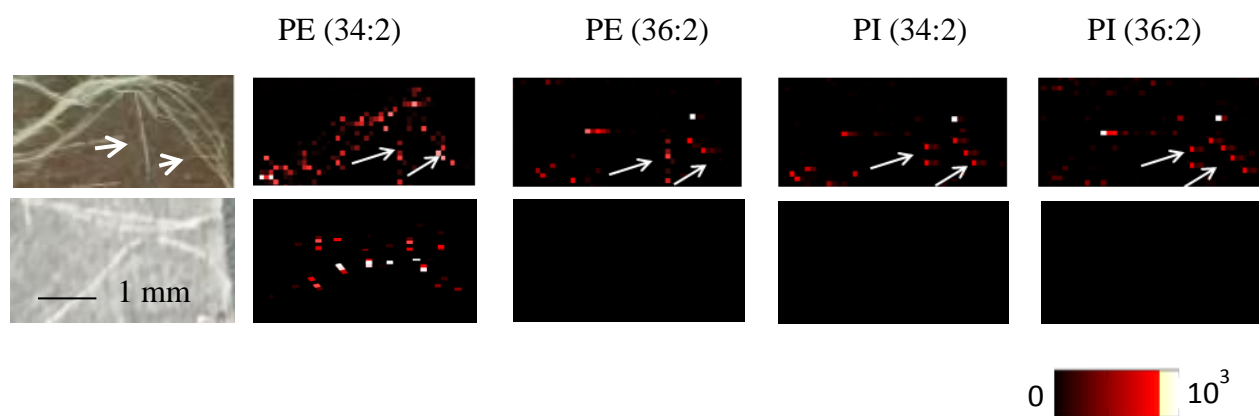
	PE (34:2)	PE (36:2)	PI (34:2)	PI (36:2)

Figure 6. Images for negative ions of *Arabidopsis* roots. A) Optical photograph wild type *Arabidopsis.* False color ion maps of B) m/z 714.5081, PE (34:2); C) m/z 742.5400, PE (36:2); D) m/z 833.5165, PI (34:2), E) m/z 861.5521, PI (36:2). *Atg5* mutant type *Arabidopsis* was also imaged, with its optical photograph in F). Only PE (34:2) was able to be imaged (m/z 714.5074), as shown G). In H-I) lipids were at lower, undetectable levels.
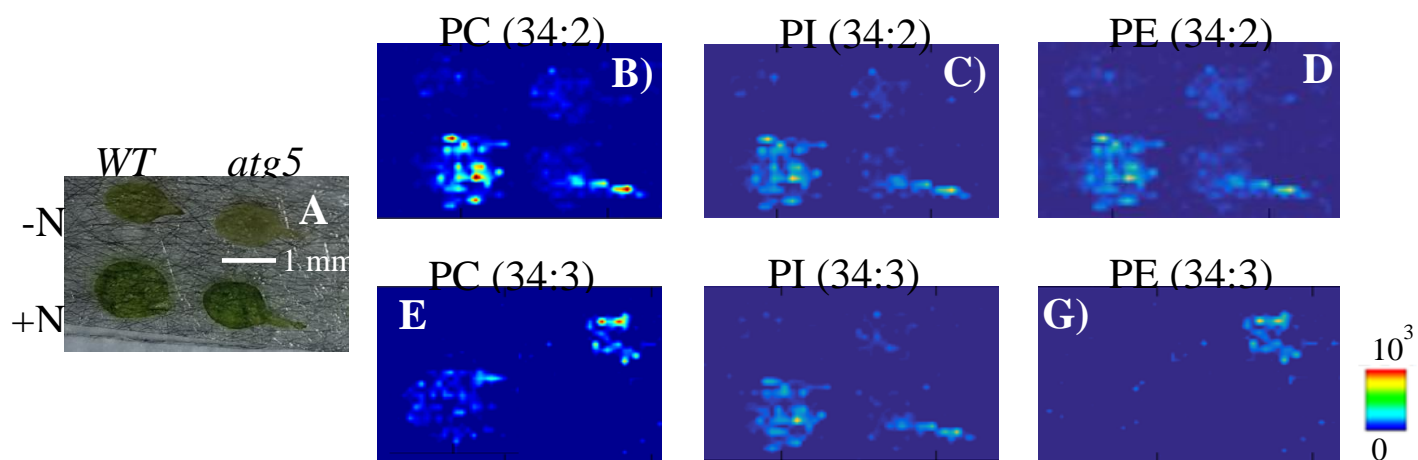
Figure 7. Images for negative ions of *Arabidopsis* in both WT and *atg5*. A) optical photograph wild type *Arabidopsis.* False color ion maps of B) PC (34:2); C) PI (34:2); D) PE (34:2), E) PC (34:3); F) PI (34:3); G) PE (34:3). Ion signals were normalized. For m/z values of each compound, please refer to table 2.
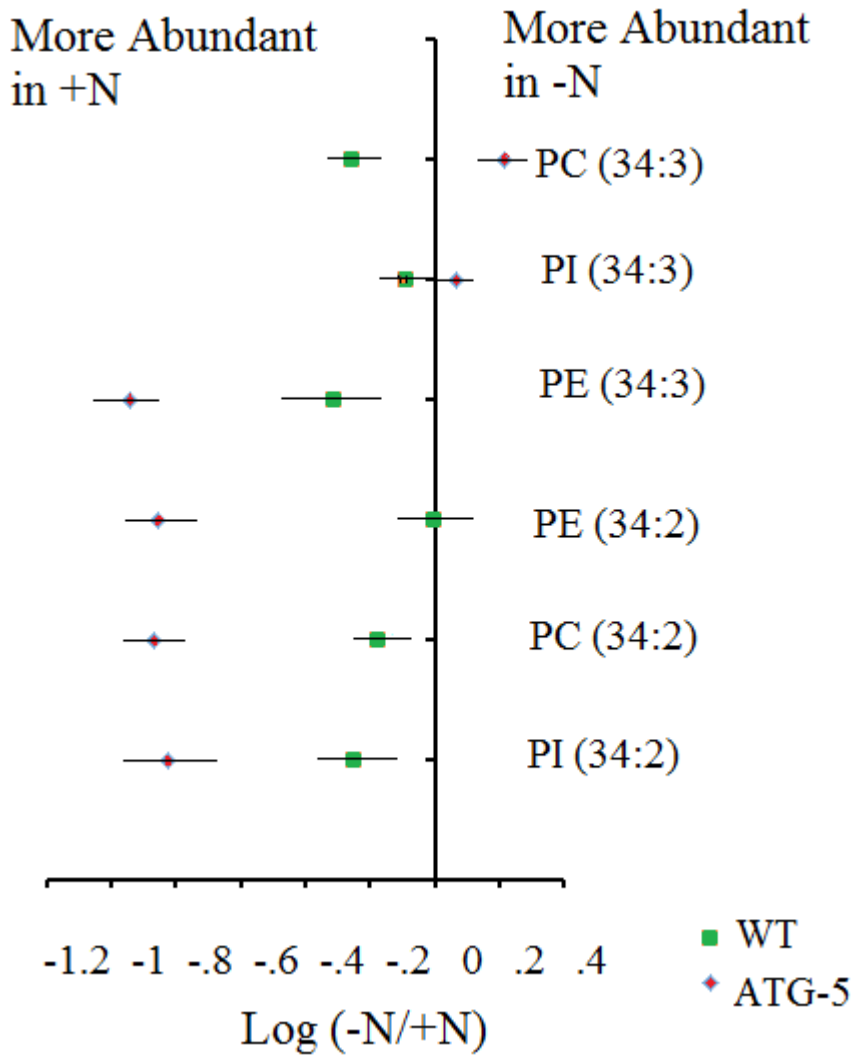
Figure 8. Log graph of wild type (green square) and *atg5* (red diamond) *Arabidopsis* in nitrogen rich and nitrogen starvation conditions calculated from specific ion intensities over total ion intensities of the lipids listed.

CHAPTER 5

GENERAL CONCLUSIONS AND FUTURE WORK

General Conclusions

Metabolomics profiling can be done easily and with little sample preparation using ultraviolet laser ablation electrospray ionization. This dissertation examined several uses of UV-LAESI in a variety of plant materials. In Chapter 2, a UV-LAESI system was described and tested using geranium, hosta, French marigold, and peony leaves. These leaves were previously studied using other forms of laser ablation, such as IR-LAESI. The resultant spectra and images were similar to those other forms of ionization, demonstrating the potential value of ambient-pressure UV-LAESI for metabolites analysis, as there is little sample preparation and no matrix coating.

In Chapter 3, UV-LAESI was further tested by determining anthocyanins, common secondary metabolites, which give rise to blue, red, and purple pigments, in two kinds of coleus leaves, Broad Street (red and green foliage) and Wizard Jade (green and yellow foliage). Anthocyanins were in high abundance in Broad Street, but surprisingly, small amounts were present in Wizard Jade as well. These anthocyanins were concentrated in the vein and stem, concluding that their presence was for damage protection against typical stressors such as UV damage. Interestingly, anthocyanins were not found in LC-MS runs of Wizard Jade, which shows the value of the spatial resolution of UV-LAESI.

In Chapter 4, the use of LAESI was used to image lipids in autophagy conditions of *Arabidopsis thaliana* leaves and roots. Autophagy was induced using a nitrogen starvation method. While lipids were of low abundance (~10^3 orders of magnitude), significant changes

were still observed in autophagy vs. normal growth methods. LAESI MSI can thus be a quicker, sensitive option to investigate biological processes than typical means. This project is part of a larger on-going lipidomic study which seeks to understand autophagy in *Arabidopsis thaliana* with the goal to have and open source data base of lipid images to serve as a model for future experiments.

Overall, UV-LAESI is a useful technique for plant metabolomics. Since it is a sensitive technique that does not require a matrix and is amenable to dry (i.e. no water containing) materials, it can be used for a wide variety of samples. When coupled with mass spectrometry imaging, UV-LAESI is useful for interpreting biological processes such as the malonylshisonin pathway and autophagy.

Future Work

Future and current work using UV-LAESI MSI focuses on its usefulness in a biological sense. Current work being performed in our lab involves light and dark studies of henna coleus leaves and uptake studies of ^{13}C glucose in Arabidopsis leaves. Future work will veer away from plant leaves and focus on materials such as pills. Using these non-plant materials will allow for further improvements of the instrument including lowering the laser spot size below 50 µm and testing the efficiency of a pneumatically assisted UV-LAESI system.